UNIVERSITÀ DELLA CALABRIA

UNIVERSITY OF CALABRIA

D.I.B.E.S.T.

LIFE SCIENCE

XXXIII CYCLE

RHEOLOGICAL ANALYSIS OF COMPLEX INTERFACES AND BULK BEHAVIOUR OF STARCHES AND PEA PROTEIN

Scientific Disciplinary Sector: ING-IND/24

Coordinator: Ch.mo Prof. Maria Carmela Cerra

Supervisor: Prof.ssa Noemi Baldino

Tutor: Prof. Bruno de Cindio

PhD student: Dott.Paleologo Mario Floro Oraldo

UNIVERSITÀ DELLA CALABRIA

UNIVERSITY OF CALABRIA

D.I.B.E.S.T.

LIFE SCIENCE

XXXIII CYCLE

RHEOLOGICAL ANALYSIS OF COMPLEX INTERFACES AND BULK BEHAVIOUR OF STARCHES AND PEA PROTEIN

Scientific Disciplinary Sector: ING-IND/24

Coordinator: Ch.mo Prof Maria Carmela Cerra

MARIA CARMELA
CERRA
27.04.2021
12:48:30 UTC

Supervisor: Prof.ssa Noemi Baldino

BALDINO NOEMI
28.04.2021 09:10:35
UTC

Tutor: Prof. Bruno de Cindio

BRUNO DE CINDIO
28.04.2021 11:47:54 CEST

PhD student: Dott.Paleologo Mario Floro Oraldo

Firma oscurata in base alle linee guida del Garante della privacy

Index

There is nothing deeper than what appears on the surface

(Hegel)

To my parents

and my grandfather

Introduction:
Aim and development of the work

This work aims to find rheological relationships for complex food systems and to use them for product design in food engineering. Foods are structured and multiphasic systems, with wide interfaces between different phases. Both the bulk and interfaces need complex constitutive equations to be modelled. For this reason, the engineering product design needs information about both the bulk and interfacial rheological properties and the stability of systems. In this work, attention was paid to systems constituted of vegetable proteins and resistant starches.

This choice was not casual. In fact, during the last few years, new dietary needs have emerged in the world population: some due to dietary diseases and intolerances; some linked to religious questions, and others to ethical issues. Because of these new emergencies, the attention of the food industry is focusing on satisfying new needs.

Proteins are an essential component of the human diet and are very much used in the food industry thanks to their capacity to stabilize multiphasic foods, constituted of emulsion or foams, because of their amphiphilic nature. The most widely-used proteins source has an animal origin, but attention is shifting to a vegetable source as an alternative, since an increasing number of people refuses food in which animal proteins are present, for healthy or ethical issues. So, in this work, pea proteins were investigated. Pea proteins are less studied than other vegetable proteins, such as soybean or hemp-derived products, but they constitute a valid alternative thanks to their functional and nutritive properties (Lam et al., 2013).

On the other hand, gluten-free products are increasingly in demand on the market, principally for health reasons. The efforts of research and the food industry are focusing on the design of gluten-free products with characteristics comparable to conventional bakery products deriving from wheat flour. The use of resistant starches can be a valid option. Resistant starch refers to the indigestible part of the total starch amount (Nugent et al., 2005). Resistant starches have good functional and nutritional properties, being important to counteract dietary diseases, such as the celiac one, obesity, diabetes (Nugent et al., 2005; Sharma et al., 2008). Thus, pea proteins/resistant starches food systems can be the basis for the design of a dietary product with a high added value.

In light of the above, the first part of this work is focused on the bulk characterization of single materials used. Bulk rheological properties dependency upon concentration, temperature, stress and frequency investigated, with special attention paid to their behaviour during thermal treatment, to

understand the evolution of the system with increasing temperature. Specifically, gelatinization onset and peak temperatures dependency upon concentration was studied, together with structural properties of systems after the gelatinization process was accomplished. This investigation is very useful to understand how gelatinization parameters and structure properties change according to the composition of materials used and suitable ingredients to obtain the desired final product properties can be chosen.

The second part of the work regards interfacial analysis both of single materials and their mixtures. The investigation was performed in static, dynamic conditions, and transient conditions. From static measurements, equilibrium surface tension and information about kinetic parameters was studied. Dynamic measurements were performed in asymptotic dilatational kinematic so that the equilibrium condition can be investigated. With this kind of investigation, intrinsic interfacial properties are studied. While the transient tests were performed to understand the characteristics of the system in non-equilibrium conditions, such as those that occur during rapid expansion or compression.

For complex systems modelling, both a classic and fractional constitutive equation were used, according to the literature and experimental data. The theoretical background on the interface refers to the classic treatment of Gibbs and the use of rheological models of bulk applied to the interfacial layer (Rusanov, 2005; Ivanov et al., 2005; Mezzenga et al., 2013).

Finally, information derived both from bulk and interfacial characterization were matched together, to understand which materials have to be used to design a final product with certain characteristics. In particular, attention is paid to bakery aerated systems. So, in the last chapter the use of the information derived both from the bulk and interfacial analysis is shown to design a product with a determined expansion capacity.

Bibliografy

Noemi Baldino, Francesca Laitano, Francesca R. Lupi, Stefano Curcio, Domenico Gabriele (2018), Effect of HPMC and CMC on rheological behaviour at different temperatures of gluten-free bread formulations based on rice and buckwheat flours, *European Food Research and Technology* 244:1829–1842

Cheng Li, Bo Gong (2020) Insights into chain-length distributions of amylopectin and amylose molecules on the gelatinization property of rice starches, *International Journal of Biological Macromolecules* 155 721–729

C. Chang, S. Tu, S. Ghosh, M.T. Nickerson (2015) Effect of pH on the inter-relationships between the physicochemical, interfacial and emulsifying properties for pea, soy, lentil and canola protein isolates, *Food Research International* 77 360–367

Ricky S.H. Lam, Michael T. Nickerson (2013), Food proteins: A review on their emulsifying properties using a structure–function approach, *Food Chemistry* 141, 975–984⇑

Ivanov, I. B., K. D. Danov, K. P. Ananthapadmanabhan & A. Lips (2005) Interfacial rheology of adsorbed layers with surface reaction: On the origin of the dilatational surface viscosity. *Advances in Colloid and Interface Science*, 114, 61-92.

Mezzenga R., Fischer P. (2013), The self-assembly, aggregation and phase transitions of food protein systems in one, two and three dimensions, *Reports on Progress in Physics* (76) 046601 (43pp)

Nugent, A. P. (2005). Health properties of resistant starch. *British Nutrition Foundation, Nutrition Bulletin*, 30, 27–54

Rusanov, Surface thermodynamics revisited, *Surface Science Reports* 58 (2005) 111–239

Sharma, A., Yadav, B. S., & Ritika (2008). Resistant starch: Physiological roles and food applications, *Food Reviews International*, 24, 193–234.

Chapter 1:
Resistant Starch and Pea Proteins: an overview

Introduction

Resistant Starch (RS) recently received the attention of the scientific community because of its interesting nutritional and functional properties, useful both for health and disorder or alimentary diseases. The benefits coming from the RS assumption comprehend the control of glycemia, cholesterol and mineral adsorption. In recent years, new technologies to isolate RS were developed, along with the design of functional healthy foods.
In this chapter, the main topics about RS are summarised.
Another important topic in food research is the vegetable proteins investigation. These last are a very important source of essential amino acids and constitute a valid alternative to meat and milk proteins sources. In this work, attention is focused upon pea proteins, their characteristics, ways of production and benefits.

1.1 Resistant Starch

1.1.1 Introduction

It is well known that starch is the most plentiful storage polysaccharide in vegetables and consequently one of the most relevant components of the human diet. Starch is the principal reserve of carbohydrates in the human diet, as well as the major storage polysaccharide present in plants. It comes in the form of granules inside the chloroplast of leaves and in the amyloplastic in tubers and seeds (Ellis et al., 1998). Cooking enhances the digestibility of starches, but the human digestive system cannot digest the total amount of starch present in foods. For at least twenty years, numerous experimental evidences have proved this last phenomenon and the concept of food “availability” is used to explain (Nugent et al., 2005). Several factors prevent the digestive system from absorbing all the nutrients, such as indigestible cell walls, the density of bulk structure, poor solubility, components able to inhibit digestion, such as dietary fibre. Otherwise speaking, processing of foods could make derivatization and establishment of cross-link among various nutrients; this kind of reactions could make the food indigestible, and part of their compounds not available (Erbersdobler et al., 1989; G. Sarwar et al., 2012). The undigestible portion of starch is called Resistant Starch (RS), and it can be classified as a kind of dietary fibre, but there is no consensus about this; in fact, in the UK they are

considered dietary fibre only not starchy products (Sharma A. et al., 2008). In recent years, the scientific community usually names dietary fibres RS naturally present in vegetable foods, while RS added in functional foods is called functional fibre. Dietary fibres are considered very important from a nutritional and functional point of view, and under this denomination can be individualized a lot of substances, each with different physical and chemical characteristics. All the definitions of dietary fibre agree within considering them as carbohydrate polymers with a certain number of monomeric units, which cannot be digested nor absorbed in the tract of the human small intestine (Mermelstein et al., 2009). The prominence of this type of substances is linked both to health and social matters. The dietary fibres can help human metabolism to control the amount of cholesterol, as well as to prevent cancer of the intestinal system. They are also helpful against obesity, a disease that affects human life not only from a physiologic but also from a social point of view. On the other side, the great demographic increase in recent years makes the use of new technologies to produce innovative functional foods to respond to global needs (Peressini et al., 2009). The nutritional function of starch is connected to its rate and extent of digestion and absorption in the small intestine. From this point of view, starches can be defined as rapidly available, slowly available and resistant starch (RS). It is not easy to understand the real mechanism that makes starches resistant, because several factors are interconnected. According to the definition of dietary fibre, the fraction of starch that the human intestine cannot hydrolyse belong to the ensemble of them and constitute a topic of great relevance in food chemistry, engineering and industry. RS can be found in cereal grains or starchy foods (Charalampopoulos et al., 2002). The fraction of indigestible starch is dependent upon the form of seeds in which it is present, especially when they are partially or totally overblown. Other factors that affect the digestibility of starch are food processing from raw materials to finite product, cooking conditions, human metabolism and health conditions (Slavin er al., 2004).

1.1.2 Resistant starch composition ad classification

From a chemical point of view, starches are polysaccharides made up of α-D-glucopyranosyl units, bonded together through two types of linkage: α-D-(1–4) and/or α -D-(1–6). They are constituted by two kinds of molecules: first, amylose, with a linear structure of polyglucan, made by 1000 glucose units, linked by α-D-(1–4) bound; the second one is amylopectin, whose structure is constituted by branched glucan, with roughly 4000 units of glucose, linked by α -D-(1–6) linkages (Sharma et al., 2008). Starch was proved to have two different crystalline structure, called respectively “A” and “B” forms, which depend upon the amount of amylopectin. The “C” form is a combination of A and B structure. This is normally founded in legumes. The digestion of starch occurs through the action of enzymes glucoamylase, amylase and sucrase-isomaltase. The digestive process leads to the formation

of units of glucose, able to be adsorbed (Nugent et al., 2005). As said above, not all amount of starch undergoes the digestive process, and the indigested part can pass through the entire gastrointestinal tract. RS is then fermented in the colon. It was proved that RS is constituted by linear molecules of α-1,4-D-glucan, characterized by a small molecular weight (Tharanathan, R. N., 2002). Several studies demonstrated that there are at least four reasons for which RS cannot be digested. First, RS has a compact molecular structure, so that digestive enzymes cannot reach the decomposition sites (Haralampu, 2000). Secondly, the starch grains could be physically unassailable by the enzymes (Nugent, A. P., 2005). Thirdly, it is known that heating in water excess process can disrupt the starch grains, by this way leading to gelatinization, offering to the enzymes the possibility to get access to the reaction sites. However, when the gel is cooled, starch crystals are formed, which is indigestible. This kind of starch is called "retrograded". Finally, certain starches undergo selected treatment, such as etherification, esterification or cross-bonding: by this way, they are made inaccessible to the enzyme action (Nugent et al., 2005; Sharma et al., 2008).

In the design of a new functional product, great attention is focused on its texture. RS has a small water-holding power, and this makes it a good ingredient to improve final product texture. Controlling process conditions can increase the total amount of RS, and through this way improve final product texture. RS takes advantage compared to other dietary fibres because it does not give marked flavour or grainy texture to the final product (Tharanathan, R. N., 2002). Four classes of RS were individuated, which depend upon physical and chemical characteristics. RS naturally presents in foods is often disrupted when manufactured. The processing of RS comprehends hydrolysis in acid conditions, thermal treatment, polymerisation, retrogradation and chemical substitution of functional groups. The characteristics of four RS classes are summarised below (Nugent, A. P., 2005; Sajilata, M. G., et al., 2006). RS1: the first-class comprehend RS physically made unavailable to digestion by entrapment inside an indigestible substrate. Digestion in the small intestine proceeds slowly and partially. Resistance to digestion can be reduced by milling and chewing. It is present in totally o partly milled grains or seeds, legumes and pasta.

1. RS2: the second class is constituted by ungelatinized granules, whose crystallinity is of type B. It is slowly hydrolysed by α-amylase action, and digestion in the small intestine occurs at a very low rate. Resistance to digestion can be totally overcome if RS2 is eaten when just cooked. It is found in raw potatoes, green bananas, certain legumes and in starches with high-amylose content (Nugent et al., 2005).
2. RS3: the third class is the retrograded starch, which is formed when foods are cooked and then cooled. In the small intestine, tract digestion occurs quite slowly and partially. The digestion rate can be increased by reheating. Processing conditions can reduce resistance to

digestion. It is present in cooked and cooled foods and in heat-treated products (Nugent et al., 2005.

3. RS4: the last class are selected and chemically modified RS, made indigestible in the small intestine tract by chemical treatment. They are also less accessible to digestibility in *vitro* systems. They are present in drinks and foods with modified starches (Nugent et al., 2005.

The first two classes, RS1 and RS2 are remains of starchy substances, that survive digestion. RS1 is physically inaccessible to digestion contribute to total RS. This kind of indigestibility can be due to the presence of intact cell walls, which makes RS1 stable also during the cooking process. For this reason, RS1 is an ideal ingredient for starchy foods design. RS2 is constituted by native uncooked grains, with a crystalline structure that makes them less hydrolysable (Hernández, et al., 2008), and with a compact form that prevents the enzymatic action. There is a very important RS2 starch, called hi-amylose maize starch that can preserve its structure also during process stages (Wepner et al., 1999.). RS3 are the retrograded starch that arises when cooked food is cooled at low or room temperature. It was shown that this kind of RS has a very high thermal stability, and it can retain its structure also when RS1 and RS2 are destroyed during heating processes (Faraj, A., et al., 2004). RS3 has also a higher water-holding power than starch in granular forms (Sanz T. et al., 2008). The global digestibility of RS is a function of the class to which it belongs to. It was estimated that 80-90% of the glucose obtained from the enzymatic action is metabolized. A range of 30-70% of the total amount of RS can be reduced to short-chain fatty acid in the human colon portion by the action of bacterial amylases. The remaining portion is directly expelled from the body. It was proved that the degree of digestibility depends on individual metabolism, in particular by the enzymatic response (Sharma et al., 2008). The last class, RS4 is an RS type produced by chemical reactions to reduce their digestibility, analogue to resistant oligosaccharides and polydextrose (Wepner et al., 1999.). RS4 can be produced by reactions of conversion, substitution, cross-linking, in such a way that the enzyme access to the reaction site is blocked, and during the chemical treatment, they can be formed unusual linkages, such as α (1 →4) and α (1 →6) (Kim et al., 2008). Understanding how much RS can be digestible is very complex, for there are also other factors that can influence the digestibility of RS. For instance, complexes amylose-lipids can be formed, or in native RS structure there can be amylase inhibitors, and the presence of non-starchy polysaccharides can influence catalytic enzymatic action. It is also important the mechanical action of mouth upon the RS food: increasing chewing can help to destroy the crystalline structure, and this can affect digestibility. Further, individual health state can affect the metabolization of RS, such as the menstrual cycle for women (Nugent et al., 2005).

1.1.2Healthy benefits of RS

One of the most important topics about RS is its connection with human health, and for this reason, RS has recently received much attention. As said in previous sections, RS constitute one of the most copious sources of dietary fibre in nature, and it is as important as non-starch polysaccharides (NSP) to ensure human large bowel health and to prevent diseases, such as inflammatory syndrome or cancer (Peressini et al., 2009). The health effects of RS can be a function of several factors, including origin, processing, concentration in foods, other than individual metabolism. Recent eating habits have probably led to a minor consummation of RS than in past (before Second World War), and this has brought a wide range of bowel diseases. New technologies to design innovative functional food with a determined RS concentration must be developed to answer new healthy and demographic emergencies. It is known that RS is fermented in the large bowel by bacteria, and short-chain fatty acids are produced (SCFA) (Englyst et al., 2005). It was shown that butyrate, a fermentation product, can reduce the probability of colon cancer onset, because it is an important component of the energy substrate of large bowel epithelial cells, and it can block one of the phases of the tumoral cells cycle. As the fermentation of dietary fibre leads to the production of butyric acid and relative salts in the human large bowel, RS, as a kind of dietary fibre, can be a fundamental ingredient for colon cancer prevention (Nugent, A. P., 2005; Sharma et al., 2008). Another important function of RS in food is to control glycemic and insulinemic responses. The glycemic response to the ingestion of starchy foods in the postprandial period can be dependent on several factors, such as amylose/amylopectin ratio, the native conditions of granules, processing conditions and gelatinization characteristics. While the conventional starchy foods are digested in a very short period after ingestion, those with RS are metabolized 5-7 hours after. The digestion action spread over 5-7 hours is useful to lower postprandial glycemic level and insulin response. Low RS digestion is also directly linked to an inferior blood glucose concentration. It was studied that foods with RS3 as a functional ingredient can lower maximum blood glucose level compared to other conventional carbohydrates (Truwell, A. S. (1992). This RS3 feature is very important to improve the metabolic cycle in people with II type diabetes. To be successful in controlling glycemic levels, RS must be present for almost 14 % of the total amount of starch in foods (Behall et al., 2002). The fourth class of RS, RS4, can also induce different glucose answers during digestion (Raben et al., 1998). RS is also intended as a prebiotic functional ingredient. Foods indigestible that can take benefit the bacteria (probiotics) in the gastrointestinal tract by promoting growth or activity are called prebiotic. It was suggested that RS can stimulate the growth of these gastrointestinal bacteria, such as Bifidus-bacterium (Brown et al., 1996). It is probable that RS, passing through the digestion process, can be a substrate for the probiotic

bacteria life cycle (Sajilata et al.,2006).

Some studies suggest that RS can strongly influence lipidic metabolism and in this way, it can bring a hypocholesterolemic effect on the human organism, although more research to confirm effectively this kind of benefit (Nugent et al., 2005).

RS is also employed to reduce the calorific power of carbohydrate present in foods and to extend the sense of satiety (Higgins et al., 2004). RS is thought to influence fat oxidation, and to induce a major fat mobilization in the postprandial period. This is probably since RS digestion leads to minor insulin secretion (Tapsell et al., 2004). RS can be also a functional ingredient to induce gut hormones secretion, which is responsible for reducing energy intake. This is a natural way to contrast obesity (Keenan et al., 2006)

It is known that great insulin secretion can lead to gall stone formation because insulin stimulates cholesterol synthesis, which in turn can lead to gall stones formation. Since RS can reduce insulin secretion and, consequently the cholesterol synthesis, it can be deduced that the RS assumption can reduce the insurgence of gall stones (Sajilata et al., 2006). Finally, RS is thought to promote the absorption of certain minerals by the human ileal tract (Morais et al., 1996).

1.1.3 RS: application in the food industry

Since RS was proved to be a food functional ingredient for its healthy and physiological benefits, great interest has raised around its application by nutritionists and food engineering, because RS was proved to have several features that other dietary fibres do not possess. In fact, foods with a high conventional insoluble fibre content usually are rough, coarse, too consistent and with very low palatability, compared to refined and processed products (Sajilata et al., 2006). Instead, RS has optimal rheologic and chemical properties, that make it desirable as an ingredient in high dietary fibres content foods. Some of the unique RS characteristics that can lead to foods are increasing viscosity, swelling, gel-forming, water binding (Sajilata et al., 2006). Moreover, RS consist of small particle, it does not alter food flavour excessively and has a white appearance. Its low water-holding power can give good handling and can enhance the texture in food (Yue et al., 1998). RS is able to confer crispness and better expansion properties, improving so sensorial feelings when the final product is eaten (Buttriss et al., 2008).

For these and other qualities, it could possible to replace flour with RS, totally or partially, without altering significantly the overall quality of the product, but anyway advances in food engineering on this topic is needed (Riva et al., 2000). RS is also employed to increase fibre content in low carbohydrate food for special dietary regimes (Nugent, 2005). The RS content may be dependent upon the process conditions, which can affect gelatinisation and retrogradation phaenomena

(Thompson, 2000). It was shown that it is possible to get functional RS by imposing determinate conditions on suspensions starch suspensions. Such conditions can be pH of suspensions, heat fluxes, time and temperature (Augustin, 2008). In addition, industrial RS is not affected by processing conditions as RS naturally present in legumes, vegetables or fruits (Nugent, 2005). A large amount of RS is recommended because of functional, processing and nutritional reasons. From a food design perspective, RS is important because it can improve the texture without altering excessively the flavour, giving also the desired consistency. One of the most important factors that make RS ingredient very important in food design is the stability it can confer to the final product, which in turn is fundamental to preserve nutritional qualities and functions of the food. The RS stability is important also from a metabolic perspective because its resistance to pass through the gastrointestinal tract give it the possibility to contrast gastrointestinal diseases (Peressini et al., 2009; Baldino et al., 2018). It is also fundamental for the design of functional products suitable for coeliac people. RS is mainly used for the manufacture of moisture-free products and bakery foods (Yue, P., & Waring, S.,1998). The use of resistant starch powder for bakery products to replace wheat flour in a gluten-free diet, since it is not easy to reproduce the same characteristics of classic bakery products (Riva et al., 2000; Peressini et al., 2009). The addition of resistant starch could lead to a decrease of texture quality and a more difficult workability (Birt et al., 2013). Anyway, efforts are being made to design products in which resistant starch replace partly or totally wheat flour (Birt et al., 2013; Foschia et al., 2017; Korus et al., 2009).

1.2 Pea proteins

1.2.1 Introduction

Dry peas are cultivated in the world for a total amount of over 12 million metric tonnes. These cultivations are important for human beings because of the dry pea protein content. Pea Protein concentrations and isolates are produced from dry peas, but the relative sales are limited because of the competition with other more diffused soy protein products, or other protein sources, such as that derived from milk and animals (Kumari et al., 2021). Despite these factors, pea proteins are a very important source of essentials amino acids for humans and constitute a valid alternative to other protein sources (Owusu et al., 2015).

1.2.2 Chemical composition

The protein concentration of field peas strongly depends on genetic and environmental variables. On average, *Pisum Sativum* is in the range of 24-39%, but this percentual is too variable to make uniform conclusions. The protein content increases with the presence of nitrogen, phosphorus, and *S*-triazine. It decreases with soil potassium. The different pea protein content between different cultivar is

decisive when products with uniform composition are to be designed and achieved with dry or wet milling technologies (R. D. Reichert et al., 1982; Kumari et al., 2021). It was shown that the amino acid composition for plantation with similar protein content is often quite similar, while the amount of each amino acid is directly proportional to protein content. However, there are several exceptions to this assertion (R. D. Reichert et al., 1982; Kumari et al., 2021). The main amino acids present in the pea protein content are isoleucine, lysine, methionine, cystine, threonine, alanine and glycine, other than arginine, aspartic acid, glutamic acid, and serine. There are several thousand specific proteins in the overall crude pea protein content and a percentual between 10-15 % of nonprotein molecules containing nitrogen. A percentage of 70-80% of the crude protein in legumes are of storage type, which constitutes a primary source of amino acid and nitrogen to develop the seeds (). The other non-storage protein is enzymes, enzyme inhibitors, hormones; there are also transport, structural and recognition proteins. Some proteins (globulins), 65-80% of the total amount, can be extracted with a salt treatment (Hartmut E. Schroeder,1982; Kumari et al., 2021). This percentage is constituted primarily of two proteins, legumin and vicilin. There is also a third type of globulin, the convicilin, whose amount is very small. This kind of protein can be found in the protein bodies, which are spheroidal organelles, bounded by a membrane, with few micron diameters (J. Mossé and J. C. Pernollet 1983; Owusu et al, 2015). In early seeds, it can be found vicilin in major quantities, because its synthesis begins during the first phases of the seedling. Instead, in mature seeds, legumin is found in major quantities, because the rate and the extent of its biosynthesis are higher. Legumin is greater than vicilin, being of about 400.000 daltons, while vicilin is about 200.000 dalton (Donald Boulter,1983; Kumari et al., 2021). Legumin has six heterogeneous pairs of subunits, where each couple is made by a basic portion of 20.000 daltons and by an acidic component of 40.000 daltons (Rod Casey 1982; Owusu et al., 2015). It was hypothesized that most of the acidic components are placed upon the surface, while the basic subunits are situated and constitute the hydrophobic core. Vicilin is thought to have the same structure, but this protein is less studied than legumin (Owusu et al., 2015). Compared to the vicilin, legumin is less soluble in saline solutions, has more difficulty coagulating at 95°C, and has a larger quantity of nitrogen and sulphur. Legumin preserves its natural structure in the pH range between 7 to 9 and undergoes dissociation at extreme pH conditions. Vicilin was shown to be soluble at about pH 5, contrarily to legumin. Vicilin has also a large amount of covalently linked sugar (Rod Casey,1982). It was shown that the amino acids composition of highly purified pea protein is quite different. Legumin has a larger amount of sulphur-containing amino acids and arginine, while vicilin is richer in isoleucine, leucine, phenylalanine and lysine (Owusu et al., 2015; Kumari et al., 2021). It is thought that increasing the ratio of legumin/vicilin can improve the nutritional property of pea proteins and their derivates (Jacques Gueguen et al., 1984). In *Pisum*

Sativum this ratio was evaluated to vary from 0.5 to 1.7. There is also a water-soluble pea protein fraction, the albumins, which have not been analysed as well as globulins. The albumin percentage results in the range between 12% and 38% (J. Gueguen et al., 1988). It was shown that the ratio in eight round-seeded *Pisum sativum* is about 1:3. There thousands of proteins that were classified as albumins. The albumin class contains enzymic and metabolic proteins. They were individuated into two major types of albumin, respectively of 8.000 and 22.000 daltons, which constitute about 34% of the total albumin amount. The albumins are characterized by a more balanced amino acids composition than globulin fraction, mainly for sulphurous amino-acids (Dr. S. Gwiazda et al., 1980). Other these two classes, albumins and globulins, there are proteins present in small quantities, but very important for processing and utilization of pea seeds. Among them, there are lipoxygenase, trypsin inhibitor and lectin (Owusu et al., 2015; Kumari et al., 2021). Generally speaking lipoxygenase in raw legumes is connected with the development of unpleasant flavour during storage, also in legumes with quite low-fat content, such as peas (J.J. Rackis 1979). Several legumes contain proteins that can inhibit the proteolytic activity of certain enzymes involved in indigestion. It was shown that dry peas contain trypsin inhibitor (Eva Guillamòn et al., 2008). Finally, lectins can be found in several legumes, and they are responsible for the agglutinating of red blood cells. Lectins are present in peas, but their effect is not toxic (I. E. Liener 1983).

1.2.3Technology of production

Pea Protein can be produced in three different forms: pea flour, pea protein concentrates and pea protein isolates. The flour can be prepared by dry milling of dehulled peas. Pea concentrate can be produced by the acid leaching method or through other dry separation technology. Pea isolate can be prepared by wet processing methods (Kumari et al., 2021).

Starches and proteins contained in non-oil seeds could be separated by dry milling and air classification. By this method, flours with different size and density are obtained. When these flours undergo air classification, proteins (fine portion) are separated from starches (grosser fraction) (Owusu et al., 2015). At the beginning of this dry process, peas are milled in a fine flour: whereas starch granules remain quite intact, the protein matrix is crushed into very small particles. The resultant flour is the air classified in an airstream with spiral flux. The resulting (25% of the total feed) fine fraction contains about 75% of the total protein, while the remaining coarser fraction (75% of total feed) contains most of the starch granules. The separation is possible because of the difference in terms of size and density between starch and protein. These resulting two fractions are then centrifugated, and then each of them is carried into its specific process line. The yield of this process

can be affected by several factors, some of which linked with pea variety and composition, others with process variables (Prof. Dr. Friedrich Meuser et al., 1995; Kumari et al., 2021). Pea protein concentrate and isolate fractions can be prepared by wet processing. The protein can be separated principally by solubilization followed by isoelectric precipitation. Other processes involve "salting out" (J.R. Bacon, 1990), "hydrophobic out" (E. D. Murray et al., 1980; Xiang Dong Sun et al., 2012) and ultrafiltration (Louis-Philippe Des Marchais et al., 2011). In isoelectric precipitation, the peas are first milled, then solubilized either in water, either in alkali or acid conditions. The following centrifugation removes the insoluble fractions. The solubilized proteins can be precipitated at their isoelectric point. The precipitate is separated by centrifugation. The resulting curd is then either just dried or neutralized first and then dried. Several factors can influence the yield of this process, such as solubilizing solvent, pH of solubilization and precipitation conditions (Vose J.R. et al.,1976.). It was suggested that an average particle size within the range of 100 µm and 150 µm is optimal for the solubilization of protein (Gueguen et al., 1988). The ultrafiltration process starts by solubilizing the protein. Then, the solution containing the solubilized protein is sent to a certain number of membranes. The retentate, rich in protein, may undergo a spray dry process to get the protein isolate. The yields for this kind of process is analogue to that of isoelectric precipitation, but the scale-up to the industrial stage is hindered by technical problems. Instead, ultrafiltered isolate protein contains a high lipid concentration (Vose J.R et al., 1976; Owusu et al., 2015). The "hydrophobic-out" process involves the extraction of protein in a salt solution having at least 0.2 ionic strength. The resulting solution is then centrifugated. The ionic strength of the extract is then adjusted by dilution with water. The proteins precipitate in micelles. In the first stage, the "salting-out" process starts with the extraction of proteins in a salt solution with high ionic strength. The salt extract undergoes fractional salting-out employing ammonium sulphate. This stage involves two steps: In the first, ammonium sulphate is added at 35% of saturation, to obtain the precipitation of certain proteins along with nucleic acids. The system is then centrifugated, and in the second step, ammonium sulphate is added to reach 65-100% of saturation. This way, the remaining protein is "salted-out". This method allows to separate the principal proteins from secondary ones, and also protein from nucleic acids (E. D. Murray et al., 1980; Kumari et al., 2021; Stone et al., 2015)

1.2.4 Nutritional properties

The nutritional pea protein properties depend upon the number of essential amino acids they contain, other than their bioavailability for the organism that must adsorb them. Pea proteins are a good source for essential amino acids, but they are lacking in sulphur-containing amino acids, methionine and

cystine (WHO, "Energy and Protein Requirements," World Health Organization Technical Report Series 724, 1985). It was suggested (G. Sarwar, 1984) that the digestibility of the single amino acids may be less efficient than that of the entire protein derived from the same source. When enriched with tryptophan, methionine and cystine, pea proteins are a valid alternative to other protein sources. The digestibility of pea protein lies in the range between 83% and 93%. It was suggested that the digestibility of protein in flours and isolate is greater than in concentrate (R.S. Bhattyet, 1984; Stone et al., 2015; Kumari et al., 2021) Other authors demonstrated that isolate protein can be hydrolysed better than concentrate from whose isolate derive. This can be because in isolate there is a higher proportion of globulins. Globulins can be hydrolysed with a rate twice greater than pea albumins by pepsin. The phytic acid present in peas could affect negatively the digestibility of pea protein (E. Carnovale et al., 1988). Heat treatment can improve the nutritional properties of pea protein-containing products and their texture. Gelation phaenomena induced by heat treatment is favoured both by globulins and albumins (Xiang Dong Sun 2010). It was demonstrated that hydrolysed pea protein can reduce starch digestibility (Nataly Lopez-Baron, 2018). Flatulence is caused by several legumes, including peas, and this could cause discomfort in people. Part of this flatulence is induced by some indigestible oligosaccharides, such as raffinose, stachyose, and verbascose (S.E Fleming and R.D. Reichert, 1983; Kumari et al., 2021). Pea proteins isolate produced by wet processes can contain a smaller concentration of these α-galactosides, because a discrete amount of the carbohydrates linked to the protein are removed in the effluent (C. Martinez-Villaluenga, et al., 2006).

1.2.5 Functional properties

Pea proteins have some functional properties very interesting for the food industry, and these make them a valid alternative both as a protein source and as a functional ingredient for protein products. Solubility is one of the most important variables for food engineering because soluble proteins can be easier processed. Protein solubility is highly influenced by the pH of the solution in which they are put. Pea proteins were shown to be highly soluble at a very acidic pH (pH 2), and the solubility decrease very quickly as pH increases to the range of minimum solubility, i.e. pH 4 to 6. Pea protein can be well-solubilized solutions with alkaline pH. It was shown that the real solubility of pea protein materials is highly variable in the pH range from 5 to 9. Instead, it was proved that at pH 7, vicilin is more soluble than legumin (H. Koyoro and J.R. Powers, 1987). Protein denaturation can lower solubility. It has also been shown that at a pH near to 7, air- classified concentrates are less soluble than flours. This can be due to scarce dispersibility or to the denaturation that occurs during the process. Another important property is the protein water-binding capacity (Stone et al., 2015). This can be a useful characteristic in food products where there is not enough water to dissolve protein,

but the ability of proteins to be hydrated can imparts structure and rheological properties. Such foods are sausages, custard or doughs. It was shown that pea protein can absorb water from 1 to 3.3 times their mass (F. W. Sosulki,1987). A further characteristic of proteins is their emulsifying power, i.e. the ability to stabilize an emulsion of oil and water. There are several ways to define and measure emulsifying properties, and for this reason, it is very difficult to make comparison among different substances (John E. Kinsella, 1976). However, it was shown that pea isolate has an emulsifying power analogue to that of soybean isolate protein (Vose J.R.,1976; Owusu et al., 2015).

The foaming property of a dispersion protein pertains to its ability to form a stable form when air is blown in it. It is measured by evaluating the maximum volume increase attained by a protein dispersion after air was beaten in. Instead, foam stability is the capacity of foam to detain the air blown in. It was shown that the foaming properties of pea proteins flours are weaker than that of other legume flours. Foam stability of pea protein flours is also very low Pea protein concentrate obtained by air-classification process showed good foaming property, but the resulting foams are not very stable (F. Sosulski and C.G. Youngs, 1979). Several studies have shown that pea protein isolate can lead to a quite good volume of foam, which is not very stable ((F. W. Sosulki and AR. McCurdy, 1987)), while it was demonstrated that spray-dried pea protein isolate can produce foam volumes even greater than that produced by soy protein isolate (Vose J.R.,1976). However, there is no consensus about the last assertion. The acylation of pea protein isolate can improve the foaming ability (E.A. Johnson and C.J. Brekke, 1983). One of the most important property that must be analysed is the flavour of pea protein-containing product. Pea flours flavour was described as bitter, metallic and astringent. It was suggested that soy saponin It is the reason for the off-flavour of pea proteins flours. Soysaponin I is found in a large amount in protein-rich fraction outgoing from the air classification process, but it can be removed by wet processes. Steaming can reduce the saponin content (K. R. Price, 1985; Owusu et al., 2015). It was also suggested that a bitter taste is due to the lipid oxidation products. Lipoxygenases and bound unsaturated fatty acids are contained in pea seeds. So, the lipid oxidation catalysed by enzymes is very probable. The oxidation products, such as esters, ketones, aldehydes can cause pea protein bitterness (Erickson M.C.1997). Anyway, it was noted that pea protein isolates prepared by ultrafiltration and isoelectric precipitation can result bland in flavour. The colour of the pea protein proteins is important when they must be included in the final products (Kumari et al., 2021; Stone et al., 2015). A colour next to white is preferable because it does not alter the visual perspective of the consumer. Pea flour colour is next to creamy yellow colour. Pea protein isolates colour is quite beige, in the function of the preparation method (F. Sosulski and C.G. Youngs,1979; Mehle et al., 2020). Generally, the functional properties can depend on the preparation method. It was shown that sodium proteinate isolate is more “functional” than pea protein produced

by isoelectric precipitation, while air-classified pea protein shown less functionality than isolates. This lesser functionality is more accentuated for foaming and emulsifying properties. Ultrafiltered pea proteins exhibit a higher solubility than acid-precipitated proteins (Owusu et al., 2015). In fact, the pH at which extraction and precipitation are carried on can affect both solubility and flow properties. For example, it was found that the viscosity of a protein in water dispersion extracted at pH 7 is lower than that of the same dispersion with protein prepared at pH 9 (70). Isolates prepared with the acid extraction method is richer in cysteine and methionine, and this can improve foaming properties (Barry G. Swanson et al., 1987). Heat treatment of pea protein prepared by air classification can lead to the decreasing of solubility and emulsifying capacity, increasing water-holding power and variable effects on oil absorption and foaming functional characteristics (A.V. Megha and D.R. Grant, 1986). It was asserted that drum drying can decrease solubility and increase emulsifying properties compared to spray drying (A. K. Sumner, 1981). They are been found different results about the dependency of pea protein functional properties on the processing method. This can be due to the different types of peas, kinds of proteins and different processing conditions (El-Sayed M. et al., 1996; Kumari et al., 2021).

1.2.6 Pea Protein uses

Nowadays, pea proteins are not so utilized as other vegetable proteins. The major trends in pea proteins utilization are in the food industry, especially in cereal and bakery products, meat and milk products, protein drinks (Kumari et al., 2021). Pea proteins flour is added to wheat ones to enrich protein content. By substituting almost 20% of wheat flours with pea protein flours it is possible to realize a good protein bread. However, till this moment, the bred produced in this way can lose increasing volume capacity and can have poor crumb content (Owusu et al., 2015). It was demonstrated that by adding a certain amount of $KBrO_3$ for 5% of pea flour and adding a lesser amount of water this effect can be minimized (S.E. Fleming et al.,1977; Mehle et al., 2020). A similar effect can be produced by adding 2 % of gluten and 1% dough conditioner to wheat flour enriched with 15% of pea protein. However, also with these precautions, products can have scarce sensory properties (F. Sosulski and C.G. Youngs 1979; Mehle et al., 2020). Similarly, to bakery products, pasta realized entirely with wheat flour does not contain a complete protein contribution. For this reason, it is desirable to enrich this kind of product to give the right protein supply. Pea protein-enriched pasta lacks flavour compared to all wheat products, but this inconvenience can be minimized by cooking the pea protein before adding it to the flours. Pea protein-fortified pasta has similar characteristics to that prepared only with wheat flours (J. A. Repetsky et al., 1981; Owusu et al., 2015). Another application in which pea protein can be used are biscuits. In some processing, they

have substituted milk protein for pea protein in the production of baking powder biscuits (E.H. Eneche, 1999). It was showed that the main characteristics, such as appearance, colour and textural properties of pea protein-containing biscuits are like those that do not contain them. Anyway, it remains the same problem about the flavour, but steam heating flours added before processing the dough can aid to minimize flavour disappointment (Mehle et al., 2020). It was observed that the viscosity of batter added with pea protein decreases with pea protein concentration (Owusu et al., 2015; Kumari et al, 2021).

Bibliography

J.R. Bacon, T.R. Noel, N. Lambert (1990), *Preparation of transparent pea protein gels: a comparison of isolation procedures*, International Journal of Food Science and Technology 25,527-537

Behall, K. M., & Hallfrisch, J. (2002). Plasma glucose and insulin reduction after consumption of breads varying in amylose content. European Journal of Clinical Nutrition, 56, 913–920.

Diane F. Birt, Terri Boylston, Suzanne Hendrich, Jay-Lin Jane, James Hollis, Li Li, John McClelland Samuel Moore, Gregory J. Phillips, Matthew Rowling, Kevin Schalinske, M. Paul Scott, and Elizabeth M. Whitley (2013), Resistant Starch: Promise for Improving Human Health, American Society for Nutrition. *Adv. Nutr*. 4: 587–601.

Donald Boulter (1983), *Protein composition of grains of the* Leguminosae, Qual Plant Plant Foods Hum Nutr 32 247-252

Miroljub B. Barać, Mirjana B. Pešić, Slađana P. Stanojević, Aleksandar Ž. Kostić and Slavica B. Čabrilo (2015), Techno-functional properties of pea (pisum sativum) protein isolates- a review, *APTEFF*, 46, 1-269

Brown, I. L., McNaught, K. J., Ganly, R. N., Conway, P. L., Evans, A. J., Topping, D. L. (1996). Probiotic compositions. Intl. Patent WO 96/08261/A1. Issued March 21,. Univ. New South Wales, Burns Philip and Co., Limited, Burns Philip Res. and Dev. Pty., Mauri Lab. Pty. Ltd., Commw. Sci. Ind. Res. Org., *Arnotts Biscuits Ltd., Good man Fielder Ingredients Li, Goodman Fielder Ltd.*

Brown, M. A., Storlien, L. H., & Brown, I. L. (2003). Cooking attenuates the ability of high amylose meals to reduce plasma insulin concentrations in rats. British Journal of Nutrition, 90, 823–827.

Buttriss, J. L., & Stokes, C. S. (2008). Dietary fibre and health: An overview. British Nutrition Foundation, Nutrition Bulletin, 33, 186–200.

Rod Casey (1982), *The genetics of pea seed storage proteins*, Qual. Plant. Plant. Foods Hum. Nutr., *31,* 281

C. Martinez-Villaluenga, J. Frias, C. Vidal-Valverde (2006), *Functional lupin seeds (*Lupinus albus L., Lupinus luteus L.*)*, Food Chemistry 98 291-299

E. D. Murray, C. D. Myers, and L. D. Barker, (1980) Process for isolation of proteins using food grade salt solutions at specified pH and ionic strength, Can. Pat. No. 1028552, *United States Patent*

Xiang Dong Sun, Susan D. Arntfield (2012), Molecular forces involved in heat-induced pea protein gelation: effects of various reagents on the rheological properties of salt-extracted pea protein gels, *Food Hydrocolloids* 28, 325-332

Charalampopoulos, D., Wang, R., Pandiella, S. S., & Webb, C. (2002). Application of cereals and cereal components in functional foods: A review. *International Journal of Food Microbiology*, 79, 131–141.

U.D. Chavan, D.B. McKenzie., F. Shahidi (2001), Functional properties of protein isolates from beach pea (Lathyrus maritimus L.), *Food Chemistry* 177-187

Commission of the European Communities (2008). Draft commission directive: Amending directive 90/496/EEC. <http://www.food.gov.uk/multimedia/pdfs/ consultation/cwd>.

Louis-Philippe Des Marchais, Mathieu Foisy, Samuel Mercier, Sébastien Villeneuve, Martin Mondor (2011), Bread-making potential of pea protein isolate produced by a novel ultrafiltration/diafiltration process *Procedia Food Science* 1 1425-1430)

E.H. Eneche (1999), Biscuit-making potential of millet/pigeon pea flour blends *Plant Foods for Human Nutrition* 54**,** 21–27

Englyst, K. N., & Englyst, H. N. (2005). Carbohydrate bioavailability. *British Journal of Nutrition*, 94, 1–11.

Faraj, A., Vasanthan, T., & Hoover, R. (2004). The effect of extrusion cooking on resistant starch formation in waxy and regular barley flours, *Food Research International*, 37, 517–525.

Foschia Martina, Paola Beraldo and Donatella Peressini (2017), Evaluation of the physicochemical properties of gluten-free pasta enriched with resistant starch, *J Sci Food Agric* **97**: 572–577

S.E. Fleming and F.W. Sosulski (1977), Nutritive value of bread fortified with concentrated plant proteins and lysine, *Cereal Chem*, 54 (6); 1238-1248

Jacques Gueguen, Ahn T. Vu, François Schaeffer (1984), Large-scale purification and characterisation of pea globulins, *Journal of Science of Food and Agriculture*, Volume 35, Issue 9

E.A. Johnson and C.J. Brekke (1983) Functional properties of acylated pea protein isolates, 722- *Journal of Food Science*,Volume 48 (79831)

J. Gueguen, J. Barbot (1988), Quantitative and qualitative variability of pea (Pisum Sativum L.) protein composition, *Journal of the Science of Food and Agriculture*, Volume 42, Issue 3.

Eva Guillamòn, Mercedes M- Pedrosa, Carmen Burbano, Carmen Cuadrado, Maria de Cortes Sanchez, Mercedes Muzquiz (2008), The trypsin inhibitors present in seed of different grain legume species and cultivar, *Food Chemistry* 107 68-74

Dr. S. Gwiazda, Dr. sc.K.D. Schwenke, Prof. Dr. A. Rutkowski (1980), Isolation and partial characterization of proteins form pea (Pisum sativum L.) *Food Nahrung* Volume 24, Issue 10.

Haralampu, S. G. (2000). Resistant starch: A review of the physical properties and biological impact of RS3. *Carbohydrate Polymers*, 41, 285–292.

Hernández, O., Emaldi, U., & Tovar, J. (2008), In vitro digestibility of edible films from various starch sources, *Carbohydrate Polymers*, 71, 648–655.

Higgins, J. A. (2004). Resistant starch: Metabolic effects and potential health benefits, *Journal of the AOAC International*, 87(3), 761–768.

John E. Kinsella & Nicholas Melachouris (1976) Functional properties of proteins in foods: A survey, *C R C Critical Reviews in Food Science and Nutrition*, 7:3, 219-280

H. Koyoro and J.R. Powers (1987), Functional properties of Pea Globulin Fractions, *Cereal Chem*. 64(2), 97-101.

Nataly Lopez-Baron, Domenico Sagnelli, Andreas Blennow, Mette Holse, Jun Gao, Lasse Saaby, Anette Müllertz, Birthe Jespersen, Thava Vasanthan (2018), Hydrolyzed pea proteins mitigate in vitro wheat starch digestibility, *Food Hydrocolloids* 79 117-1216.

Higgins, J. A., Higbee, D. R., Donahoo, W. T., Brown, I. L., Bell, M. L., & Bessesen, D. H. (2004). Resistant starch consumption promotes lipid oxidation, *Nutrition & Metabolism*, 1, 8.

Helmut F. Erbersdobler (1989), Protein Reactions during Food Processing and Storage - Their Relevance to Human Nutrition, Somogyi JC, MUller HR (eds*): Nutritional Impact of Food Processing. Bibl Nutr Dieta*. Basel, Karger, N 043, pp 140-155

Keenan, M. J., Zhou, J., Mccutcheon, K. L., Raggio, A. M., Bateman, H. G., Todd, E., et al. (2006). Effects of resistant starch, a non-digestible fermentable fiber, on reducing body fat, *Obesity*, 14, 1523–1534.

Kim, M. J., Choi, S. J., Shin, S. I., Sohn, M. R., Lee, C. J., Kim, Y., et al. (2008). Resistant glutarate starch from adlay: Preparation and properties, *Carbohydrate Polymers*, 74, 787–796.

Korus J, Witczak M, Ziobro R, Juszczak L. (2009), The impact of resistant starch on characteristics of gluten-free dough and bread. *Food Hydrocoll*; 23:988–95.

Tapasya Kumari, Sankar Chandra Deka (2021), Potential health benefits of garden pea seeds and pods:A review, *Legume Science*; e82.

Morais, M. B., Feste, A., Miller, R. G., & Lifichitz, C. H. (1996). Effect of resistant starch and digestible starch on intestinal absorption of calcium, iron and zinc in infant pigs, *Paediatric Research*, 39(5), 872–876.

Hannah Mehle, Laurianne Paravisini and Devin G. Peterson (2020), Impact of temperature and water activity on the aroma composition and flavor stability of pea (Pisum sativum) protein isolates during storage, *The Royal Society of Chemistry, Food Function.*

Mermelstein, N. H. (2009). Analyzing for resistant starch, *Food Technology*, 4, 80–84.

Prof. Dr. Friedrich Meuser, Norbert Pahne, Matthias Moller (1995), Extraction of high amylose starch from Wrinkled Peas, *swrch/starke* 47 Nr. 2. S. 56-6

Nugent, A. P. (2005). Health properties of resistant starch. British Nutrition Foundation, *Nutrition Bulletin*, 30, 27–54.

Y. J. Owusu-Ansah a & S. M. McCurdy (2015), Pea proteins: A review of chemistry, technology of production, and utilization, *Food Reviews International*.

Raben, A., Andersen, K., & Karberg, M. A. (1997). Acetylation of or B-cyclodesetrin addition to potato starch: Beneficial effect on glucose metabolism and appetite sensations, *American Journal of Clinical Nutrition*, 66, 304–314.

Raben, A., Tagliabue, A., Christensen, N. J., Madsn, J., Holst, J. J., & Astrup, A. (1994). Resistant starch: The effect on postprandial glycemia, hormonal response and satiety, *American Journal of Clinical Nutrition*, 60, 544–551.

Donatella Peressini, Alessandro Sensidoni (2009), Effect of soluble dietary fibre addition on rheological and breadmaking properties of wheat doughs, *Journal of Cereal Science* 49, 190–201

K. R. Price, N. M. Griffiths, C. L. Curl & G. R. Fenwick (1985), Undesirable Sensory Properties of the Dried Pea (Pisum sativum) The Role of Saponins, *Food Chemistry* 17 105-115)

R. D. Reichert and S. L. MacKenzie (1982), Composition of Peas (Pisum sativum) Varying Widely in Protein Content, *J. Agric. Food Chem*., 30, 312.

Riva M, Fessas D, Schiraldi A. (2000), Starch retrogradation in cooked pasta and rice. *Cereal Chem*. 77:433–8.

El-Sayed M. Abdel, Frank W. Sosulski1, A. Adel Y. Shehata2 & Mohamed M. Youssef (1996), Nutritional, functional and sensory properties of wheat, rice and fababean blends texturized by drum drying, *International Journal of Food Science and Technology*, 31, 257–266

Sajilata, M. G., Singhal, R. S., & Kulkarni, P. R. (2006). Resistant starch – A review. Comprehensive Reviews,*Food Science and Food Safety*, 5, 1–17.

G. Sarwar (1984), Available Amino Acid Score for evaluating Protein Quality for Foods, *J. Assoc. Off. Anal. Chem.*, 67, 623.

G. Sarwar Gilani, Chao Wu Xiao and Kevin A. Cockell (2012), Impact of Antinutritional Factors in Food Proteins on the Digestibility of Protein and the Bioavailability of Amino Acids and on Protein Quality, *British Journal of Nutrition*, 108, S315–S332

Sharma, A., Yadav, B. S., & Ritika (2008). Resistant starch: Physiological roles and food applications, *Food Reviews International*, 24, 193–234.

Carsten Schulz, Michael Wickert, Claudia Kijora, Johnny Ogunji & Bernhard Rennert (2007) Evaluation of pea protein isolate as alternative protein source in diets for juvenile tilapia (Oreochromis niloticus), *Aquaculture Research*, 38, 537^545

F. W. Sosulki and AR. McCurdy (1987), Functionality of flours, protein fractions and isolates from field peas and faba bean, 1012-*Journal Of Food Science*-Volume 52, No. 4.

F. Sosulski and C.G. Youngs (March 1979), Yield and functional properties of air-classified protein and starch fractions from eight legume flours, *J. Am. Oil Chemists' Soc*., (vol. 56).

Andrea K. Stone a, Anna Karalash a, Robert T. Tyler a, Thomas D.Warkentin b, Michael T. Nickerson, (2015), Functional attributes of pea protein isolates prepared using different extraction methods and cultivars, *Food Research International* 76 (2015) 31–38

Tapsell, L. C. (2004). Diet and metabolic syndrome: Where does resistant starch fit in? *Journal of the Association of Analytical Chemists International*, 87(3), 756–760.

Tharanathan, R. N. (2002). Food-derived carbohydrates: Structural complexity and functional diversity, *Critical Reviews in Biotechnology*, 22(1), 65–84.

Thompson, D. B. (2000). On the non-random nature of amylopectin branching, *Carbohydrate Polymers*, 43, 223–239.

Truwell, A. S. (1992). Glycemic index of foods, *European Journal of Clinical Nutrition*, 46(2), 91–101.

Vose J.R., Basterrechea M.J., Gorin P.A.J., Finlayson A.J. (Nov 1976),., Air classification of field peas and horsebean flours: chemical studies of starch and protein fractions, *Cereal-Chemistry* (USA). v. 53(6) p. 928-936.

Yue, P., & Waring, S. (1998). Resistant starch in food applications, *Cereal Foods World*, 43(9), 690–695.

Chapter 2
Materials and Methods

This work aims to study interfacial characteristics of complex mixtures, composed of resistant starch and vegetable proteins. In particular, three different resistant starches were used, described in the following section. As far as vegetable proteins are concerned, peas were used. The experimental work was divided into two phases: the first was focused on the bulk properties of single materials, which were analysed using rheometric procedures. From this kind of characterization, the behaviour of materials as a function of concentration, stress, frequency and temperature was investigated. The second part was focused on interfacial properties, both single materials and mixtures. The investigation was performed both in static and dynamic conditions. The results of the rheological bulk analysis were used also to design the procedure of interfacial investigation, as will be explained in the following sections. For this reason, this chapter is divided into three sections: the first being concerned with generic information about the material utilized, the second with bulk rheological analysis, the third with an interfacial one. The last two sections each contain a subsection relative to the preparation of samples, one pertinent to the kind of test performed, and one in which the method for the data interpretation are described.

2.1 Materials

Three different resistant starches (RS), Hi-Maize, Hylon VII and Amioca, and Pea Protein isolate (PP) and their mixtures were analysed. All the materials were kindly provided by INGREDION® (Westchester, Illinois, USA) and in Table 2.1 the materials IDs are reported.

Materials	Materials ID
Hi-Maize	M
Hylon VII	H
Amioca	A
Pea Protein	PP

Table 2.1: ID of materials utilized

PP isolate powder utilized in this work has a purity of 80%. Pea proteins are principally globulin (at least 50%), whose molecular weight varies in the range of 300-310 kDa (Franco et al.1999) and are quite soluble at neutral pH (Lam et al.2018). The remaining percentage is constituted of albumins, and other insoluble proteins (Leterme et al.1990). Pea storage proteins are constituted of two main fractions: the 11S (legumin) and 7S (vicilin) subunits. The legumin consists of a hexameric protein, with a molecular weight in the range 350–400 kDa; vicilin is trimeric and its molecular weight is about 150 kDa (Makri et al., 2005; Klassen & Nickerson, 2012; Mession, Assifaoui, Cayot, & Saurel, 2012).

The resistant starch powders utilized have a different ratio of amylose and amylopectin. Amylose and amylopectin are both polysaccharides, with the molecular formula $(C_6H_{12}O_6)_n$ and molecular weight of $(180,6)_n$. The difference between the two species is in their chemical structure: amylose has a short linear chain, while amylopectin has a very branched structure (J.Jane et al. 1999). Amylopectin average molecular weight is MDa magnitude order, while amylose is kDa (Chen Li et al., 2020). They appear both as white powders. Hylon VII has an amylose content of about 70%, while in the remaining percentage should be present amylopectin, and also a little part of other fibres. Amioca consists almost of pure amylopectin, which is present at 98% w/w. Maize has an intermediate composition between Hylon VII and Amioca, with an amylose content of 56%, while the rest is composed of amylopectin and other fibre (Ingredion technical documents). These three starchy powders were chosen to investigate the behaviour of resistant starch in the function of the content of their major components, namely amylose and amylopectin. In fact, amioca represent an extreme, being almost pure amylopectin; hylon represent the other extreme, i.e. a resistant starch powder rich in amylose. Hi-maize starch has a composition similar to hylon, but a major percentage of amylopectin. So, its behaviour was expected somewhat intermediate between amioca and hylon.

2.2 Bulk characterization

Bulk characterization was performed to understand the rheological behaviour of the materials utilized, as a function of temperature, concentration, stress and oscillation frequency.

It was performed by strain controller rheometer (ARES-RFS, TA Instrument, USA), with a Peltier control system. For all the performed tests, parallel plate geometry was used, with a diameter of 40 mm. The gap used for all the samples was 2.0 mm ± 0.2 mm. All tests here described were repeated twice.

Two types of tests were performed: time cure test and frequency sweep test. The first type of test was performed on samples prepared only solubilizing the ingredients at room temperature and the second

type on pregelatinized samples. Preliminary time sweep tests on suspensions at various temperatures (25°C, 40°C, 60°C) were performed, to investigate if gravity settling phaenomena occur, especially at low concentrations. Considering that for all time sweep tests dynamic moduli, G' and G'', were constant in time, it was concluded that in test conditions does not occur gravity settling.

The time cure tests were performed in the range between 10°C to 100°C by using a heating rate of 1°C/min and a frequency of 1 Hz. Sample drying was avoided by surrounding it with silicon oil. The tests were performed in linear conditions previously determined by time and strain sweep tests on samples prepared at room temperature. Although cooking conditions are different in terms of ramp temperature and then viscoelastic functions evolution, time cure tests are important for a preliminary evaluation of materials evolution from a rheological and textural point of view and kinetic parameters evolution. In fact, from time cure tests dynamic moduli, G' and G", are derived and they are able to give us information about the principal phenome occurring during heating, like the onset of gelatinization temperature and ending of the kinetics and the structuring process (Baldino et al.2018).

On pregelatinized tests frequency sweep in linear conditions were performed at T=25°C. The linear conditions were evaluated by a stress sweep test at the same temperature. The frequency was varied in the range between 0.1 to 10 Hz to obtain the viscoelastic functions versus frequency. From the interpretation of data, information about structure was obtained, like the consistency and texture of materials after thermal treatment.

Finally, comparing results derived both from bulk investigation and interfacial analysis, two mixtures constituted by RS/PP systems were prepared and analysed during thermal treatment. Time cure tests were performed on each mixture in the linear region, in order to understand the evolution of the system during thermal treatment. The same strain-controlled rheometer was used (Ares TA instrument). Parallel plate geometry was used for all the performed tests, with a diameter of 40 mm. The gap used for all the samples was 2.0 mm ± 0.2 mm. All the tests described here were repeated twice. The range of temperature analysed was 20-100 °C, with a ramp of 1°C/min and at 1Hz frequency. From the time cure data, the onset and peak temperatures were evaluated according to the same procedure described above (Baldino et al., 2018). On the same mixtures, a cooking process was performed: samples of each system were placed in an oven (BINDER, GmBh) at 180 °C for an hour. After cooking, samples were sectioned to observe the internal section. No baking powder was used for the formulation of cooked mixtures.

2.2.2 Samples preparation

Samples constituted only of a single RS and water or by water and PPs were analysed in the range between 5 and 50% w/w. Specifically speaking, between 5 and 20 %w/w the percentage was increased by 5%w/w, while between 20 and 50%w /w every 10. On solutions prepared in this way, time cure tests were performed. Dry RS powder was mixed with the right amount of distilled water. Solutions were agitated on a magnetic stirrer (AREX Heating Magnetic Stirrer, Velp Scientifica, Italy) for 30 minutes at room temperature, preventing in this way the gravity settling of starch suspensions. . Sample drying was avoided by surrounding it with silicon oil. The same procedure was used for the samples prepared with PPs before performing rheometric analysis.

For dynamic frequency sweep tests, it was necessary to pregelatinize the samples. Then solutions of RS or PPs were kept under stirring for 1 h at T=120°C in an oil bath. The temperature chosen to pregelatinize the starches is in agreement with the complex modulus evolution during the temperature sweep test. Particularly, it was set at 120°C because, from the analysis of time cure data, it was possible to conclude that all the phenomena are finished at this temperature. In particular, this is evident by the decrease after the peak of G* at high temperature. This choice was supported also by comparing the onset and the peak temperatures for similar systems found in the literature (Fengwei Xie at al. 2009) In this way, it was possible to obtain the swelling of the starch and the gel structure formation. After 1 h of stirring, the solutions were cooled down at room temperature in a cold-water bath at 20 °C and after a rest time of 15 minutes (that is, the time it takes to let the system cool down), frequency sweep tests were performed at 25°C after evaluation of the linear conditions. For all the ingredients solutions were prepared at a different concentration ranging between 5 and 30% w/w (5, 10, 20 and 30% w/w).

After analysing single component solution bulk and interfacial behaviour, and investigating RS/PP mixtures interfacial properties, bulk and interfacial results were matched together to study bulk properties of RS/PP systems. Two different mixtures were prepared; in each one, 50% dry powder and 50% water were present. For these mixtures, the same materials were used. The dry powder composition is summarised below:

1. Mixture A: dry powder with a composition of 20% PP and 80% RS. Of RS starch powder, 70% was constituted of H and 30% of A; on dry powder basis, the percentage of resistant starch (amylose and B-type amylopectin present in Hylon) is 56%, while the percentage of normal starch, namely amylopectin in Amioca, is 24%. So, in this mixture the resistant starch percentage is more than double the normal.
2. Mixture B: dry powder with a composition of 20% PP and 80% RS. Of RS starch powder, 70% was constituted of A and 30% of H; on a dry powder basis, the normal starch percentage

is 56%, while resistant starch is 24%, including both amylose and B-amylopectin. Specifically, on a dry basis, the amylose percentage is 15%, while B-type amylopectin is 7.2%; so, in this mixture resistant starch is present for less than half of the normal one.

Mixtures were prepared by mixing the dry powder with water using a magnetic stirrer (AREX Heating Magnetic Stirrer, Velp Scientifica, Italy) for 30 minutes at room temperature, to guarantee the homogenization of samples.

2.2.3 Rheological data interpretation

From frequency sweep data about storage and loss moduli are obtained. The data must be then interpreted through constitutive models. Generally speaking, classic rheological models of linear viscoelasticity are based upon the superposition principle, for which elastic and viscous contributes can be linearly combined. An alternative to the superposition principle is represented by the intermediacy principle, for which the material behaviour is not a linear combination between elastic and viscous constitutive equations but is "intermediate" between them. For this purpose, the fractional analysis must be used. The choice between these two approaches is determined by the rheological data trend obtained from the experimental analysis.

2.2.3.1 Time cure tests data interpretation

Time cure data were interpreted according to the procedure found in the literature and used for analogous systems (Baldino et al. 2018). In this way, two important temperatures can be evaluated: the onset temperature, at which dynamic moduli suddenly increase as a consequence of the gelatinization, and the peak temperature, at which dynamic moduli assume their maximum value. This trend is physically related to the end of the gelatinization mechanism. Both temperatures are important to understand the behaviour of materials during thermal treatment (Baldino et al. 2018). From Time Cure, G' and G'' were determined as the function of temperature. As it can be seen in Fig. 2.1 the T_o can be obtained from the knee point of the G' curve. Considering the linear approximation of the liquid-like part of the interpolated curve, and the linear approximation of the increase of G', owing to the gelatinization, the T_o can be evaluated at the intersection of the two straight lines. T_o is an interesting parameter because it is related both to the gelatinization phenomena and therefore at the change of the mechanical behaviour, from liquid-like to solid-like (Baldino et al. 2018). Thus, T_o can be considered as the transition temperature.

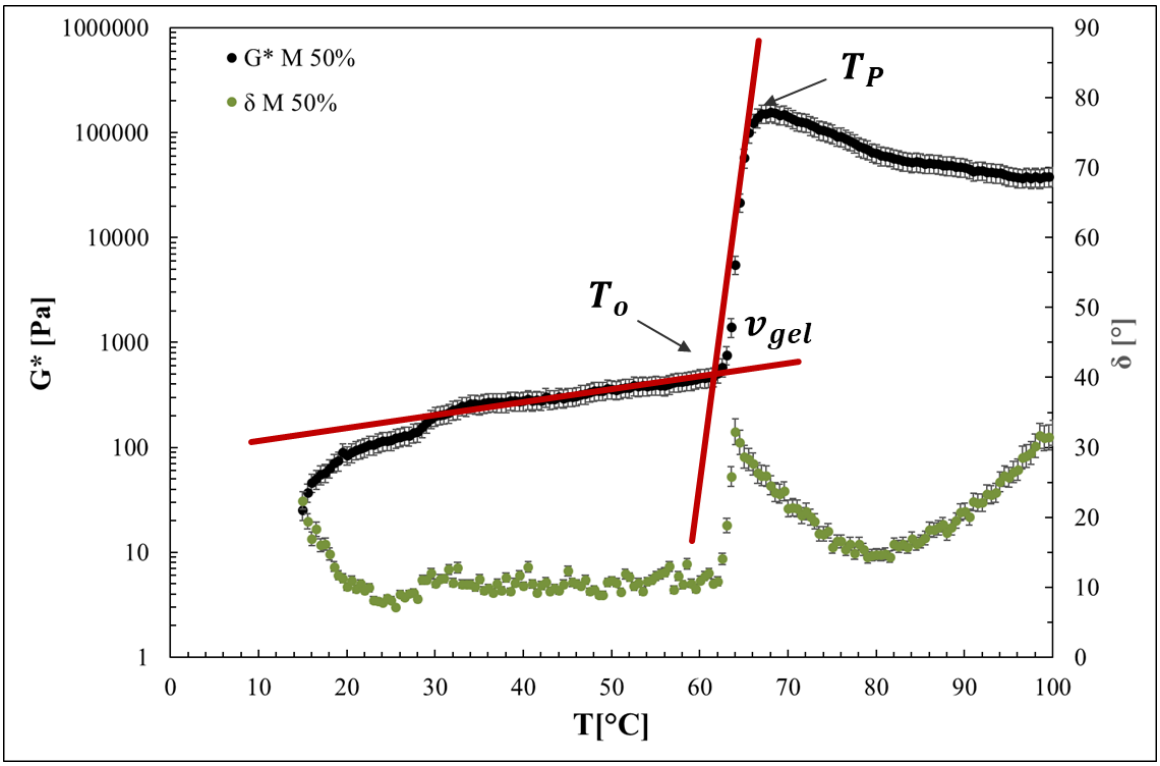

Figure 2.1: Trend of G* of M50%solution during Time cure test. T_o and T_p example evaluation.

The T_p, i.d. the temperature at which G* assumes its maximum value and can be found by searching the higher G' value and evaluating the temperature at which this occurs.

2.2.3.2 Frequency sweep data interpretation

Frequency sweep tests are performed in shear asymptotic kinematic to evaluate the intrinsic characteristics of the material. Tests data can be interpreted both with classical rheological viscoelastic models, based upon the superposition effects principle, in which it is assumed that the solid part of the material can be added together to describe the material's behaviour. On the other hand, the fractional approach is based upon the intermediacy principle, which states that the material behaviour is not the linear combination between solid and liquid components, but it is "intermediate" between them. First, the classic approach will be shortly discussed.

In frequency sweep tests on the sample a sinusoidal deformation in shear kinematic is applied, as stated in the following equation (Bird et al, 1987):

$$\rho = \rho_0 \sin(\omega t) \tag{2.1}$$

For viscoelastic materials, the stress answer can be expressed as:

$$\sigma = \sigma_0 \sin(\omega t + \delta) \tag{2.2}$$

It is possible to define the dynamic modulus G as:

$$G\,(\omega t) = \left(\frac{\sigma_0}{\rho_0}\cos\delta\right)\sin\omega t + \left(\frac{\sigma_0}{\rho_0}\sin\delta\right)\cos\omega t = G'(\omega)\sin\omega t + G''\cos\omega t \tag{2.3}$$

On the right member, the storage modulus, G', and the loss modulus, G'' appear. From the ratio, $\tan\delta$ can be evaluated:

$$\tan\delta = G''/G' \tag{2.4}$$

This material function is able to "weigh" the liquid-like behaviour and the solid-like one. It is useful to introduce the complex modulus, G*, as follows:

$$G^* = G' + iG'' \tag{2.5}$$

$$|G^*| = \sqrt{G'^2 + G''^2} \tag{2.6}$$

The analysis in small amplitude led to the G' and G'' trend reported in Fig.2.2:

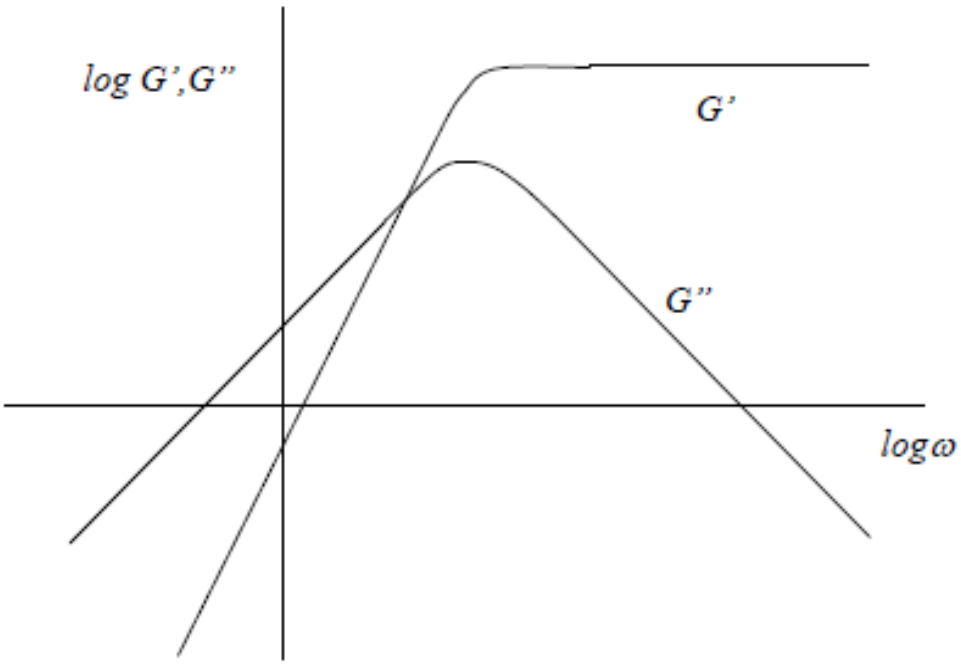

Figure 2.2: G' and G'' function graph vs ω in viscoelastic theory for small oscillations analysis.

As it can be seen from Fig. 2.2, the G' slope at very low frequency is equal to 2 and at high frequency is zero, while G" slopes are 1 and -1 respectively at low and high frequencies. For foods materials, in the frequency range investigated, G' and G'' trends are almost parallel, as shown in Fig.2.3 as example:

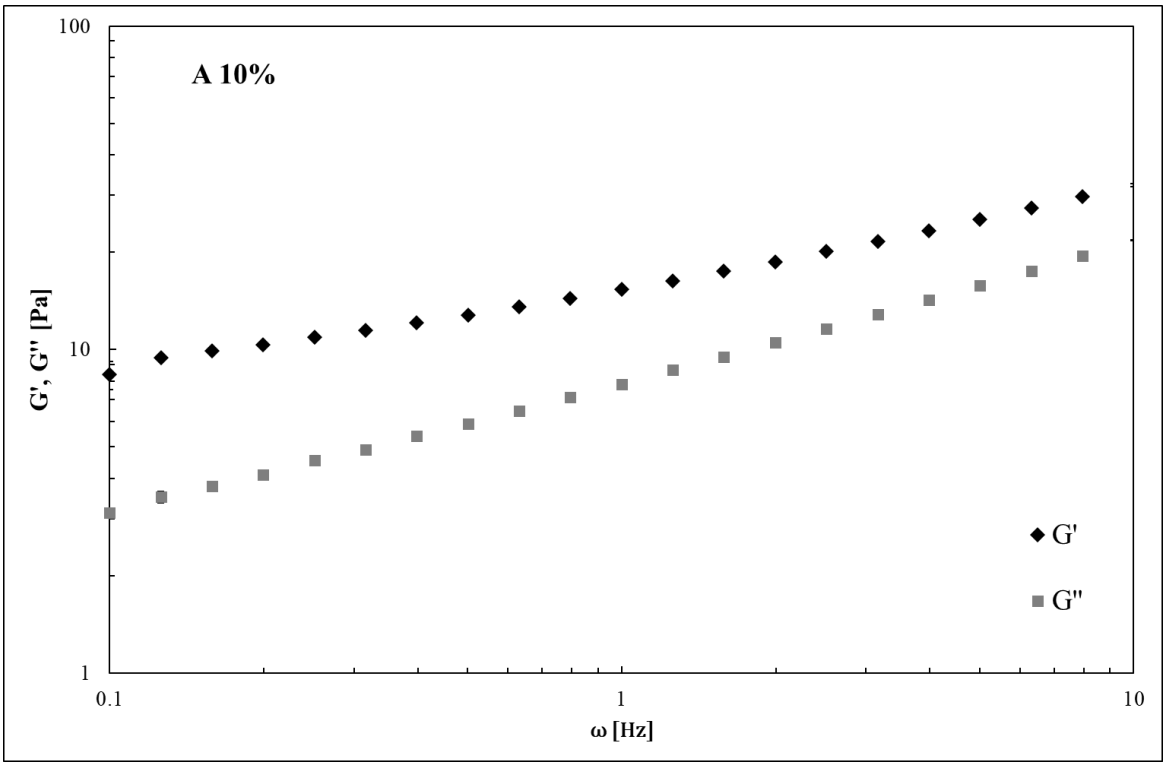

Figure 2.3: G' and G'' trends vs ω for A30% sample.

For samples analysed, the G* trend as a function of the frequency is linear, as shown in Fig.2.4, so data can be well fitted with a power-law equation, i.e., in viscoelastic theory, with a gel model, as reported in the literature for similar systems (Baldino et al.2018), that can be seen as a three-dimensional network:

$$G^*(\omega) = A\omega^n \tag{2.7}$$

Where the parameter A can be related to the strength of the structure: higher values of A are related to stronger network. The exponential factor, n can be considered a measure of the network extension: higher values are related to a less extended network, namely to a more liquid-like behaviour. Low n values, vice-versa, indicates a more extended network, and the system tends to solid-like behaviour.

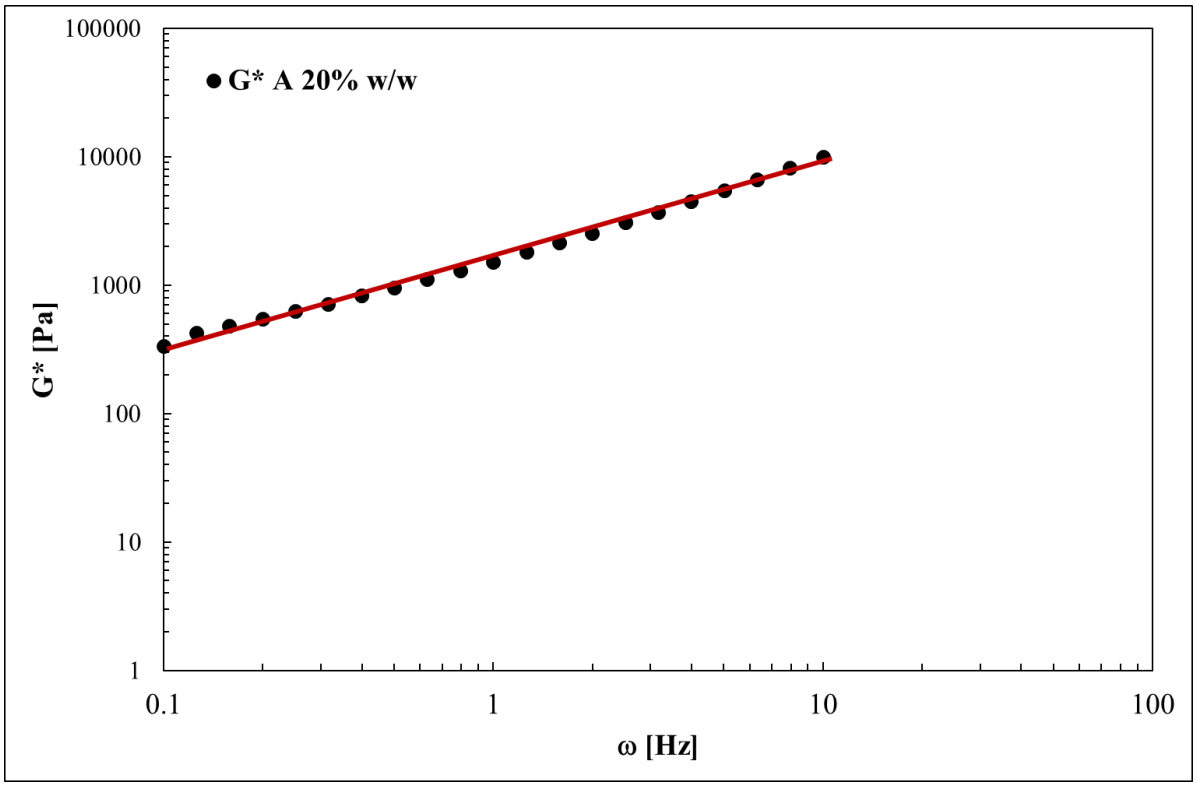

Figure 2.4:G* trend vs ω for A20%

If the viscoelastic theory is not considered valid for this kind of system, the fractional model can be used. Using a single fractional element, the following relationship can be found:

$$G^*(\omega) = \mathbb{G}\omega^{\alpha} \tag{2.8}$$

Where $\mathbb{G}$ is a quasi-property and α is the order of the differential equation that describe the fractional constitutive equation. As can be seen, the fitting equation is the same as the gel model, but the physical interpretation is very different, starting from the principles upon which they are founded. Moreover, while in viscoelastic theory this kind of system is considered networks, fractional models refer to them as clusters or softy materials (Faber et al.,2017).

2.3 Interfacial characterization

The second part of the experimental work was performed to understand the interfacial characteristics at the A/W interface, both of the single materials and their mixtures. From interfacial characterization equilibrium in static conditions, dynamic stability and transient behaviour of this kind of complex interface can be investigated. This information will finally be compared with bulk results in final applications. All tests for interfacial analysis were performed with the Pendant Drop Method, whose characteristics and operating principles will be described in the following section.

2.3.1 Pendant Drop Method

In this work for all interfacial tests, a Pendant Drop Tensiometer (FTA200, First Ten Angstroms, USA) was used. The principle of operation is based upon the formation of a drop, merged in a fluid of different density; from the drop geometrical analysis interfacial tension is evaluated. The instrument is composed of the following components: a cell, where the contact with two fluids with different density is achieved; an illumination device in front of the cell; a viewing apparatus by which the drop is visualized, and geometric data acquired; an automatic pump controlled by the instrument software, that can attain the formation of the drop and different kinds of volume or interfacial area variation in time (sinusoidal, Dirac impulse, square wave, etc.). Different types of syringes and needles can be attached. Through the use of the Axisymmetric Drop Shape Analysis (ADSA), the software of the instrument can evaluate the instantaneous interfacial tension by transforming the geometric variables of the visualized and captured drop image. The images of the drop are visualized and captured by a camera, whose capture triggering options are controlled by the software. The measurement of interfacial tension by the pendant drop method consists of four steps. First, through the automatic pump, the drop is formed; second, through the camera, drop images are captured and digitalized. Thirdly, the outline of the drop is extracted, upon which the software performs a smoothing, and in this way, geometric parameters are evaluated. In the last step, by the use of a fourth-order Runge-Kutta method and by comparing the experimental value with the theoretical one deduced with the Laplace equation, the software determines the interfacial tension (Araschiro 1999; Berry et al. 2015). With the software commands, it is also possible to control an automatic pipetting system that allows maintaining the drop volume constant during the measure of dynamic tensions, γ. Evaporation phaenomena cannot be controlled.

All experimental tests were performed at room temperature, i.d. (22 ±1 °C), putting the aqueous solutions that must be investigated in a glass Hamilton syringe (1710TLL) of 100 ml. The syringe used for all tests was equipped with a stainless-steel needle (D = 20 gauge), and it was attached to the pump system, which under the software commands allows forming the drop of the desired volume. The drop is created in an optical quartz cuvette, filled with a certain amount of inert liquid to saturate the system and to minimize the evaporation phenomena. All the interfaces obtained and analysed are A/W. A CCD camera is connected to a computer and records the images of the drop during the test period.

The interfacial tension measurement is performed until the drop evaporation reduces the volume drop, and in this way compromises the validity of the measure. Further details of this instrument can be found in Biresaw, Liu, and Erhan (2008).

2.3.2 Tests performed

The effect of pea protein, resistant starches and their mixtures on interfacial properties were analysed in static, dynamic and transient conditions. All tests described in this section were repeated twice.

The static measurements are useful to obtain equilibrium interfacial tension and kinetic parameters, by which information about diffusion, adsorption and rearrangement mechanisms of the various species upon the interface. Static measurements were led by making a drop of the desired volume form and registering the evolution of geometrical parameters during the time. Instrument software evaluates the surface tension from these geometrical data using the Laplace equation. Static interfacial tension measurements were performed at T=22±1°C, maintaining drop volume constant; for all static tests, the period was 2 h.

Dynamic oscillating tests in dilatational kinematic were performed by making a drop of desired volume form, subjecting the interfacial area to cycles of expansion and compression that follow a sinusoidal time function. The duration of the tests was 30 minutes and they were performed at room temperature. Oscillating amplitude is chosen in the linear region, previously determined with amplitude oscillating tests. From these tests, dynamic dilatational moduli E' and E'' are derived as a function of the frequency. Data are interpreted according to rheological models, by which information about interface structure can be derived.

Relaxation tests were performed by making the drop form and leaving it in static conditions, so it could reach equilibrium conditions. After this lag-time, the interfacial area underwent square-wave cycles of expansion and compression. In other terms, the interface was subjected to a sudden expansion, and it was maintained in static condition for an established time. Then, it was subjected to a sudden compression, and it remained in static condition for the same time that followed expansion. In this way, it was possible to obtain information about the relaxation mechanism of the interface after the expansion/compression. It can be said that while oscillating tests give information about equilibrium interface structure, relaxation tests allow inferring knowledge about the interface time-dependency (Wustneck et al. 1997; Saulnier et al. 2001). The relaxation tests can be carried out only for a short range of time, because in log time, evaporation of the drop is too pronounced, and the test is no longer valid. The imposed variation of volume was determined out of the linearity region. Relaxation tests are useful to investigate the time dependency of interfacial properties. Relaxation tests were performed at room temperature, for 40 minutes.

Elasticity and viscosity are derived from relaxation tests, together with information about relaxation and recovery mechanisms following respectively an expansion or compression. Further details will be given in the data interpretation section.

2.3.3 Samples preparation

The samples analysed were prepared always with RSs and PP and according to the following procedure:

- The powder of protein and the resistant starch, previously weighted using a precision balance (KERN ABJ-NM/ABS-N), were put in solution in Milli-Q ultrapure water (Millipore, USA), for at least one hour at room temperature on a magnetic stirrer (AREX Heating Magnetic Stirrer, Velp Scientifica, Italy);
- Then, the solutions were centrifugated at 2900 rpm for 30 minutes (Centrifuge 5810, Eppendorf, Italy) to separate the fibre portion from the supernatant liquid. This last one was successively analysed.

In the first phase of this work, the adsorption isotherm on the pure component was achieved to evaluate the CMC value for each RS and the PP. This was accomplished by performing static surface tension measurement on solutions of the single component, prepared at different concentrations, varying between 2 and 10^{-4} % w/w for RS solutions, and between 1 and 10^{-5} % w/w for PP. In the second phase, binary mixtures were obtained mixing pea protein and each resistant starch was prepared. The ratios utilized are summarized as follows:

- PP/A: 1/1; 1/3; 1/5;
- PP/H: 1/1; 1/1/2; 1/1/3;
- PP/M: 1/1; 1/2; 2/1.

The ratios were chosen considering that H is the most resistant starch, containing the highest amylose content; on the contrary, A is the weakest one, since the amylopectin is almost pure. Since M has a content of amylose intermediate between the two, a mixture with a higher PP content and another one with lesser PP content was investigated. These considerations were derived from the results obtained with the bulk characterization of the materials investigated. The concentration of each component in mixtures was chosen above the respective CMC, to guarantee the saturation of interface during dynamic surface tension tests. It is worth noting that no aqueous solution with a surface tension greater than the value of pure water (72 - 73 mN/m at 20 °C) was used.

2.3.4 Interfacial data interpretation

From the different tests performed, it is possible to obtain various pieces of information about the complex interfaces analysed (Sagis et al., 2014). From static measurements, thermodynamic and

kinetic information is inferred. From the dynamic oscillating tests, rheological parameters about structure in equilibrium conditions are obtained, while from relaxation tests time dependency can be investigated.

2.3.4.1 Static measurements

From static measurements, interfacial tension in function of time is derived. A typical trend is shown in Fig.2.5:

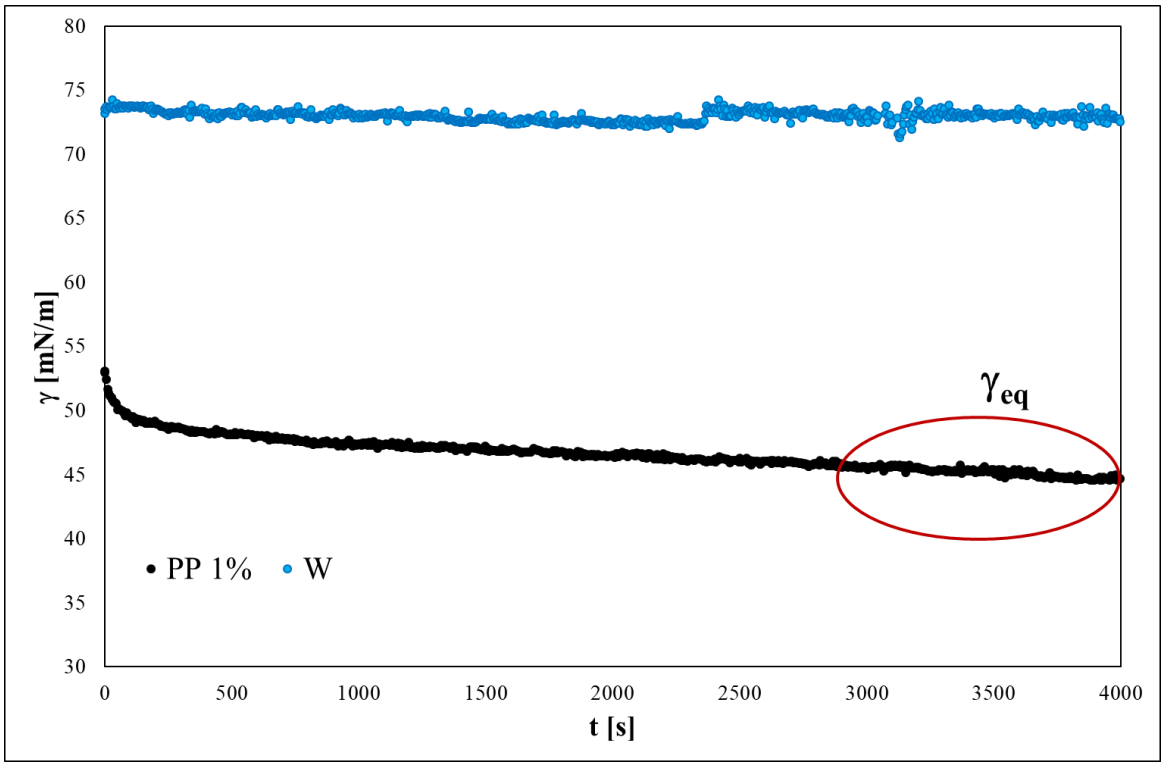

Figure 2.5: Interfacial tension versus time for PP 1% w/w and pure water, W.

As it can be seen from the Fig.2.7, the interfacial tension value for pure bi-distilled water is about 72±0.5 mN/m for all the duration of the test, while for PP1% it varies with time because of the interfacial activity of pea proteins. It is possible to obtain the equilibrium interfacial, γ_{eq}, assuming that equilibrium is reached if the interfacial tension does not vary more than 0.5 mN/m during 30 min of measurement (Mileti et al. 2019). So, equilibrium interfacial tension is the average of the values included in the red oval in Fig.2.7.

From the same data, kinetic parameters can be derived. According to literature, the kinetics of proteins as surfactants can be described in three main steps (Seta et al. 2012):

- diffusion of proteins in the bulk toward interface;
- adsorption of molecular proteins at the interface;

- rearrangement in interfacial layers;

The diffusion step can be described by the Ward-Torday equation:

$$\pi = C_0 KT \frac{D_{diff}\theta^{\frac{1}{2}}}{\Pi} \quad (2.9)$$

In the equation above, π is the surface pressure, i.e. the difference between the sub-phase interfacial tension (namely water surface tension) and that of the solution for any instant θ, C_0 is the bulk component concentration, K is the Boltzmann constant, T the absolute temperature of the system, D_{diff} the diffusion coefficient, θ is the diffusion time, Π is the pi Greco number. If the plot of π versus $\theta^{\frac{1}{2}}$ is linear, the diffusion is the controlling step and from the slope of the curve, it is possible to evaluate the diffusion rate as the slope of the curve. (Mileti et al. 2019; Camino et al. 2009), as it can be seen in Fig.2.6:

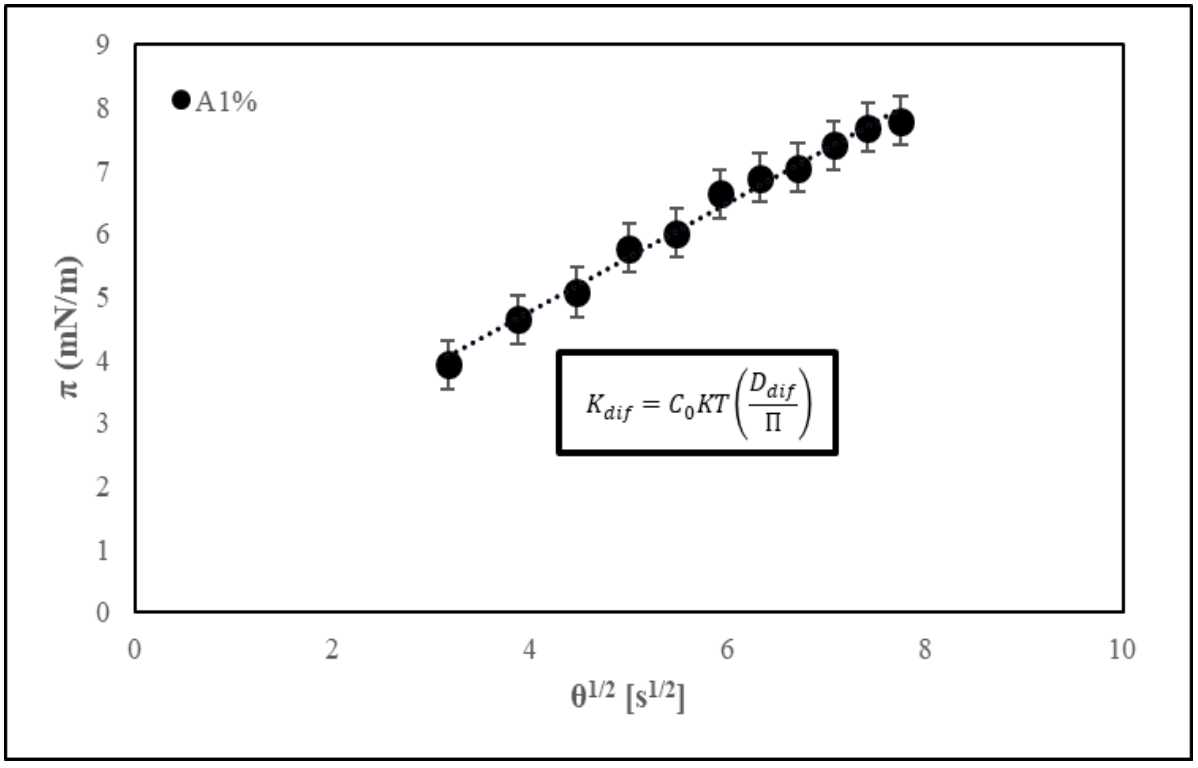

Figure 2.6: π versus $\theta^{\frac{1}{2}}$for A1%. The slope of the curve is the diffusion rate coefficient.

The other two steps can be modelled with Graham and Phillips equation:

$$ln\frac{\pi_f - \pi_t}{\pi_f - \pi_0} = -k_i t \quad (2.10)$$

The equation above can describe both adsorption and rearrangement steps. In the relationship, π_f, π_0 and π_t represent respectively the surface pressure at the last time of the step analysed, at the first time and at any time, while k_i is the first order constant. From the data plot, as shown in Fig.2.7,

it is possible to distinguish two slopes, the first being the adsorption constant, k_{ads}, and the second the rearrangement one, k_r (Mileti et al. 2018; Camino et al. 2009).

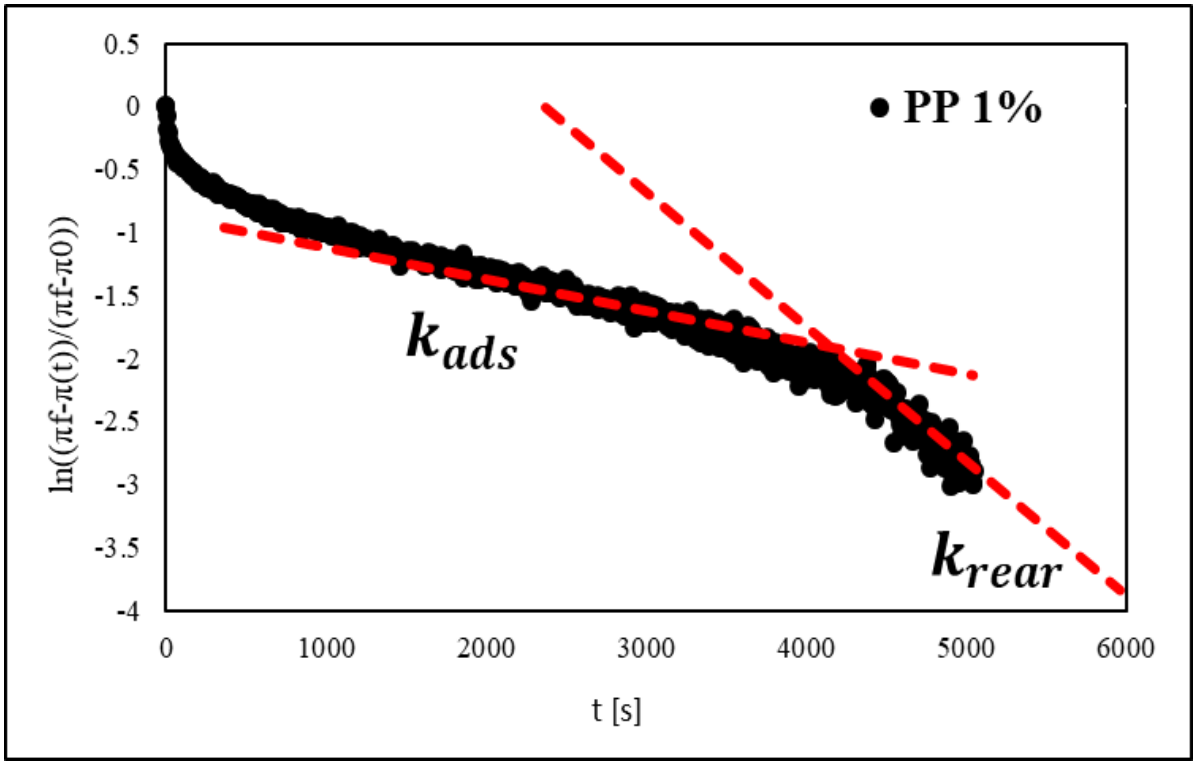

Figure 2.7: Graham Philips plot to evaluate adsorption and rearrangement constants.

As it is shown in Fig.2.9, from the first slope k_{ads} can be evaluated, while similarly from the second slope k_{rear} can be determined.

2.3.4.2 Dilatational oscillating tests data interpretation

The dilatation properties of interfaces can be studied with the oscillating pendant drop method; the analogue of the frequency sweep test performed in bulk rheology. As said above, in this method, the drop of the solution to be analysed undergoes periodical cycles of compression/expansion, where the volume varies with a sinusoidal function, whose amplitude and period are imposed through the software. The drop of the desired volume is firstly, and then, starting from the initial static condition characterized by an undisturbed initial area A_0 and an initial surface stress γ_0, the surface area underwent a sinusoidal variation of an established value ΔA_0 amplitude, as described by the equation (Ivanov et al., 2005; Mileti et al., 2019):

$$A - A_0 = \Delta A_0 \sin(\omega t) \tag{2.11}$$

Small oscillation must be used to prevent the effects of higher frequency harmonics, so the suitable ΔA_0 to be imposed is determined by amplitude test, in which, maintaining the oscillation period constant, ΔA_0 is varied, and in this way, the linearity region can be founded. Thus, ΔA_0 is chosen in this region.

Applying the area variation established by equation (2.11), the dilatation stress varies in response with the following sinusoidal functionality, a constant amplitude $\Delta\gamma_0$:

$$\gamma - \gamma_0 = \Delta\gamma_0 \sin(\omega t + \delta) \tag{2.12}$$

where δ is the phase angle between the input function, the variation of area, and the consequent response of the surface stress. Manipulating equation (2), follows equation (3):

$$\gamma - \gamma_0 = \Delta\gamma_0 \cos\delta \sin\omega t + \Delta\gamma_0 \sin\delta \cos\omega t \tag{2.13}$$

Since the variation of the surface area is imposed, the time function $A = A(t)$ is known, and consequently $\Delta A(t) = A(t) - A_0$. Thus, it is possible to evaluate the surface area deformation, α, and the rate of surface area deformation $\dot{\alpha}$ (t), defined as follows (Ivanov et al. 2005):

$$\dot{\alpha}(t) \equiv \frac{1}{A}\frac{dA}{dt} = \frac{d\alpha(t)}{dt} \tag{2.14}$$

$$\alpha(t) = \int_0^t \dot{\alpha}\, dt = ln\frac{A(t)}{A_0} \approx \frac{\Delta A}{A_0} \tag{2.15}$$

Eq.3 is divided by the area deformation, complex modulus E_d^* can be found as the function of frequency, taking the basic harmonic wave as reference:

$$E_d^*(\omega) = \frac{\gamma - \gamma_0}{\Delta A_0/A_0} = \frac{\Delta\gamma_0 \cos\delta}{\Delta A_0/A_0} \sin\omega t + \frac{\Delta\gamma_0 \sin\delta}{\Delta A_0/A_0} \cos\omega t \tag{2.16}$$

In analogy with bulk rheology, the two following factors can be respectively indicated as storage dilatational modulus $E_d{}'$ and loss dilatational modulus $E_d{}''$:

$$E_d{}' = \frac{\Delta\gamma_0 \cos\delta}{\Delta A_0/A_0} = E_0 \cos\delta \tag{2.17}$$

$$E_d{}'' = \frac{\Delta\gamma_0 \sin\delta}{\Delta A_0/A_0} = E_0 \sin\delta \tag{2.18}$$

Thus, interfacial $tan\delta$ can be defined as:

$$tan\delta = \frac{E''}{E'} \tag{2.19}$$

This parameter is useful because it can give immediate information about the behaviour of the interface (solid or liquid-like). Usually, in frequency analysis complex functions are used. Thus, a complex dilatational modulus can be introduced and defined as:

$$E_d^*(i\omega) = E' + iE'' \tag{2.20}$$

The complex modulus represents the correlation between the surface area variation and the corresponding answer in terms of dilatational stress, in a small oscillation amplitude field (Ravera,

Loglio and Kovalchuk 2010); (Seta et al. 2012)). In the definition of complex modulus stated in eq. (11), storage contribute, E' and loss modulus, E'', are present, respectively as real and imaginary parts. $E'$is related to the solid behavior, and E'' to the liquid one.

The absolute value of the complex modulus can be reached as follows:

$$|E_d^*(i\omega)| = \sqrt{E'(\omega)^2 + E''(\omega)^2} \tag{2.21}$$

In this work, according to the theoretical background described above, for all the solutions investigated, the linear region was determined, choosing an intermediate frequency, 0.025 Hz, and performing several dilatational oscillating tests at different amplitudes. From these tests, an equilibrium complex modulus is evaluated as the media on data obtained in the last part of the test. Finally, a plot of equilibrium complex modulus versus amplitude is obtained. A suitable amplitude is chosen in the region where the complex modulus is constant. Once this is chosen, it is possible to perform oscillation tests, at the desired amplitude, varying the frequency of oscillations. Finally, a plot of equilibrium complex modulus versus frequency is obtained. In a log-log diagram, data can be well fitted by a power-law equation:

$$E^* = A\omega^n \tag{2.22}$$

An example is shown in Fig.2.8:

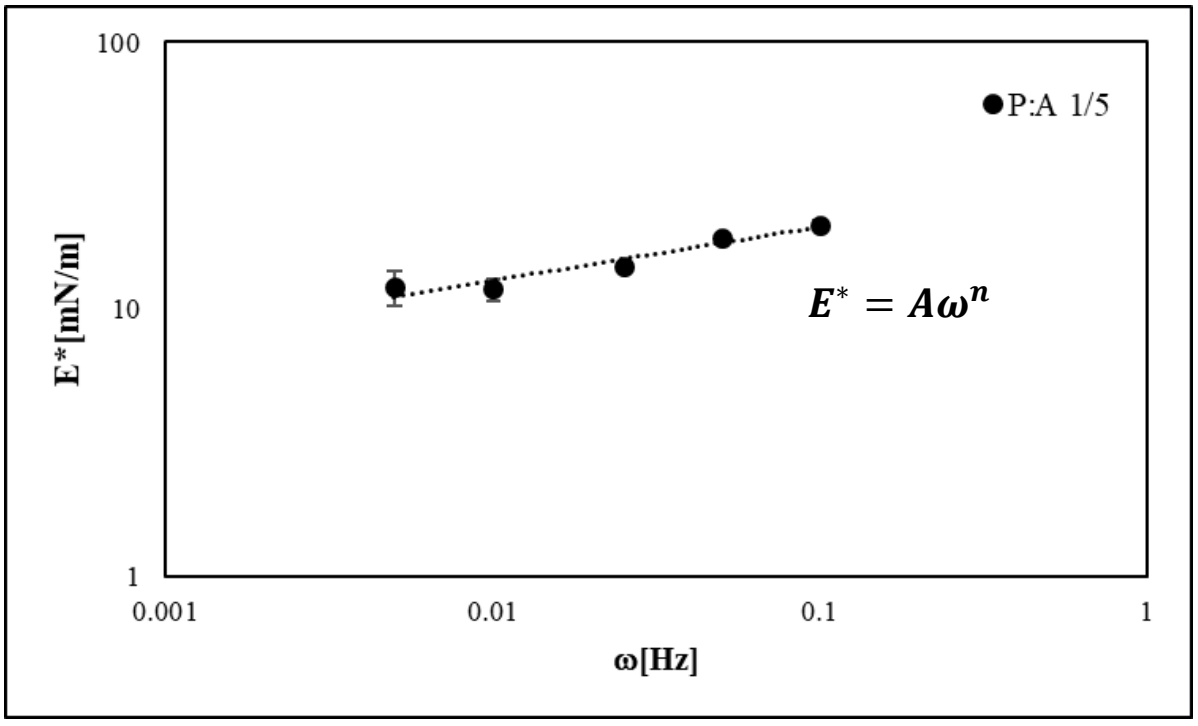

Figure 2.8: E* vs ω plot, with power-law fitting equation

If the viscoelastic theory is assumed valid for this kind of system, eq.2.22 can be considered the Winter gel model for interfaces. This model uses two parameters: A, which is a measure of interfacial layer strength, so the higher the A, the stronger the interface and n, which is a structure index, the

higher is n, the lower is the structuring of the interface, and vice-versa. The interpretation is analogous to that introduced for bulk systems.

In a fractional model with a single Scott Blair model, the complex dilatational modulus can be related to the frequency as follows (Faber, Jaishankar and McKinley 2017b, Jaishankar and McKinley 2013):

$$E^*(\omega) = \mathbb{E}(i\omega)^{\alpha} \tag{2.23}$$

Consequently, the storage and loss modulus can be evaluated as follows:

$$E'(\omega) = \mathbb{E}\omega^{\alpha} cos\left(\frac{\pi\alpha}{2}\right) \tag{2.24}$$

$$E''(\omega) = \mathbb{E}\omega^{\alpha} sin(\pi\alpha/2) \tag{2.25)}$$

Thus, the phase angle is:

$$tan(\delta) = \frac{E''(\omega)}{E'(\omega)} = tan(\pi\alpha/2) \tag{2.26)}$$

And finally, the complex modulus is:

$$|E_d^*(\omega)| = \sqrt{E_d'(\omega)^2 + E_d''(\omega)^2} = \mathbb{E}\omega^{\alpha} \tag{2.27)}$$

In a log-log plot, the complex modulus varies linearly versus frequency, with a slope α, as reported in the figure below: In this model, the quasi-property $\mathbb{E}$ is the analogue of elasticity, but considered in a fractional equation, with the dimension of [Pa s^{α}]. The parameter α corresponds to the order of the derivative that appears in the constitutive equation. Parameter α is related to the slope of the curve, while the value of E_d^* at 1 Hz, gives the quasi-property $\mathbb{E}$.

It is worth noting that the fitting equation is the same for both points of view, classic viscoelastic theory and the fractional model, so are the numeric values of parameters, but their physical meaning is very different. In the first case, superposition effects principle and network theory are considered, while in the second, intermediacy principle and cluster-like systems are assumed.

2.3.4.3Interfacial stress-relaxation test

Complex interfaces can exhibit a quite strong time dependency; for this reason, the interfaces of solutions to be investigated were subjected to the surface stress relaxation test. As can be observed in the figure below, from a static condition, the interface undergoes a sudden expansion in terms of volume, which increases the interfacial area; consequently, the surface tension increases suddenly and then decreases because of relaxation mechanisms (Saulnier et al., 2001). Then, a compression follows, with a decrease of volume and the surface area, and, in analogy, a recovery mechanism can be observed. The repetition of the sequence expansion/compression gives a square wave, with period T and amplitude ΔA. To the variation of area, corresponds a change of interfacial tension $\Delta\gamma$, as shown in Fig.2.9 .

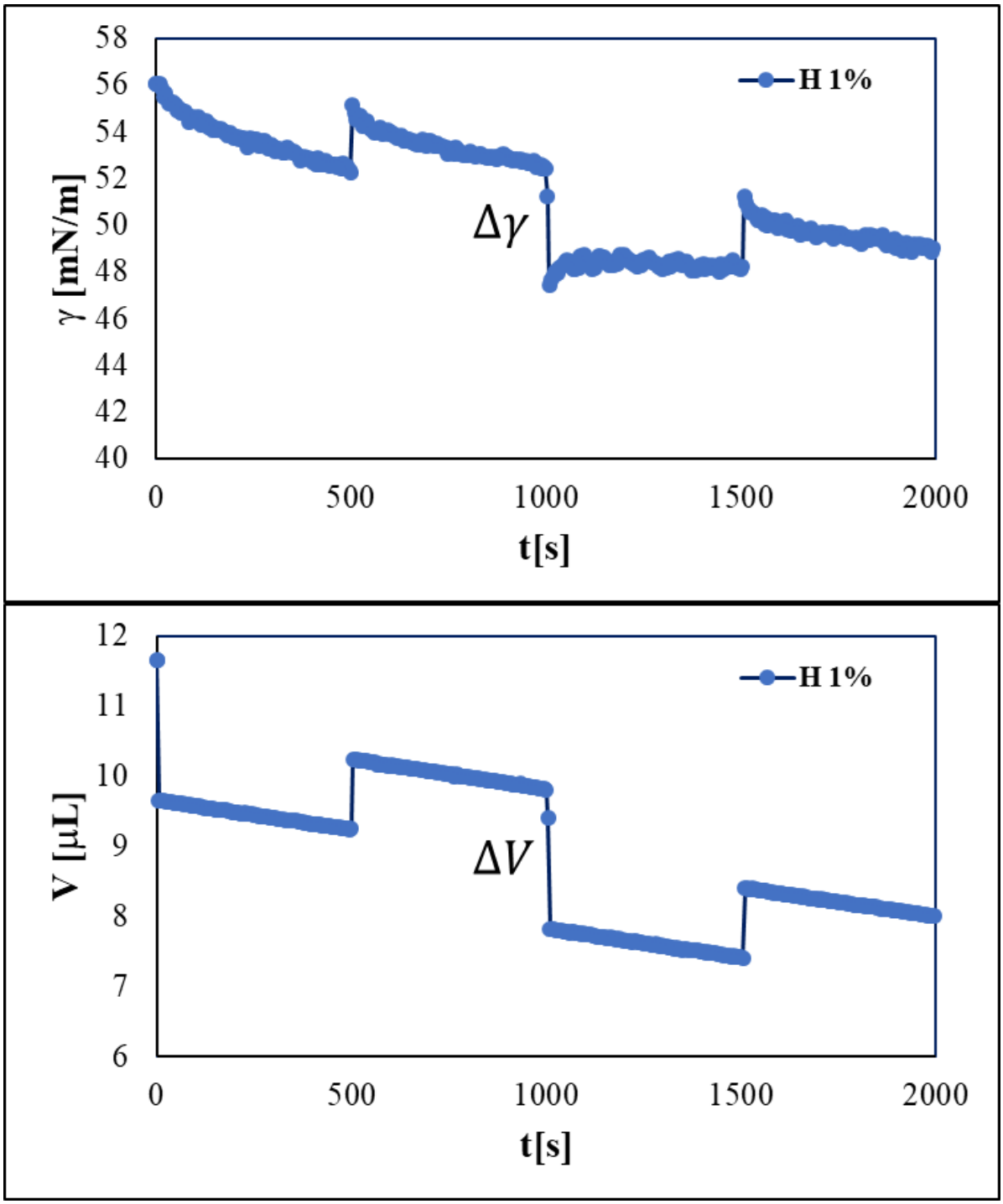

Figure 2.9: partial sequence of a relaxation test for H1%, in which is shown how a variation of volume corresponds to a variation of surface tension.

Experimental data can be well fitted with a stretched exponential decay model or William-Watts equation:

$$ln\frac{\pi(t)-\pi_\infty}{\pi_0-\pi_\infty} = -\left(\frac{t}{\tau}\right)^\beta \qquad (2.28)$$

Where $\pi(t)$ is the surface pressure, defined as the difference between the interfacial tension of water in the air, and the actual surface tension of the solution analysed, $\gamma(t)$; τ is the mean relaxation time, while the exponent β is a measure of the relaxation spectrum width and describes the intensity distribution, or spreading, of the relaxation spectrum. It can assume values between 0 and 1. When $\beta < 1$, the stress relaxation time distribution is characterized by a long tail of a short one, and thus τ is not so far from the peak of a continuous relaxation spectrum. Moreover, when $\beta < 1$ there are several relaxations (or recoveries) mechanisms involved, which act in different moments of the test. This can be due to the presence of different molecules that relax in different ways. Rheological parameters, i.e., dilatational elasticity and viscosity can be evaluated from a classical viscoelastic rheological model, as suggested in (Saulnier et al., 2001; Wustneck et al. 1997):

$$E_d = \frac{\Delta\gamma}{\frac{\Delta A}{A_0}} \tag{2.29}$$

$$\eta_d = \frac{\Delta\gamma}{\frac{\frac{\Delta A}{\Delta t}}{A_0}} \tag{2.30}$$

As can be observed from the equations above, both elasticity and viscosity are related to the instantaneous answer of the interfacial area to a sudden expansion or compression. Elasticity is referred to the variation of the interfacial area compared to the previous condition, while viscosity is related to the rate of the interfacial area changing.

Bibliografy

Arashiro E. Y. and Demarquette N.R. (1999), Use of the Pendant Drop Method to Measure Interfacial Tension between Molten Polymers, *Materials Research* (2), 23-32

Noemi Baldino, Francesca Laitano, Francesca R. Lupi, Stefano Curcio, Domenico Gabriele (2018), Effect of HPMC and CMC on rheological behavior at different temperatures of gluten-free bread formulations based on rice and buckwheat flours, *European Food Research and Technology* 244:1829–1842

Biresaw, G., Liu, Z. S. & Erhan, S. Z. (2008) Investigation of the surface properties of polymeric soaps obtained by ring-opening polymerization of epoxidized soybean oil. *Journal of Applied Polymer Science*, 108(3), 1976-1985.

Bird, Hassager, Armstrong (1987), Dynamic of polymeric liquids, *Wiley-Interscience*.

C.Saldanha do Carmo, A.N.Nunes, I.Silva, C.Maia, J.Poejo, S.Ferreira-Dias, I.Nogueira, R.Bronze, C.M.M. Duarte (2016), Formulation of pea protein for increased satiety and improved foaming properties, *RSC Advances* (6), 6048-6057

Chen P., Kwok D.Y., Prokop R.M., del Rio O.I., Susnar S.S., Neumann A.W. (1998), Axisymmetric Drop Shape Analysis (ADSA) and its applications. In: Möbius D. and Miller R. Editors, Drops and Bubbles in Interfacial Research, *Elsevier Science*, 61-136.

Cheng Li, Bo Gong (2020), Insights into chain-length distributions of amylopectin and amylose molecules on the gelatinization property of rice starches, *International Journal of Biological Macromolecules* 155 721–729

T.J. Faber, A. Jaishankar, G.H. McKinley (January 2017), Describing the firmness, springiness and rubberiness of food gels using fractional calculus. Part I: Theoretical framework, *Food Hydrocolloids*, Volume 62, , Pages 311-324

Franco J.M., Partal P., Ruiz-Marquez D., Conde B., Gallegos C. (2000), Influence of pH and Protein Thermal Treatment on the Rheology of Pea Protein-Stabilized Oil-in-Water Emulsions *JAOCS* (77), no.9

Fengwei Xie, Long Yu , Bing Su, Peng Liu, Jun Wang, Hongshen Liu, Ling Chen (2009), Rheological properties of starches with different amylose/amylopectin ratios, *Journal of Cereal Science* 49 371–377.

Jaishankar, A. & G. H. McKinley (2013) Power-law rheology in the bulk and at the interface: quasi-properties and fractional constitutive equations. *Proceedings of the Royal Society a-Mathematical Physical and Engineering Sciences*, 469.

J. Jane, Y. Y. Chen, L. F. Lee, A. E. McPherson, K. S. Wong, M. Radosavljevic, and T. Kasemsuwan (1999), Effects of Amylopectin Branch Chain Length and Amylose Content on the Gelatinization and Pasting Properties of Starch, *Cereal Chem*. 76(5):629–637

INGREDION® (Westchester, Illinois, USA) technical ddocuments, https://www.ingredion.com

Ivanov, I. B., K. D. Danov, K. P. Ananthapadmanabhan & A. Lips (2005) Interfacial rheology of adsorbed layers with surface reaction: On the origin of the dilatational surface viscosity. *Advances in Colloid and Interface Science*, 114, 61-92

D.R. Klassen, M.T. Nickerson (2012), Effect of pH on the formation of electrostatic complexes within admixtures of partially purified pea proteins (legumin and vicilin) and gum Arabic polysaccharides, *Food Research International* 46 167–176

C. Y. Lam, A. Can Karaca, R. T. Tyler & M. T. Nickerson (2018) Pea protein isolates: Structure, extraction, and functionality, *Food Reviews International*, 34:2, 126-147.

J.-L. Mession, A. Assifaoui, P. Cayot, R. Saurel (December 2012) Effect of pea proteins extraction and vicilin/legumin fractionation on the phase behavior in admixture with alginate, *Food Hydrocolloids* Volume 29, Issue 2 Pages 335-346

Makri.E, Papalomprou E., Doxastakis G. (2005), Study of functional properties of seed storage proteins from indigenous European legume crops (lupin, pea, broad bean) in admixture with polysaccharides, *Food Hydrocolloids* (19), 583-594

Mileti Olga, Noemi Bandino, Bruno de Cindio, Domenico Gabriele (2019), Interfacial Rheology of structured food, PhD Thesis, *DIMES, University of Calabria UNICAL*.

Pascal Leterme, Thierry Monmart and Evelyne Baudart (1990) Amino Acid Composition of Pea (Pisum sativum) Proteins and Protein Profile of Pea Flour, *J Sci Food Agric* 53, 107-1 10.

Ravera F., Loglio G., Kovalchuck V. I. (2010), Interfacial dilational rheology by oscillating bubble/drop methods. *Current Opinion in Colloid & Interface Science* (15), 217-228

Saulnier, P., F. Boury, A. Malzert, B. Heurtault, T. Ivanova, A. Cagna, I. Panaiotov & J. E. Proust (2001), Rheological model for the study of dilational properties of monolayers. Comportment of dipalmitoylphosphatidylcholine (DPPC) at the dichloromethane (DCM)/water interface under ramp type or sinusoidal perturbations. *Langmuir*, 17, 8104-8111.

Sagis, L. M. C. & E. Scholten (2014) Complex interfaces in food: Structure and mechanical properties. *Trends in Food Science & Technology*, 37, 59-71.

Seta L. (2011), Interface Rheology, PhD thesis, University of Calabria

Seta, L., N. Baldino, D. Gabriele, F. R. Lupi & B. de Cindio (2012) The effect of surfactant type on the rheology of ovalbumin layers at the air/water and oil/water interfaces. *Food Hydrocolloids*, 29, 247-257.

Wustneck, R., N. Wustneck, D. O. Grigoriev, U. Pison & R. Miller (1999) Stress relaxation behaviour of dipalmitoyl phosphatidylcholine monolayers spread on the surface of a pendant drop. *Colloids and Surfaces B-Biointerfaces*, 15, 275-288.

Chapter 3
Bulk characterization: Results and Discussions

In this chapter, bulk rheology characterization results are given and discussed. The chapter will be divided into two sections, the first dedicated to resistant starches investigation, the second to pea proteins. In this chapter time cure data with the relative parameters, the temperature of onset gelatinization and the peak temperature with the relative viscoelastic functions, are shown. The frequency sweep tests are reported too, and the data are commended together with fitting parameters and their physical interpretation.

3.1 Resistant starches results and discussion

3.1.1 Time cure analysis

In the first part of this section, a qualitative description of the resistant starches behaviour during the time cure test is given. Information about material trend during thermal treatment can be inferred by looking at the thermo-rheological behaviour.

In the following picture are reported G* and δ trends for M 40% w/w sample by way of example.

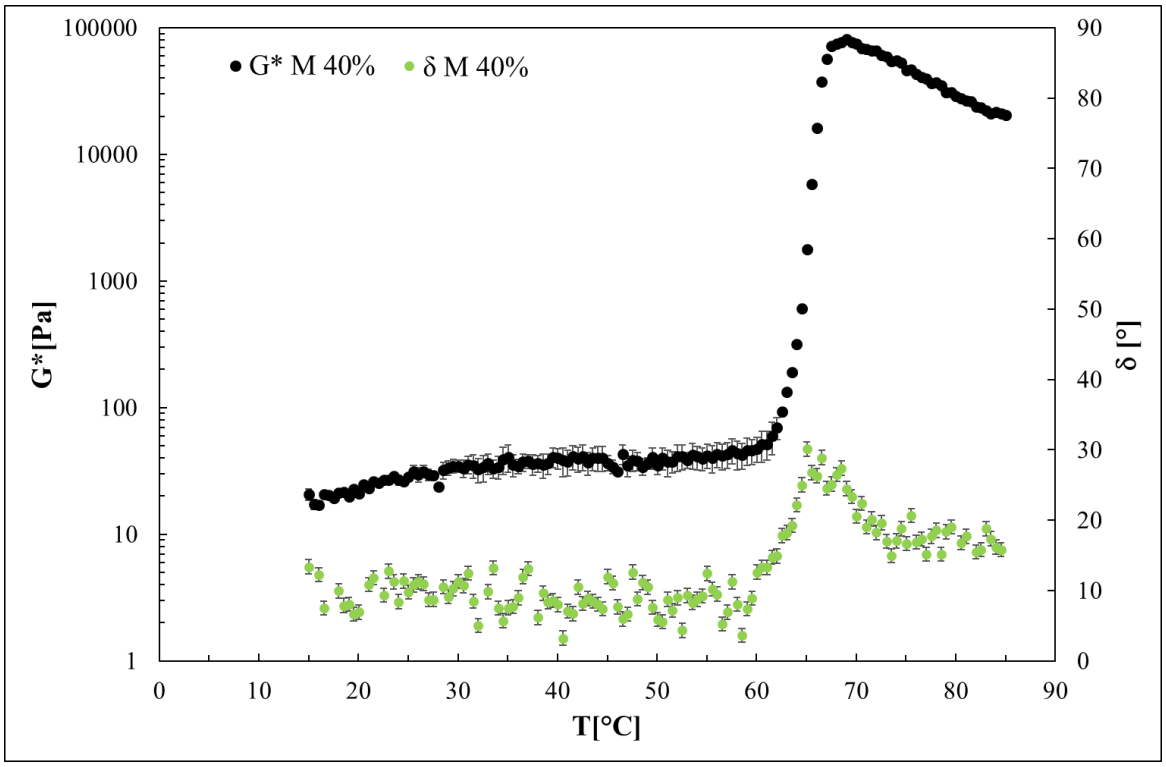

Figure 3.1: Complex modulus, G*, and phase angle, δ, for M40% w/w sample, shown as an example of typical RSs trend during temperature ramp test.

The trend shown in Fig. 3.1 is similar for all the other samples prepared with Hi-Maize and Hylon. As it can be seen, in the first part of the graph, G* slightly varies because of kinetic effect (Baldino et al., 2018), due to the temperature rise that makes molecular energy increase; of consequence, there is a "softening" effect of the sample (Hui Huang Chen et al, 2008). This part is followed by a strong G* increase, caused by the gelatinization process, during which resistant starch granules swell and try to fill the entire volume in the system (Baldino et al., 2018; Fweng Xie et al.,2009). From a macroscopic point of view, starting from the onset temperature, introduced in Chapter 2, the system undergoes a phase transition, going from suspension of granules to a gelatinised phase, more or less ordered, depending upon the kind and amount of resistant starch molecules, namely amylose and amylopectin. (Fweng et al., 2009; Chen Li et al., 2020; Baldino et al., 2018). From a microscopic point of view these molecules in granules are in a crystallised form before onset temperature; after gelatinisation starts, amylopectin and amylose exit from swollen granules, and in presence of water, generate gelatinised phase, whose characteristics will be introduced afterwards (Fweng et al., 2009). Further, the progressive swelling of granules makes molecules occupy the available volume and packaging in a compact structure, (Fweng et al., 2009; Chen Li et al., 2020), regardless if it is a network or cluster phase. If the viscoelastic theory is considered, it can be assumed that a 3D model is formed. G* increases till it reaches a maximum, corresponding to the value at the peak temperatures. After this point, the gelatinization process can be considered concluded. The decrease of G* can be again related to kinetic effects, that alter molecular energy and mobility (Baldino et al., 2018), and this results in a softening of the structure (Hui Huang Chen et al.,2008). An alternative hypothesis provides that the temperature increase can alter or melt the crystalline structure; the structure melting or altering can be responsible for the G* decrease (Fweng et al., 2009; Chen Li et al.; 2020). However, over peak temperature, the system must be still considered in evolution, both for kinetic effects and structure evolution (Fweng et al., 2009; Chen Li et al., 2020). These considerations are confirmed also by the phase angle trend: at low temperature, it remains almost constant, confirming that the structure does not undergo any significant modifications in terms of structure. In correspondence with the onset temperature, the phase angle increases, as a consequence of the transition phase process. Then, at the onset temperature, the phase angle increases as a result of the transition phase mechanism due to the gelatinization process. During the further increase in temperature, the phase angle tends to decrease, suggesting the evolution of the system toward a solid-like behaviour. This kind of behaviour is like that found in the literature for similar dough systems (Baldino et al.,2018; L.Yu et al, 2000; Teyssandier et al., 2011).

Amioca samples showed slightly different behaviour from the other two samples. By way of example, the G* and δ trends for A 50% w/w sample are shown in the following Figure 3.2.

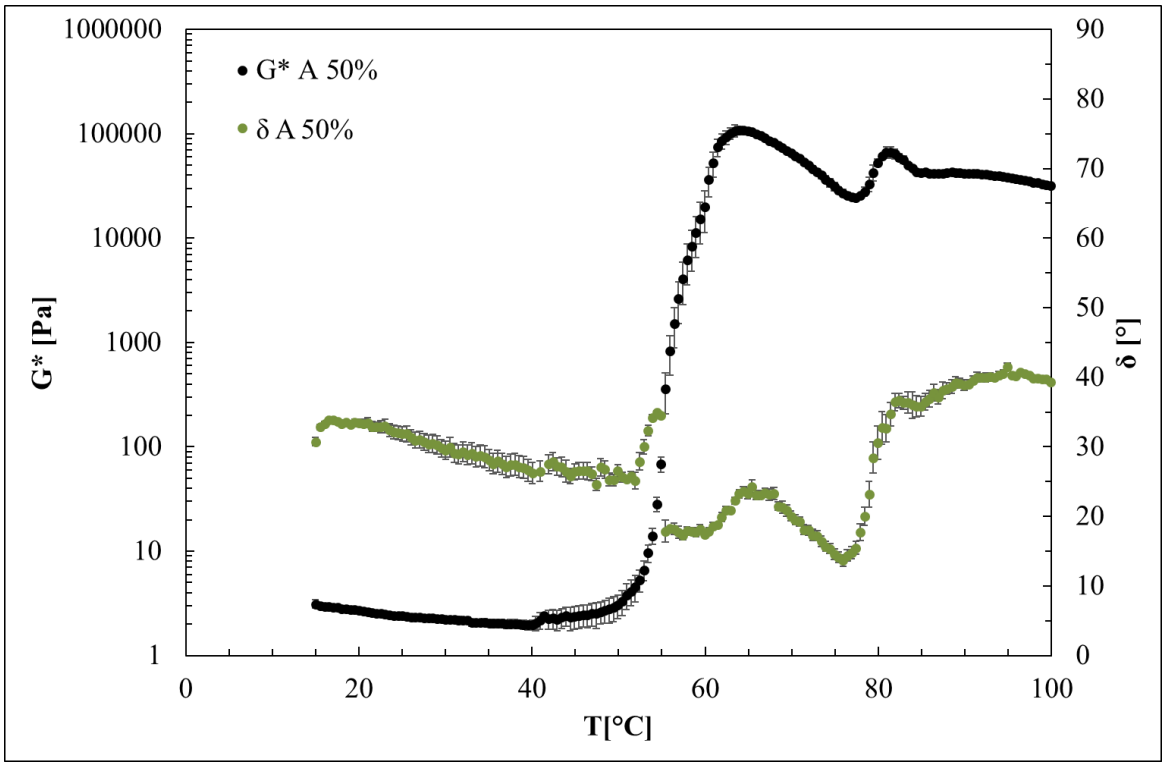

Figure 3.2: Complex modulus G* and phase angle δ trends for A50% w/w.

As it can be seen from Fig. 3.2, in the first part of the graph, at low temperatures, G* and δ slightly vary only for kinetic effects, for the same reasons introduced above (Baldino et al., 2018; Hui Huang Chen et al., 2008). As the temperature increase, at the first onset temperature, a first phase transition occurs, corresponding to a first gelatination process, during which G* sharply increases, for the same reasons introduced above, and the system is moving again from suspension to a gelatinised structure (Hui Huang Chen et al., 2008; Fweng Xie et al., 2009). This is evident also observing the decrease of phase angle, suggesting a more solid-like behaviour. After the first peak of temperature, it follows a G* decrease, due both to kinetic effects induced by temperature increase, and evolution of the system (Chen et al., 2008).t the same time, a decrease of δ is observed. This evidence can be the result of the higher molecular mobility caused by temperature increase, together with a modification in the structure system since phase transitions could not be concluded (Baldino et al, 2018; Chen et al., 2008; Jinchuan et al., 2020).

As temperature rises, a second transition phase occurs, evident by the presence of a second onset temperature and by the sudden increase of G*, suggesting that the system is moving from a kind of structure to another one, more liquid-like than the previous, as it can be seen from the δ rise. The

second gelatination process can be considered terminated at the second peak temperature. In the last part, G* and δ vary for kinetic effects and continuing phase transition (Jinchuan et al., 2020) .

Multiple starch transitions, as above described, are confirmed also in literature (Jinchuan et al., 2020;). This behaviour is more evident at higher concentrations and, at low concentrations, the behaviour is not so clear, and it was difficult to individuate the second onset and the peak temperatures.

Since amioca is amylopectin almost pure, this kind of behaviour can be ascribed to this molecule. For Hi-Maize and Hylon samples, containing amylose in a higher percentage than amylopectin, it can be speculated that the two transitions of Amilopectin are hidden by a unique transition that includes also the amylose transition. Amylose molecules can form a very stable structure, being capable to entangled each other thanks to their linear configuration (Chen li et al., 2020).

As reported in the literature (Fengwei Xie et al, 2009; Takahiro Noda et al., 1998), amylopectin is not able to form a strong structure, as many-branched molecules. Because of the weak structure of amylopectin jellified phase, a further increase in temperature can activate a second transition phase, as shown in Fig.3.2.The strength and the stability of the structure can be also linked to amylose/amylopectin interaction (Chen et al., 2020; Jinchuan et al., 2020). This topic will be discussed more extensively later. In Fig.3.3, the onset temperature trend for all three resistant starches is shown; for A, data are relative to the first onset temperature.

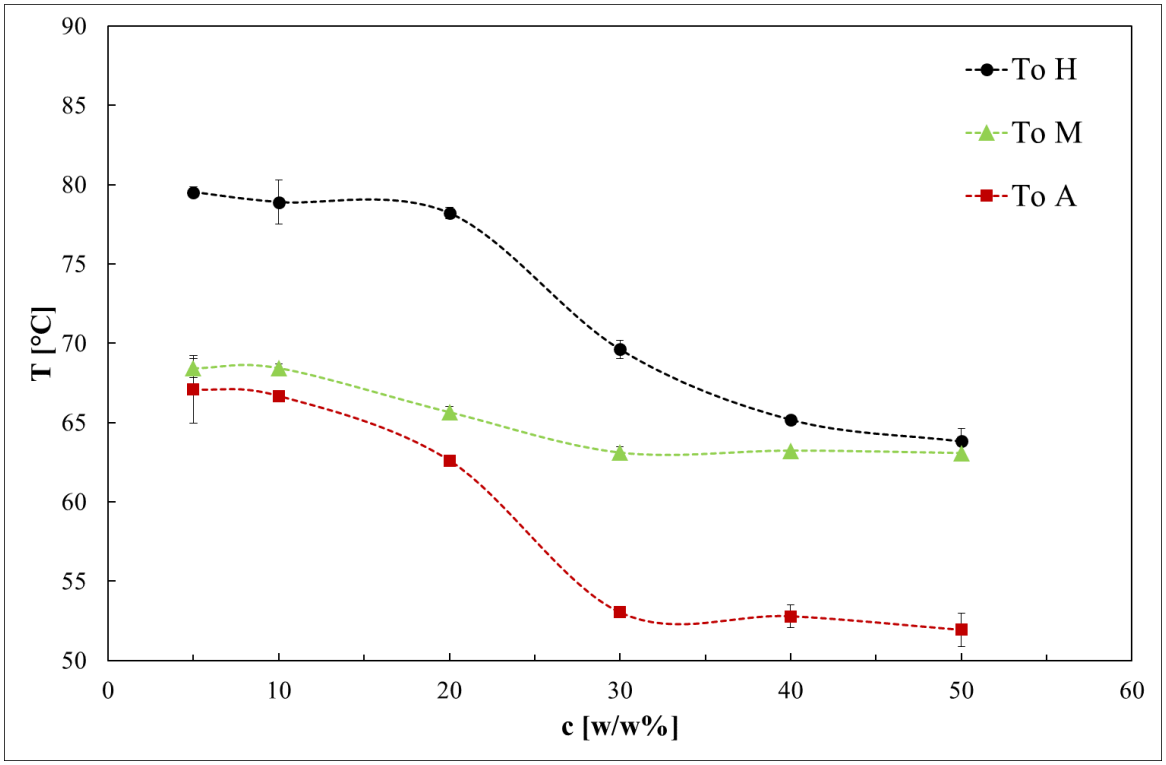

Figure 3.3: T_o trend for all the RS as a function of the concentration

In 3.4, second onset temperature trend about A samples is shown:

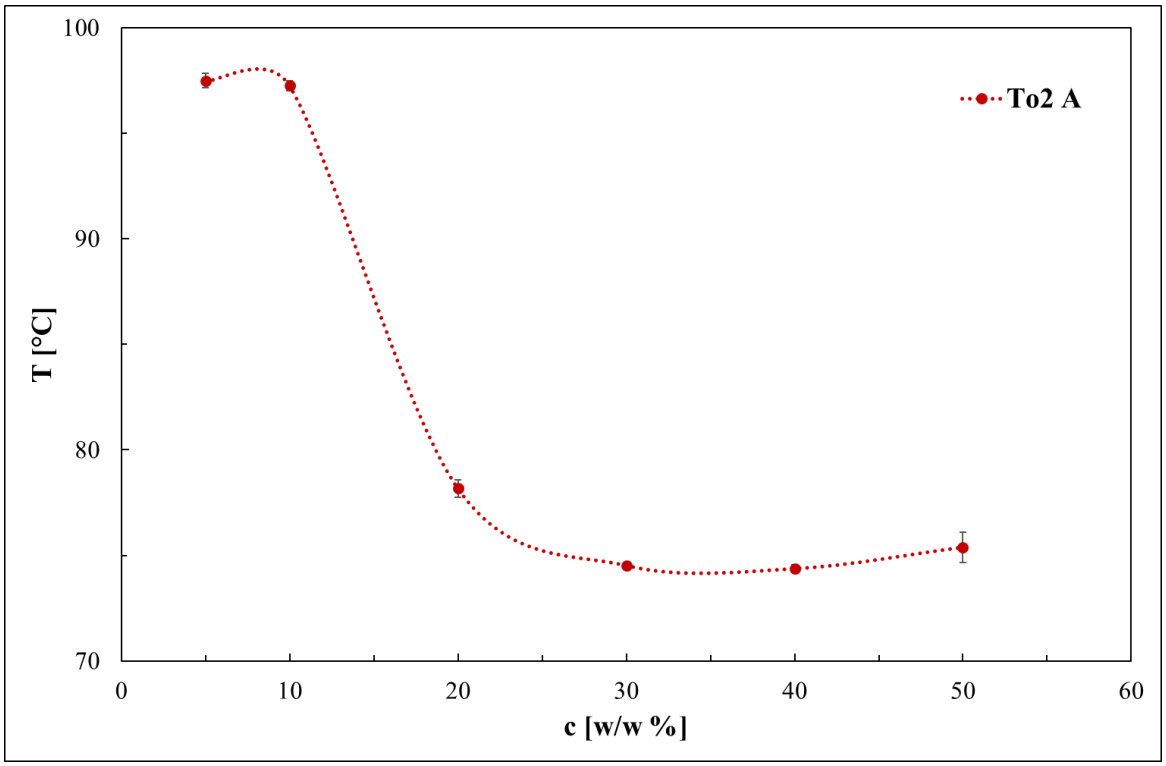

Figure 3.4: The onset temperature trend of the second transition phase, T_{02}, for A samples as a function of concentration.

All the onset temperatures are reported in Table 3.1. For A samples two columns are present: on the left, the first onset temperature is reported; on the right, the second one.

c [w/w%]	T_0 [°C]			
	H	M	A	
5	79.52±0.31	68.43±0.11	67.10±0.39	97.50±0.35
10	78.90±0.36	68.43±0.10	66.68±0.21	97.25±0.23
20	78.20±0.33	65.31±0.16	62.61±1.1	78.17±0.43
30	69.62±0.86	63.23±0.18	53.03±0.17	74.52±0.20
40	65.18±0.51	63.01±0.32	52.80±0.14	74.37±0.17
50	63.81±0.72	63.20±0.10	51.92±0.53	75.40±0.73

Table 3.1: Onset temperature T_0 values for the three different RSs at different concentrations analyzed systems.

As it can be seen from Figs 3.3 and 3.4, for all the three resistant starches investigated, the trend is sigmoidal, with two plateaus, the first at low concentrations and the second at high concentrations. The sigmoidal trend is generated by a double effect: temperature and concentration. It is not easy to give a physical reason for this kind of behaviour since starch gelatinization is a complex phenomenon,

involving several factors (Flory, 1953; Fweng Xie et al., 2020; Chen et al., 2020). Several attempts were made to explain the functionality of onset and peak temperature upon concentration, as water availability theory, (Donovan 1979), crystallite stability theory (Eliasson, 1980), but no one can consider all the variables. Moreover, there is also evidence that the crystallinity of the constituting molecules plays a fundamental role (Vermeylen et al., 2006; Ratnayake and Jackson, 2007).

As it can be observed in Fig.3.4, for amioca second onset temperature a sigmoidal trend can be found. At lower concentrations, a higher plateau is observed. Increasing concentration, second onset temperature decreases exponentially, till a lower plateau is reached.

Observing Fig. 3.3, it is possible to note that the T_o curves are shifted downwards passing from H to M and finally to A. This evidence can be explained by the following considerations, suggested by the literature (Fengwei Xie et al, 2009; Chen Li et al., 2020) on this kind of systems, or similar ones. The gelatinization mechanism for this kind of systems depends strongly on the amylose/amylopectin ratios and from the molecular conformation of the amylopectin present in the resistant starch investigated. Two kinds of structure can be hypothesized: a 3D network (Chen Li et al., 2009) or clusters (Fengwei Xei et al., 2009). As concerns the first one, it is possible to say that amylose molecules conformation is linear, so they can entangle each other and generate a three-dimensional system, whose strength depends upon the concentration. The gelatinization process involving amylose systems can produce a very stable crystalline phase, and of consequence, the mechanism requires higher activation energy (Chen Li et al., 2020). This consideration can partly explain why H and M samples have a higher onset temperature. Amylopectin molecular conformation is branched, with lateral chains of different chains, depending upon the origin of the starch. Usually, in normal starch, amylopectin has not a very ordered crystalline form, and its molecules have short length lateral chains. For this reason, this kind of amylopectin can gelatinize with low activation energy and it is not able to generate a very ordered and crystalline phase. This can explain why A sample, being at 98% pure amylopectin (dry basis), has a lower onset temperature and can undergo multiple phase transitions as temperature increases.

It is known from the literature that resistant starches have an amylopectin type with a more ordered crystalline form compared to normal starches one, having longer lateral chains, (Shi & Seib, 1995; Lingshang Lin et al.,2016), and for this reason, the gelatinization mechanism needs higher activation energy than in normal starch. More specifically, it is known from the literature (Jinchuan et al., 2020) that there exist three forms of amylopectin. The classification of these three forms is based upon the lateral branches length: A type, amorphous, with the low lateral branches length; it is the dominant form in normal starch. B type, more branched and more crystallized having a longer lateral chain than A type; it is often present in resistant starches. Finally, C type, that results in a mixing of A and B

type. For these considerations, it can be speculated that H and M have a higher onset temperature with respect to the A sample.

Moreover, it has been suggested that in resistant starch systems, the structure is the results of the mutual interaction between amylose and amylopectin, since linear chains of amylose molecules can fit among the double helixes of amylopectin structure, generating a very strong network (Chen Li et al., 2020) as represented in Fig. 3.5. This consideration can give a reason why H and M samples have higher onset and peak temperature.

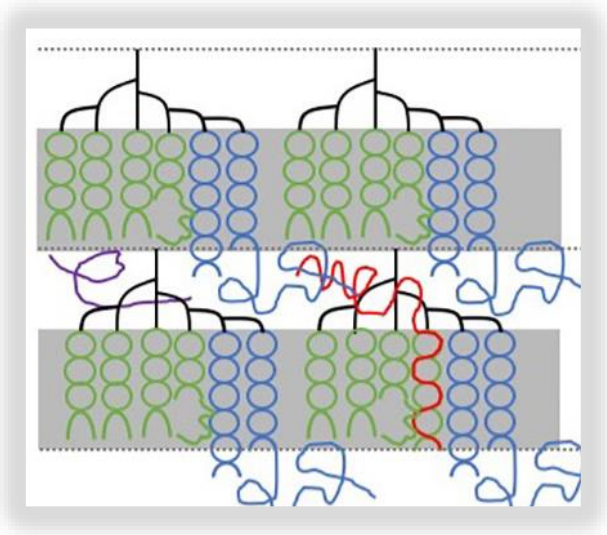

Figure 3.5: Linear chains of amylose fit in double helixes of amylopectin to generate a stronger network (Chen Li et al.,2020)

Another explanation concerns the possible type of assumed configuration for this type of systems. In fact, the literature suggests cluster or gel-ball configuration for amylose/amylopectin systems (Fweng et al., 2009). In this hypothesis, the amylopectin short-length lateral chains can form gel-balls, surrounded by linear amylose molecules, as depicted in Fig. 3.6. The entanglements among this kind of conformation are naturally less than those present among linear chains such as amylose. So, it can be said that in systems containing amylopectins, such as A ones, gel-balls or clusters structure can be considered prevalent. The activation energy for these systems is lower than high amylose ones, and this can explain why the onset temperatures for A systems are lower.

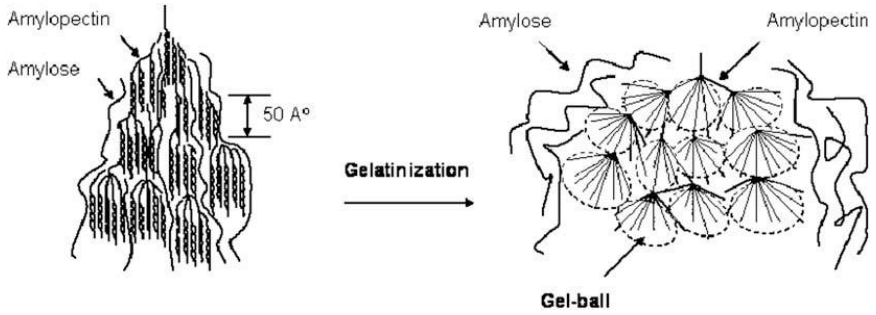

Figure 3.6: Schematic depiction of gel-ball formation during gelatinization process (Fengwei Xie et al.,2009)

It is worth noting that high amylose systems, with a very extended network, can be analysed with viscoelastic models, but the amylopectin rich systems, being essentially clusters, can be modelled with fractional models (Faber et al.,2017). It is also possible that amylose/amylopectin system structures contain both network and clusters. The same analysis performed for the T_o, was performed for the T_p. In the Fig. 3.7, peak temperature trends for all resistant starches are reported.

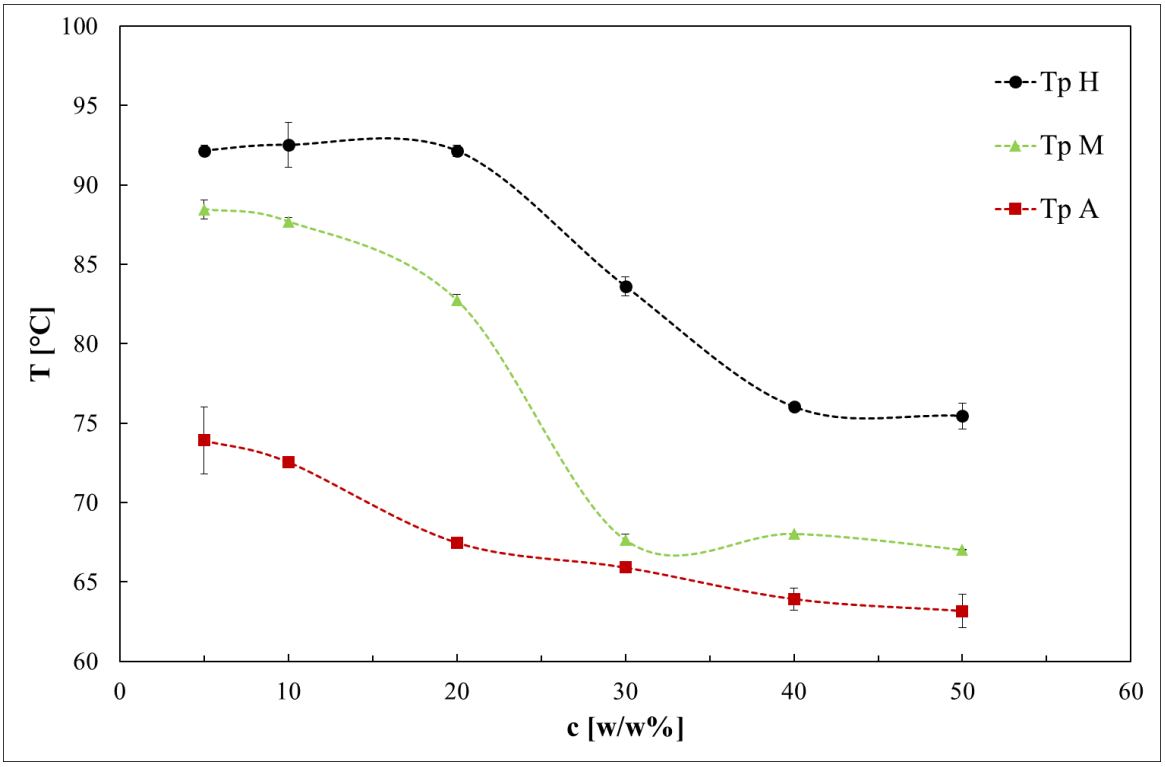

Figure 3.7: Peak temperature, T_p, for all three Rs in the function of concentration.

In Table 3.2, peak temperature data are reported. For A samples two columns are present: on the left, the first peak temperature is reported, while on the right the second one. At low concentrations, the second peak temperature is not defined in the temperature range analysed(n.d.), since it is registered only an increase of G* without maximum reaching.

c [w/w%]	T_p [°C]			
	H	M	A	
5	92.16±0.34	88.46±0.61	73.91±2.12	n.d.
10	92.51±1.40	87.70±0.27	72.5±0.2	n.d.
20	92.15±0.34	82.2±0.90	67.47±0.10	n.d.
30	83.62±0.60	67.65±0.36	65.91±0.13	88.15±0.40
40	76.02±0.14	68.03±0.16	63.91±0.70	84.50±2.52
50	75.45±0.82	67.02±0.5	63.17±1.06	79.50±0.30

Table 3.2: Peak temperature data for all the three RSs investigated to the concentration variation.

As it can be seen from Table 3.2 and Fig. 3.7, also the T_p trend as a function of the concentration is sigmoidal, maintaining the same order as onset temperature trends. Comparing Figures 3.3 and 3.7, it is possible to observe that the peak temperature trend for each resistant starch is translated upwards compared to the relative onset temperature trend. This type of behaviour can be attributed to the delay in the start of gelatinization. Further considerations can be deduced by observing the difference between the peak temperature and the onset temperature for each concentration, summarized in Table 3.3:

c [w/w%]	$\Delta T = T_p - T_o$ [°C]		
	H	M	A
5	12.63±0.23	20.04±0.50	6.81±1.73
10	13.61±1.03	19.26±0.17	5.88±0.1
20	13.90±0.9	17.09±1.06	4.86±1.12
30	13.93±0.27	4.55±0.53	12.88±0.16
40	10.84±0.5	4.80±0.32	11.13±0.84
50	11.63±0.82	3.95±0.28	11.24±1.13

Table 3.3: Differences between peak temperature T_p and onset temperature T_o for each concentration of RS investigated.

From Table 3.3 it is possible to evaluate the temperature interval between the beginning and the end of gelatinization and it is possible to observe that for H samples the ΔT is almost constant with concentration, with the trend slightly decreasing at very high concentrations. For M samples, the ΔT decreases increasing the starch concentration in the mixing, denoting an increase in the ending of the gelatinization processes for these systems. It seems that, for M samples, the higher the amylopectin content, the faster the gelatinization. Similar situation for A samples, but in this case, there is an

increase in the temperature interval between low and high concentrations. This could be due to the different kind of amylopectin present in M and A, leading for this to different structures (Fweng et al., 2009), but also interaction between amylose and amylopectin (Chen et al., 2020). The information inferred from table 3.3 can be useful to understand the evolution of the system. If the temperature range between peak and onset temperatures is short, it implies that the system crystallizes soon, with scarce further evolution possibilities, even if the temperature is increasing. On the contrary, a large range implies a slower system evolution. These considerations are important in rheological product design. For example, it can be said that in the aerating system, the expansion of the system is determined also by the gelatinization time. In fact, a structure that crystallizes rapidly prevents the aerated systems from expanding and evolving as would a structure that instead has a longer gelatinization time. So, in this case, it will be a concentration range in which gelatinization time is longer. These considerations will be discussed further in the final application's sections.

From time cure data, is also possible to evaluate the gelation velocity, as the slope of the linearized trend of G* before the onset temperature, and the linearized trend of the G* sharp increase after onset temperature, as shown in Figure 2.3 (Chenet al., 2020). The results are summarised in the following Fig.3.8.

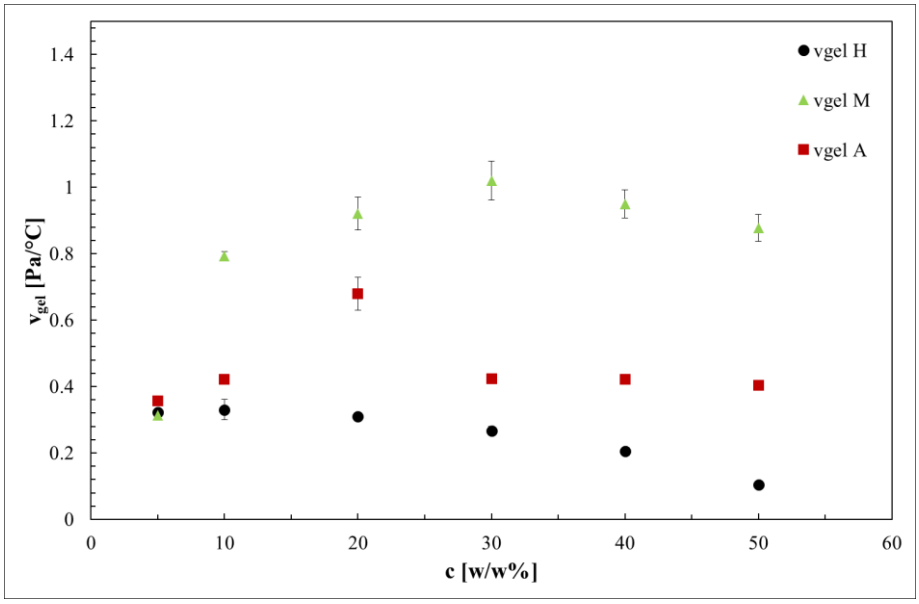

Figure 3.8: Gelatinization velocity for all the resistant starches analyzed in function of concentration.

As it can be seen from Fig.3.8, there is not a very defined trend. The trend for H samples is almost constant with concentration, decreasing slightly in the last part. For all the samples the velocity seems to increase near a certain concentration to decrease after this peak that is more or less pronounced depending on the RS investigated. Although velocity trend is not well defined, the comparison

between ΔT in table 3.3 and gelatinization velocity in Fig.3.8, suggests some considerations. The H samples ΔT is quite the same in the concentration range analysed and almost the same holds for velocity values. This could suggest the existence of a single gelatinization mechanism (Jinchuan et al., 2020; Chen Li et al., 2020). The M samples have two ΔT value, the lower at low concentration range [5%-20%] and the higher at high ones [30%-50%]. For the former range, gelatinization velocity increases with concentrations and has a lower value compared to high concentrations. So, it can be concluded that the gelatinization mechanism takes more time and it is slower. In the second range, ΔT is shorter than in the first, and gelatinization velocity is higher than in the first interval. Thus, the gelatinization mechanism can be considered shorted and faster. Similar consideration can be assumed for A samples, but only in terms of ΔT since gelatinization velocity has not a defined trend. In the first interval [5%-20%], the gelatinization mechanism can be considered faster because of ΔT values, while in the second, slower. The formation of different phases by different gelatinization mechanism for systems having different ratios of amylose/amylopectin is suggested also by Fengwei Xie et al. (2009), Chen Li et al. (2020). Moreover, other than the dependence upon concentrations, there is also a dependency upon the molecular conformations of amylose and amylopectin species present in each resistant starch analysed.

Finally, the complex modulus at peak temperature, G^*_p, is reported in Fig. 3.9 and Table 3.4 with concentration.

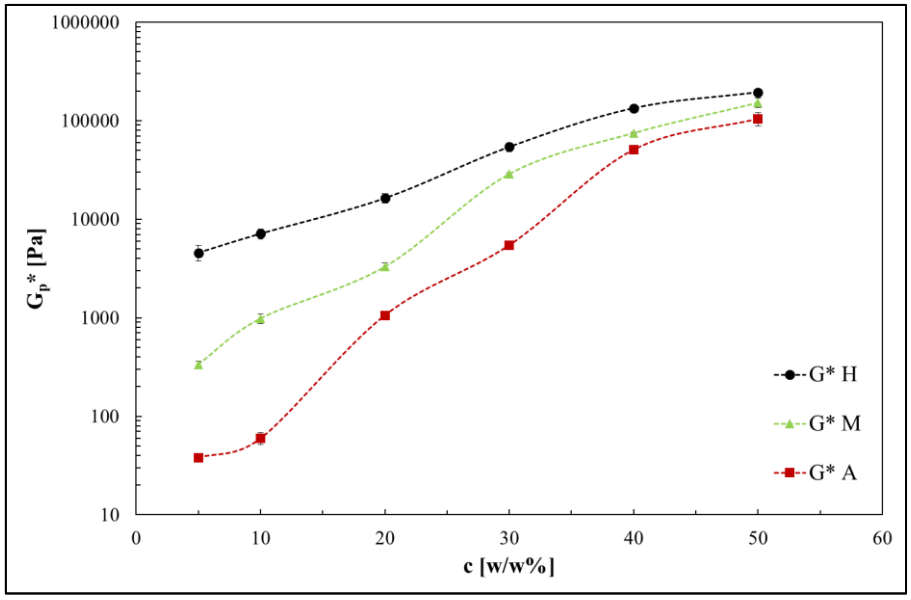

Figure 3.9: Complex modulus at peak temperature G^*_p as a function of concentration for all resistant starches.

c [w/w%]	G^*_p [Pa]		
	H	**M**	**A**
5	5173.2±215.4	336.2±26.4	38.0±1.1
10	7113.5±800.5	981.4±98.3	59.5±8.2
20	16295±1828	3293.4±322.9	1056.3±88.2
30	54057±5421	28770±566	5430±219
40	133725±10008	75026±1110	50706±676
50	193901±10331	152210±16878	104246±15139

Table 3.4: G^*_p at T_p for all RSs at various concentrations

From Fig. 3.9 it is possible to observe that for all resistant starches analyzed G^*_p increases monotonically with concentration. For this reason, it can be concluded that the higher the concentration, the higher the modulus at peak temperature. Moreover, it can be observed that the G^*_p curve for Hylon is higher compared to Hi-Maize and Amioca. This evidence suggests that H samples are more consistent than the other two resistant starches mixtures at all the concentration.

The amount of amylose seems to play a central role in the structuration of the system. As said above, the linear chains of amylose can entangle each other very effectively, so the higher number of amylose molecules are present, the stronger structure can be generated (Chen Li et al.,2020).

In the end, it can be concluded that the obtained behaviour can be ascribed to the amylose as concern the "consistency" of the system inside which it is inserted. In fact, increasing the amylose increase the final complex modulus (Fig.3.9).

3.1.2 Frequency sweep tests analysis and interpretation

As written in previous sections, the frequency sweep tests were performed on gelatinised samples. Analysis can then give information on the structure of these systems after temperature conditioning. In Fig. 3.10, a typical trend of the complex modulus as a function of frequency is shown. In the range of frequency analyzed, the G* trend for samples analyzed is linear, with different slopes for the different samples. This behaviour is confirmed also in literature for similar systems (Lovedeep K.et al., 2007; Baldino et al., 2018; Baixauli et al., 2008). The data can be well interpreted by a power law equation ($G^* = A \cdot \omega^n$), as explained in Chapter 2, eq.2.7. Both for viscoelastic gel and fractional models, the equation is the same, only the physical interpretation changes. The pre-exponential factor, *A*, is a direct measure of the network strength, while the exponent *n*, indicates the network extension. Smaller *n* values correspond to a more extended network (Baldino et al., 2018).

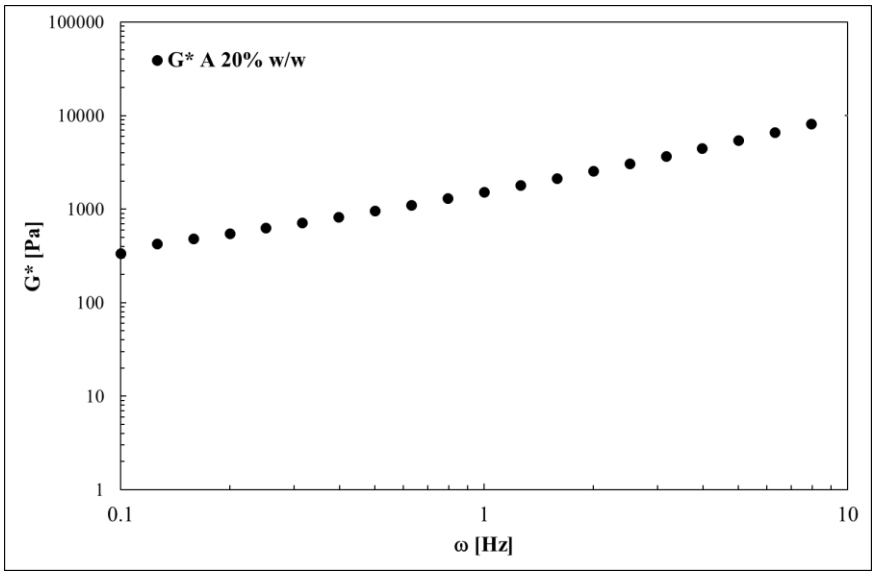

Figure 3.10: Typical trend of G* modulus as a function of frequency.

Since frequency sweep test is carried out on pregelatinized samples, retrogradation phaenomena could occur. This term is used to indicate the starch recrystallization occurring during the cooling following thermal treatment. These structure changes occur because starchy gelatinised systems are not in thermodynamic equilibrium conditions (Gudmundsson, 1994; Frost et al.,2009). However, as it will be shown below, time cure and frequency results give similar information about the structure strength of the three resistant starches investigated: at the same concentration, H has the stronger structure while A the weaker one, M being intermediate between them. This could be due to the fact that amylose-rich systems reach attains a stable structure very quickly, while amylopectin ones take a very long time (several weeks) to undergo retrogradation (Gudmundsson, 1994; Frost et al., 2009). Since pregelatinized samples were investigated soon after cooling, their structure does not undergo drastic changes compared with the hot gels (Gudmundsson, 1994).

In Tables, 3.5, 3.6 and 3.7, gel model parameters for all samples analysed are summarized and discussed.

c_H [% w/w]	A [Pa]	n [-]
5	308±23	4.96E-02 ± 9E-04
10	17434±698	5.48E-02 ± 5.4E-03
20	112731±5061	5.71E-02±1.6E-03
30	99335±4772	5.42E-02±1.5E-03

Table 3.5: Frequency sweep fitting parameters for H at various concentrations.

From data reported in Table 3.5, it can be observed that *A* increases with concentration, suggesting a direct proportionality between concentration and network strength. The network extension, indicated by the *n* parameter, is almost the same for all the concentrations investigated, indicating that the resistant starch type H is able to generate a stronger structure, independently from the concentration used, in the range investigated. These data confirm the considerations inferred from time cure tests data analysis.

c_M [% w/w]	A [Pa]	n [-]
5	93.4 ± 0.2	7.60E-02 ± 1.4E-03
10	230.1 ± 0.6	7.54E-02 ± 1.9E-03
20	5885 ± 8	5.95E-02 ± 1E-03
30	38261 ± 87	5.81E-02 ± 1.6E-03

Table 3.6: Frequency sweep fitting parameters for M at various concentrations.

From data reported in Table 3.6, it is possible to notice that as concentration increases, network strength increases too and also the network extension exhibits the same dependency with the concentration since the mean *n* values decrease as it increases. It is worth noting that for 5% and 10% w/w of H, *n* values are quite similar, and the same can be said for samples at 20 and 30% w/w suggesting that the different crystalline phases are generated in dependence on the used concentration (Fweng et al., 2009).

c_A [% w/w]	A [Pa]	n [-]
5	7.31 ± 0.03	4.81E-01±3E-03
10	293.3 ± 0.6	7.00E-01 ± 5E-03
20	1461 ±32	8.26E-01 ± 6E-03
30	5192 ± 76	1.04E +00 ± 6E-03

Table 3.7: Frequency sweep fitting parameters for A at various concentrations.

Analysing the data from Table 3.7 for the mixtures pregelatinized with starch A, it is observable that *n* value increases with concentrations, suggesting that the network is less extended when a higher amount of this resistant starch is present in the system. This behaviour finds confirmation in literature (Fweng Xie et al., 2009; Chen Li et al.,2009; Yu et al., 2005) and in particular, it can be confirmed that amylopectin in normal starch cannot generate a well-extended network, since lateral branches cannot entangle in a very effective way. On the other hand, it is possible that samples made with A

starch, do notgenerate networks, but a cluster structure (Fweng et al.,2009), so being modelled also with fractional models (Faber et al., 2017).

In the following histograms, a comparison among three resistant starches is introduced, both for *A* and *n* parameters.

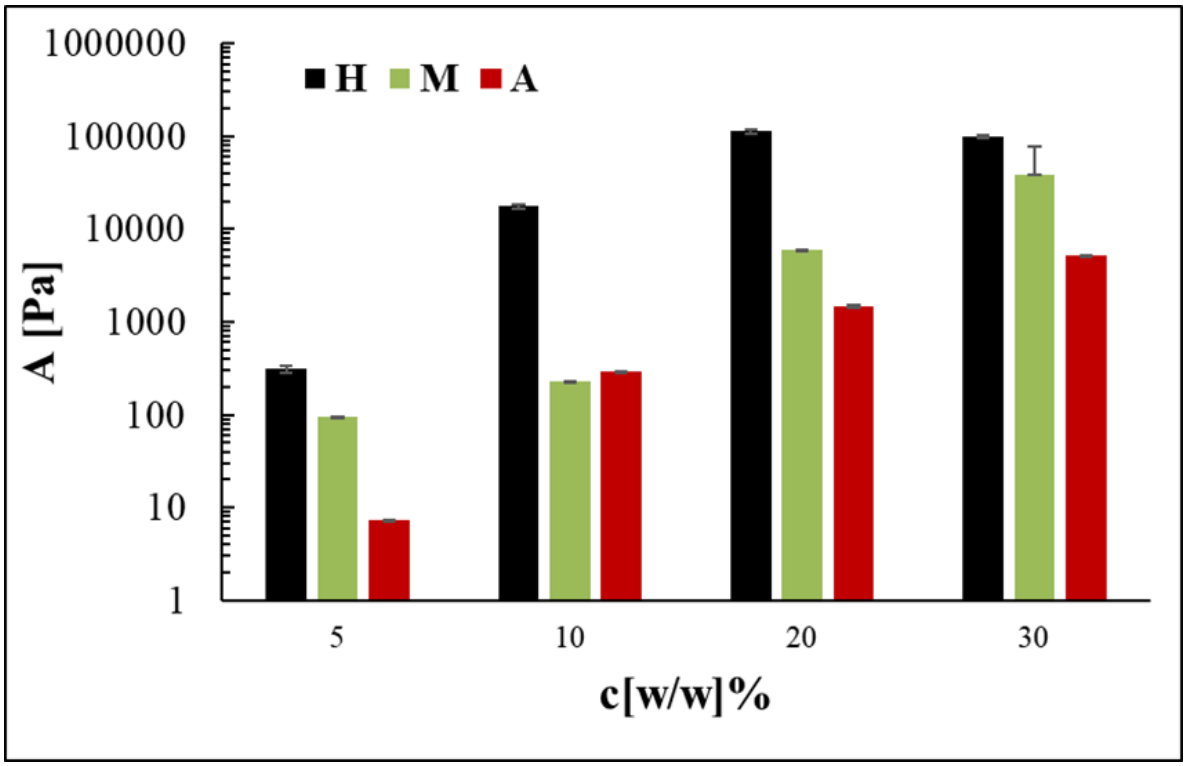

Figure 3.11: Comparison of network strength, *A*, for all the resistant starches investigated as a function of concentration

From Fig.3.11, it can be seen that H samples have the stronger network, while A the weaker, and M samples are intermediate between H and A. This is due to the presence of amylose, which can generate a strength network by entangling linear molecules. Of consequence, a major amount of amylose can generate a stronger structure. It can be also observed that over a certain concentration, the system can be considered saturated, and the structure strength does not vary anymore. This is evident by comparing H samples at 20% and 30%, H and M samples at 30%. The comparison among *A* values can be very important for rheological product design. The strength of the network (or any type of structure) is strictly related to technological and sensorial final product properties, such as firmness, springiness, rubberiness and so on (Faber et al., 2017). Thus, if a strong consistency material has to be designed, and amylose rich resistant starch blend is suitable, near to hylon and maize materials; while if more soft food is desired, the blend will be rich in amylopectin, since it has been shown that has the weaker structure among all resistant starches investigated. These considerations will be resumed in the final applications section.

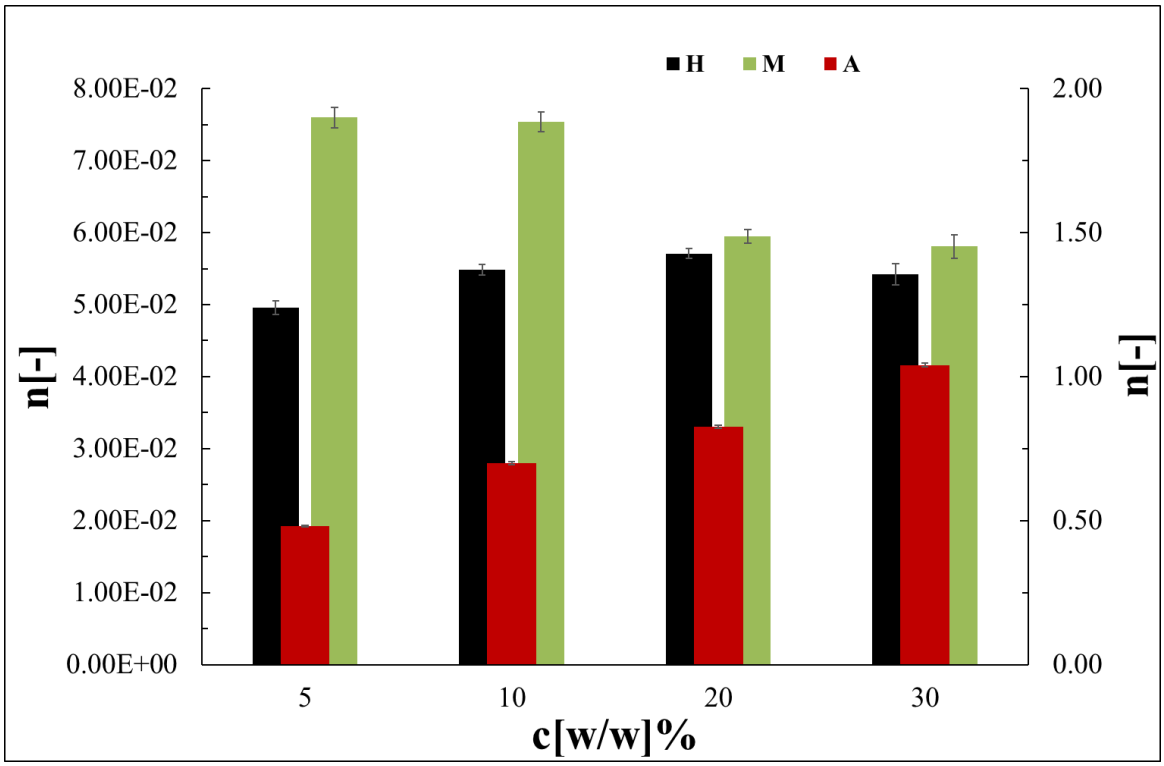

Figure 3.12: comparison among n parameters for three resistant starches in the function of concentrations.

In Figure 3.12, a comparison among *n* parameter values for three resistant starches is shown. Values relative to H and M samples are shown on the left vertical axis, while for the A sample the parameter value is reported on the right axis.

It can be said that A samples are less structured than the other resistant starches, confirming that amylopectin is not able to generate an extended network, or that does not get a network structure. As suggested in the time cure section, the network characteristics do not depend only on the amount and the presence of amylose, but also on the interaction between the form of amylopectin contained in resistant starches, more crystallized than that contained in normal starch (Chen Li et al,, 2020; Richardson et al.,2000), and amylose, as explained in the previous section. If a cluster structure is assumed for A samples (Jinchuan et al., 2020), the *n* paramenter assumes the meaning of the derivative order relative to the constitutive equation able to describe the system

3.2 Pea protein results and discussion

3.2.1 Time cure

Time cure tests on pea proteins at different concentrations were performed to obtain information on the thermo-rheological properties of these proteins. In the following Figure 3.12, an example of the complex modulus and phase angle of pea proteins samples.

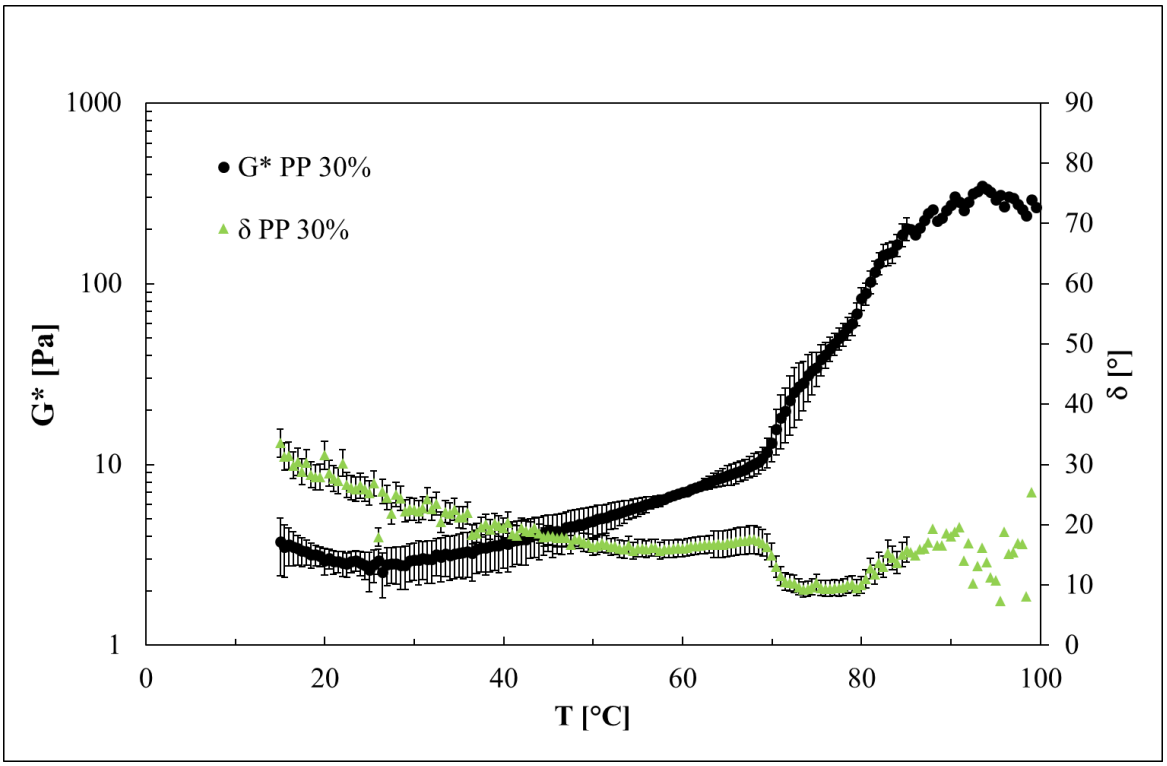

Figure 3.13: Typical trend of G* and δ for Pea proteins mixtures.

In Fig.3.13, it can be seen that the G* modulus and δ angle slightly decrease for kinetic effects, while, after a certain temperature, there is a sudden increase of G* modulus and a decrease of phase angle due to the denaturation of proteins. Differently from the gelatinization mechanism of starches, for proteins, a denaturation process is suggested, during which proteins lose their quaternary structure and can aggregate in a gel aggregate. In this case, the denaturation of globular pea protein led to an unfolding of the protein, that lose its spherical shape. Of consequence, interaction sites results exposed and become able to make linkages with other sites. This results in the clustering of the system. ((Shand et al., 2007; Munialo et al., 2015; Clark et al., 2001). Pea proteins are a mixture of different species and are very complex molecules, so several mechanisms in gel formation can be supposed. In fact, according to literature, there at least three steps involved in globular protein forming gel (Clark et al., 2001). The first provides the unfolding of proteins with the increase of temperature, during which tertiary and quaternary structure is loosed; the second step involves the formation of fibrils, namely cylindrical aggregates among unfolded proteins. This kind of structure can be formed both for an irreversible chemical reaction involving functional protein groups (as classic Flory's gelation theory provides) and physical interactions, that can be reversible (Clark et al., 2001). Finally, in the third step, a network or cluster structure can be formed by fibril aggregation. This sequence is strongly temperature and concentration dependent, as observed in time cure test analysis. From data, it was possible to evaluate the onset temperature of denaturation, while peak

temperatures were not always well identifiable. In the following Table 3.8 and Fig. 3.14 onset temperatures were reported.

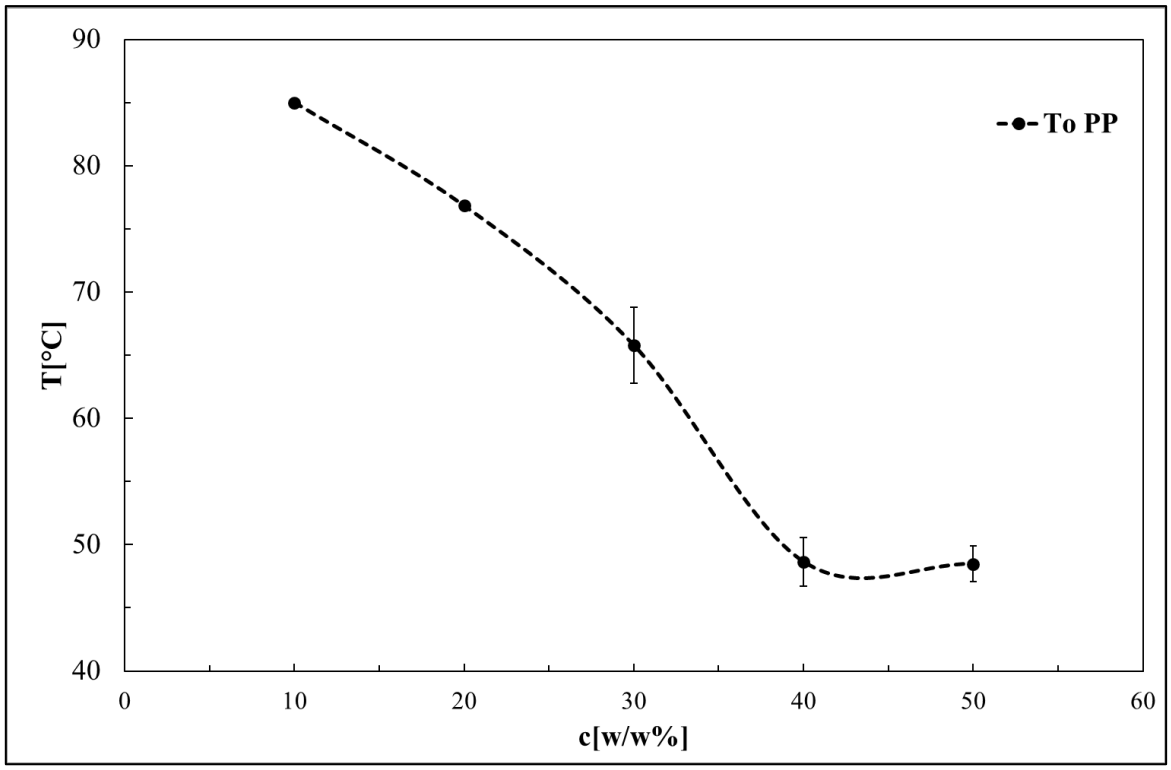

Figure 3.14: Onset temperature trend for Pea proteins as a function of concentration.

c [w/w%]	T_o [°C]
	PP
10	85.0 ± 0.1
20	76.8 ± 0.4
30	61.9 ± 0.9
40	48.6 ± 1.9
50	48.5 ± 1.4

Table 3.8: Onset temperature, To, for pea proteins at the different concentration analysed.

From the trend reported in Fig. 3.14, it possible to observe that going from low to high concentrations, T_o decreases, till it reaches a plateau at 40% w/w. This can be because a higher amount of proteins in the systems can form a gel at a lower temperature. The onset temperature individuated from data is

the temperature in correspondence of which a visible variation in terms of G* and δ is observed. This temperature decreases with the increase of concentration, clearly indicating that more amount of proteins is present in the system before the gel aggregates can be obtained, as can be inferred from the above considerations (Clark et al., 2001).

3.2.2 Frequency sweep tests results

Frequency sweep tests performed on pregelatinized pea proteins samples can give information about the strength and the extension of the structure. The trend of G* is almost linear for all the concentrations analyzed, so again a power-law equation can be used. If the viscoelastic gel model is used, the parameters obtained assume the same meaning explained in the previous section. The gel-like answer in the frequency sweep test is confirmed also in literature (Clark et al., 2001). Numerical values are reported in Table 3.9.

c_{PP} [% w/w]	A [Pa]	n [-]
5	1043 ± 70	1.10E-01 ± 3E-03
10	1320 ± 140	1.09E-01 ± 1E-03
20	8070 ± 505	1.09E-01 ± 3E-03
30	38283 ± 2050	1.40E-01 ± 1E-03

Table 3.9: Frequency sweep parameters for PP samples at different concentrations.

From Table 3.9 it is evident that the strength of these samples increases with concentration. This can be explained by suggesting that a larger amount of proteins can generate a stronger gel either forming a stronger network among the denatured protein chains, either by aggregating a higher number of clusters, linked together by electrostatic forces, which results in a stronger jellified phase (Munial et al., 2005). In light of protein gelation theory introduced in literature (Clark et al., 2001), both network structure and clusters aggregate is present in the system. As concerning the *n* parameter, it is observable that don't change changing the concentration, suggesting that the structure formed is almost the same. Moreover, the low numerical value of *n*, suggests a well-extended value and a solid-like behaviour (Munial et al., 2005).

Bibliography

R. Baixauli, T. Sanz, A. Salvador, S.M. Fiszman (2008), Muffins with resistant starch: Baking performance in relation to the rheological properties of the batter, *Journal of Cereal Science* 47 502–509

Blanshard, J.M. V. (1979). Physicochemical aspects of starch gelatinization, ‘‘*Polysaccharides” in Foods’’ (J. M. V. Blanshard and J. R. Mitchell, eds.), pp. 139–152. Butterworths & Co.(Publishers) Ltd., London.*

Noemi Baldino, Francesca Laitano, Francesca R. Lupi, Stefano Curcio, Domenico Gabriele (2018), Effect of HPMC and CMC on rheological behavior at different temperatures of gluten-free bread formulations based on rice and buckwheat flours, *European Food Research and Technology* 244:1829–1842

Cheng Li, Bo Gong (2020), Insights into chain-length distributions of amylopectin and amylose molecules on the gelatinization property of rice starches, *International Journal of Biological Macromolecules* 155 721–729

A.H. Clark, G.M. Kavanagh, S.B. Ross-Murphy (2001), Globular protein gelation-theory and experiment; *Food Hydrocolloids* 15 383-400

Donovan, J. W. (1979). Phase transitions of the starch-water system. *Biopolymers* 18, 263–275.

T.J. Faber, A. Jaishankar, G.H. McKinley (January 2017), Describing the firmness, springiness and rubberiness of food gels using fractional calculus. Part I: Theoretical framework, *Food Hydrocolloids*, Volume 62, Pages 311-324

T.J. Faber, A. Jaishankar,, G.H. McKinley (2017), Describing the firmness, springiness and rubberiness of food gels using fractional calculus. Part II: Measurements on semi-hard cheese, *Food Hydrocolloids* 62 325e339

Frost Kris, Daniel Kaminski Gemma Kirwan EdmondLascaris, RobertShanks (2009), Crystallinity and structure of starch using wide angle X-ray scattering, *Carbohydrate Polymers*, Vol.78, 3, 543-548.

Gudmusson M. (1994), retrogradation of starch and the role of its components, *Thermodinamica Acta* 246, 329-341,

Eliasson, A.-C. (1980). Effect of water content on the gelatinization of wheat starch. Starch/Starke. *Verlag Chemie*. GmbH, D-6940 Weinheim, 270–272.

Fengwei Xie, Long Yu, Bing Su, Peng Liu, Jun Wang, Hongshen Liu, Ling Chen (2009), Rheological properties of starches with different amylose/amylopectin ratios, *Journal of Cereal Science* 49 371–377

Flory, P. J. (1949). Thermodynamics of crystallization in high polymers. IV. A theory of crystalline states and fusion in polymers, copolymers, and their mixtures with diluents, *The Journal of Chemical Physics*, 17, 223–240.

Hui-Huang Chen *, Hong-Yi Kang, Su-Der Chen (2008), The effects of ingredients and water content on the rheological properties of batters and physical properties of crusts in fried foods, *Journal of Food Engineering* 88 45–54.

Jinchuan Xu, Andreas Blennow, Xiaoxi Li, Ling Chen, Xingxun Liu (2020), Gelatinization dynamics of starch in dependence of its lamellar structure, crystalline polymorphs and amylose content, *Carbohydrate Polymers* 229 115481

Gohar Khachatryan, Lidia Krzeminska-Fiedorowicz, Ewelina Nowak, Maciej Fiedorowicz (2014), Molecular structure and physicochemical properties of Hylon V and Hylon VII starches illuminated with linearly polarised visible light, LWT, *Food Science and Technology* 58 256e262

Lingshang Lin, Canhui Cai, Robert G. Gilbert, Enpeng Li, Juan Wang, Cunxu Wei (2016), Relationships between amylopectin molecular structures and functional properties of different-sized fractions of normal and high-amylose maize starches, *Food Hydrocolloids* 52 359e368

Claire D. Munialo, Erik van der Linden, Komla Ako, Hamen H.J. de Jongh (2015), Quantitiative analysis of the network structure that underlines the transitioning in mechanical responses of pea protein gels, *Food Hydrocolloids* 49 104-117

Ratnayake, W. S. and Jackson, D. S. (2007). A new insight into the phase transition process of native starches. *Carbohydr. Polym*. 67, 511–529

Sara Richardson, Gunilla S. Nilsson, Karl-Erik Bergquist, Lo Gorton, Petra Mischnick (2000), Characterisation of the substituent distribution in hydroxypropylated potato amylopectin starch, *Carbohydrate Research* 328 365–373

P.J. Shand, H. Ya, Z. Pietrasik, P.K.J.P.D. Wanasundara (2007), Physicochemical and textural properties of heat-induced pea protein isolate gels, *Food Chemistry* 102 1119–1130

Takahiro Noda, Yasuhiro Takahata, Tetsuo Sato, Ikuo Suda, Toshikazu Morishita, Koji Ishiguro, Osamu Yamakawa (1998), Relationships between chain length distribution of amylopectin and gelatinization properties within the same botanical origin for sweet potato, and buckwheat, *Carbohydrate Polymers* 37 153–158

F. Teyssandiera, Cassagnaua, J.F. Gérardb, N. Mignard (2011), Sol-gel transition and gelatinization kinetics of wheat starch, *Carbohydrate Polymers* 83 400-406.

Vermeylen, R., Derycke, V., Delcour, J. A., Goderis, B., Reynaers, H., and Koch, M. H. J. (2006). Gelatinization of starch in excess water: Beyond the melting of lamellar crystallites, A combined wide- and small-angle X-ray scattering study, *Biomacromolecules* 7, 2624–2630.

Yong-Cheng, Shi Paul, Seib (1995), Fine structure of maize starches from four wx-containing genotypes of the W64A inbred line in relation to gelatinization and retrogradation, *Carbohydrate Polymers*, Volume 26, Issue 2, Pages 141-147

Chapter 4:
Interfacial analysis: results and discussion

In this chapter, interfacial analysis results are exposed and discussed. Before discussing results, resistant starch and pea protein solubility investigation is reported. Then, in the first part, data related to static measurements at the interface and their interpretation is reported, while in the second part dynamic oscillatory results, together with model parameters are discussed. Finally, in the third part, transient relaxation test results are reported with their explanation and discussion.

4.1 Resistant starch and pea protein solubility

RS are not very soluble in water at room temperature, but anyway, their solutions have some interfacial activity. For this reason, two kinds of solubility test, one qualitative and one quantitative, were performed on the solution at 1% w/w of each in pure twice-distilled water at room temperature, since interfacial measurements were performed on samples prepared in these conditions. The solutions were mixed for 1 hr using a magnetic stirrer (AREX Heating Magnetic Stirrer, Velp Scientifica, Italy), and then centrifugated to separate the insoluble part from the rest of the solution, using Centrifuge 5810, Eppendorf, Italy, at 2900 rpm, for 30 minutes, following the same procedure used to obtain the solutions for the interfacial measurements. Resulting solutions were analysed.
The qualitative test was conducted by adding the Lugol reagent to the solutions, and noting the colour variation, as shown in Fig. 4.1:

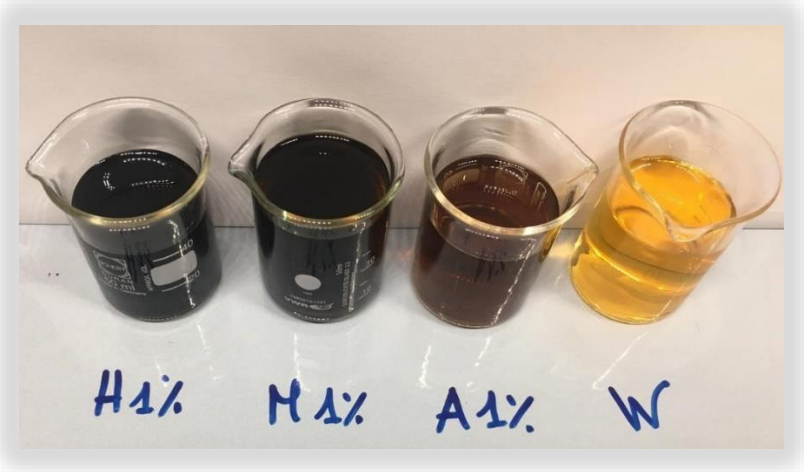

Figure 4.1: Colour comparison of RS starches solutions and pure distilled water.

As can be observed in Fig.4.1, there are evident colour differences among the RS starch solutions. Lugol reactive can complex with both amylose and amylopectin: in the first case, the colour of the solution changes to dark blue, black, while in the second, the solution changes to dark brown. Adding Lugol reactive to pure water causes it to turn yellow. In the light of the above, H1% and M1% solutions colour change to black because these RS starches contain a high percentage of amylose. A1% solution, because it contains almost pure amylopectin, changes to dark brown. It can be concluded that in solutions there is an amount of RS solubilized. To obtain also quantitative information, precipitate solutions were analysed with a TGA analysis, using a Simultaneous Thermal Analyser (STA 449 F1 Jupiter®, NETZSCH, Germany), to evaluate the residual humidity and the results are shown in the Table 4.1.

	RS mass [g]	**Residual RS in solution [g]**	**Percentage of RS solubilized [%]**
M	1.030±0.007	0.527±0.013	51.1±5.0
A	1.083±0.094	0.574±0.071	53.1±2.1
H	1.002±0.002	0.403±0.094	40.3±2.3

Table 4.1: Single materials solubility results

Similarly, to understand the degree of solubility of PP, ζ-potential and spectrophotometry tests were performed on 1%w/w solution, whose results are shown in Fig.4.2:

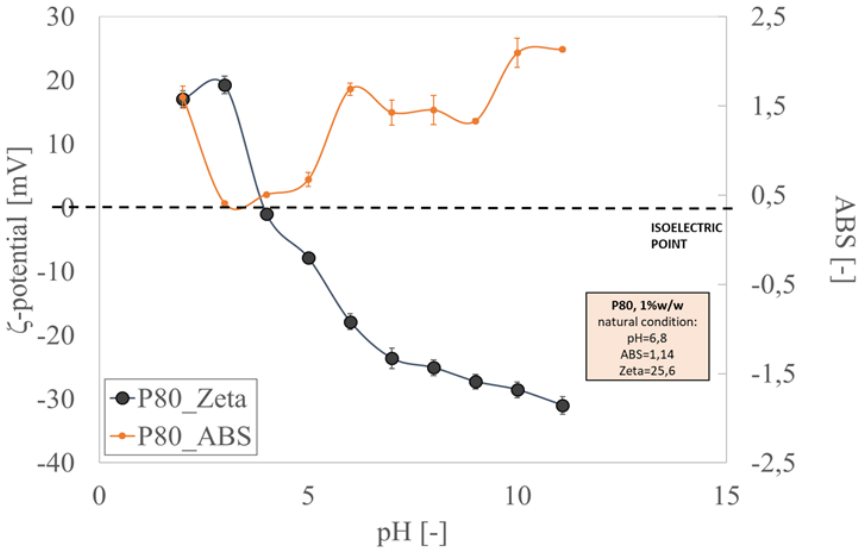

Figure 4.2: ζ-potential and spectrophotometry result for PP 1% w/w solution.

It was possible to evaluate the isoelectric point of the proteins used in correspondence with the pH value for which ζ-potential is zero, that is, around 4. At natural conditions, i.e. for a pH value of 6.8, the protein can be considered quite solubilized, considering that the ζ-potential value is negative, and this corresponds to solubilized species. The evaluated isoelectric point value is in agreement with that reported in the literature (Franco et al.2000).

4.2 Static measurement

In this section, static measurements results are given. The adsorption isotherm for a single component is illustrated, together with the equilibrium interfacial tension of the mixtures, while the kinetic parameters have been obtained and reported thanks to a single tension curve analysis.

4.2.1: Adsorption isotherm of single components and mixtures equilibrium surface tension

Interfacial tension measurements were performed on single component solutions, both for RS and PP at various concentrations to obtain a Gibbs isotherm, in which equilibrium interfacial tensions are plotted versus concentration. Equilibrium interfacial tension for each concentration was calculated by computing the mean value of the data when the interfacial tension reaches a constant value.

In Fig. 4.1 below, a comparison among the three Gibbs adsorption isotherms obtained for the three resistant starches is shown. Three significant features can be recognised for each curve: on the right of the figure, there is the Critical Micellar Concentration (CMC), namely the concentration in correspondence to which the interface can be considered completely saturated, over which a further increase in concentration does not produce any effect upon equilibrium surface tension. As concentration decreases, there is a decrease in the equilibrium interfacial tension until it reaches a minimum value. Finally, the further decrease in concentration causes equilibrium interfacial tension until it assumes the pure water value at very low concentrations.

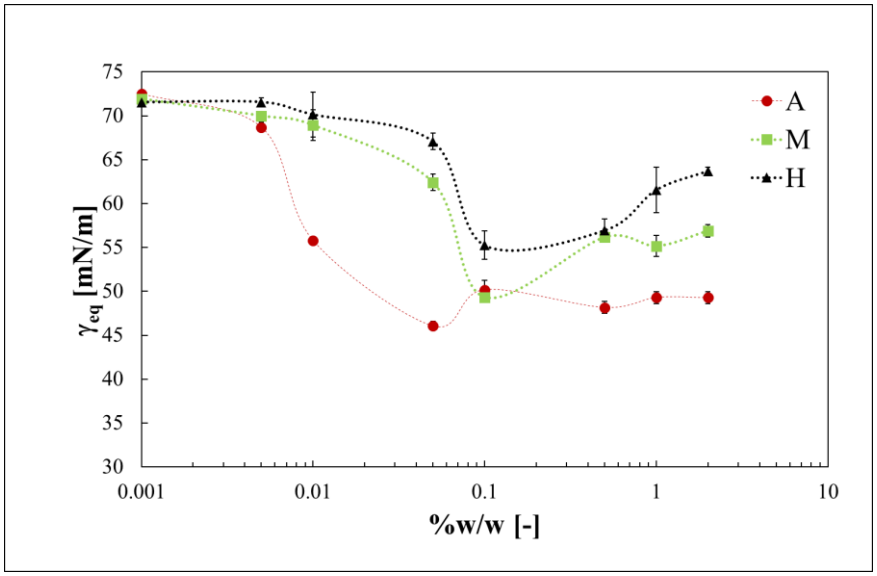

Figure 4.3: Comparison among adsorption isotherms for all three resistant starches analysed.

This type of behaviour reported in Fig. 4.3 is not common in the literature and it is very different from the sigmoidal behaviour exhibited by proteins (Seta et al.,2012). Moreover, the interfacial properties of starchy molecules have not been widely studied yet. Therefore to understand the characteristics of the interfaces analysed, it can be useful to introduce two molecular models, representative of spatial conformation of amylopectin and amylose (Ettalaie et al., 2016). These two models are pictured in Fig.4.4.

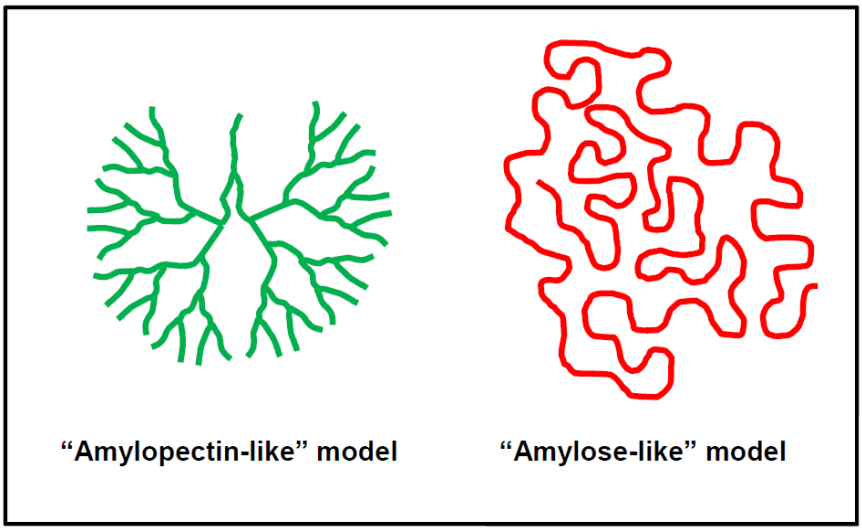

Figure 4.4: Molecular conformation models for amylopectin and amylose (Ettalaie et al., 2016)

The branched amylopectin structure and the linear conformational amylose are confirmed in several works (Fweng Xie et al., 2009; Chen Li et al.,2020). The interfacial behaviour exhibited by prepared

starchy solutions can be the result of several factors, among the more important are: electrostatic interaction, such as hydrogen bonds and Van der Waals forces (Israelachvili 2011); steric factors and relative degree of hydrophilicity and hydrophobicity (Ettalaie et al., 2016). Generally, amylopectin and amylose, having a certain degree of hydrophilicity, tend to avoid hydrophobic interfaces. This can be linked to the unfavourable entropy variation of these molecules near hydrophobic surfaces, such as air/water. However, amylopectin, because of its molecular branched conformation, has a lesser degree of swelling, because of the constraints imposed by its conformation, which prevents it from changing its structure to interact with the solvent. So, amylopectin is more hydrophobic than amylose (Ettalaie et al., 2016). From this point of view, amylopectin behaviour can be strictly compared with that of hard spheres, which can form a compact layer at the interface, thereby lowering interfacial tension. It was shown that amylopectin layers are thinner and denser than amylose ones. On the other hand, amylose, thanks to its flexible structure, can interact in a better way in the solvent, remaining in bulk and with consequently the worst interfacial power. In the amylose system, the interfacial layer is thus more diffused, with a less defined edge (Ettalaie et al., 2016). The systems analysed in this work are a mixture of amylopectin and amylose, as indicated in chapter 2; thus, the interaction between two species should be considered. A system composed of amylopectin and amylose can be assimilated to that constituted of globular and flexible proteins (Ettalaie et al., 2016; Parkinson&Dickinson 2004). The combination between a hard-sphere like a molecule with a flexible one can enhance the interfacial properties. This phenomenon was explained by introducing the "overgrown" garden model (Parkinson et al., 2005). In this perspective, spherical species, such as amylopectin, are dominant at the interface, while linear molecules of amylose can stabilize the system for electrostatic and steric interaction between the bulk and interfacial layer (Ettalaie et al., 2016). This kind of consideration can also be useful to explain the interfacial properties of resistant starch/pea protein mixtures. In the light of the above, adsorption trends in Fig.4.1 could be explained suggesting that at high concentrations, corresponding to the respective CMC, the H and M interfaces have a higher equilibrium interfacial tension than A interfaces, since they are richer in amylose than in amylopectin. On the other hand, A solutions, being almost pure amylopectin, have the higher interfacial power.

It can be speculated that the minimum of the curves, especially for samples H and M, can be due to the amylopectin that could be able to enrich quickly the interface with respect to amylose, but that is displaced from this last linear starch with a consequent increase in the interfacial tension when it is present in a higher concentration. Moreover, it is interesting to observe that the higher the amylose quantity the higher the interfacial tension.

The adsorption isotherm for pea proteins is also obtained and the result is reported in Fig. 4.3.

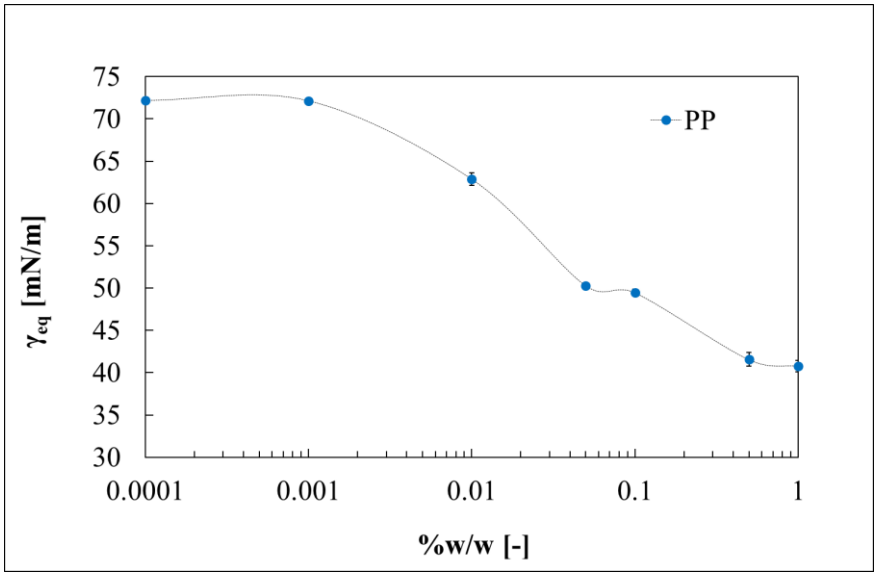

Figure 4.5: Adsorption isotherm plot for PP, where it is shown the trend of equilibrium interface tension of PP versus concentration.

The trend shown in Fig. 4.5 is almost sigmoidal as typically for a large variety of vegetable proteins (Mileti et al., 2018; Seta et al., 2012). At high concentrations, a lower plateau is present, corresponding to CMC, over which no changes in interfacial tension are recorded. As concentration decreases, there is an evident inflexion of the curve, in middle concentrations, between 0.1% and 0.05% w/w. The flattening of the curve can be because pea proteins are a mixture of different species, that, according to concentration, can form different kinds of interfacial layers (Bos et al., 2001). Finally, the concentration decrease causes an interfacial tension to increase until it reaches the pure water value.

The trend observed is consistent with the pea proteins composition. They are constituted, for the most part, of globulins (55%-65%), and the remaining by albumins (18%-25%), other than a little fraction of gliadin and glutenin (Barac et al., 2015; Tamnak et al., 2016). Globulins are made up of three species: legumin, which can be classified as the 11S fraction; vicilin and convicilin, namely, the 7S fraction. Legumin is characterized by a strong quaternary structure, stabilized by electrostatic, hydrophobic interactions and via disulphide bridges. Hydrophobic basic polypeptides are situated in the inner portion of legumin, while acid ones are facing outwards of the protein structure. It is a hexamer with an average molecular weight of 380 kDa (Barac et al., 2015). Vicilin has a trimeric constitution, which cannot be stabilized via disulphide because it lacks cysteine residues. Its average molecular weight is about 150-170 kDa. It is a heterogeneous protein since it has many residues with a net electrostatic charge, and others with a high degree of hydrophobicity. Finally, convicilin is similar to vicilin, but differently from the latter, it can be stabilized via disulphide. Its average

molecular weight is about 210 kDa. The core of protein is very similar to the vicilin one, but convicilin contains more charged hydrophilic residues, while the percentage of hydrophobic ones is like vicilin. In Fig.4.6 legumin, vicilin and convicilin just described characteristics are pictured.
The other class of proteins, albumins, have a flexible structure (Carter et al., 1994), variable average molecular weight in the range between [23-480] kDa (Karaka et al., 2011).

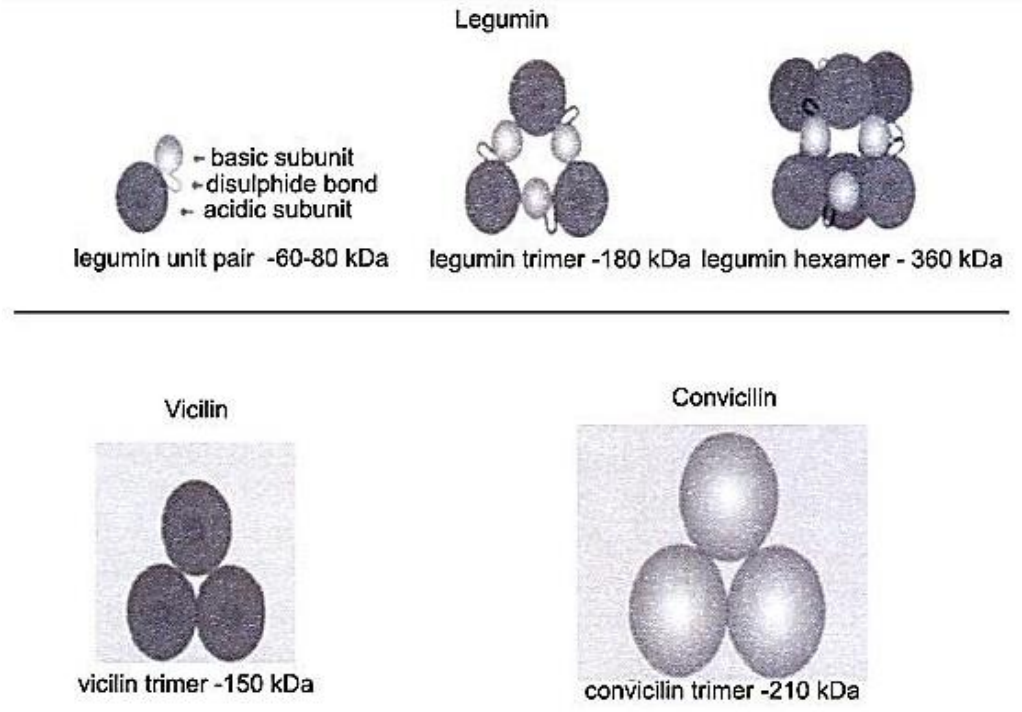

Figure4.6: Schematic representation about the structure of pea legumin, vicilin and convicilin (Barac et al., 2015)

Although the higher percentage of pea proteins is made up of globulin rather than albumins, the albumins role cannot be neglected. In fact, the shape of the isotherm can be attributed to the competition between them and this can justify the trend because from the literature species having a flexible quaternary structure such as albumins, show a tendency to unfolding and rearranging during adsorption at the interface, thus hard proteins, that do not show any significative changes during adsorption and rearrangement phaenomena (Mezzenga et al., 2013). The albumin rearrangement at interfaces and the possible displacing of pea globulin results in a lowering of equilibrium interface tension (Mezzenga et al., 2013; Bos et al., 2001; Arai&Norde 1990; Seta et al., 2011).
After evaluating the equilibrium interfacial tensions of the individual materials with varying concentrations, the focus was placed on the mixtures between each resistant starch and pea proteins. The ratios utilized were summarised in chapter 2. For each mixture, equilibrium interfacial tension was evaluated, according to the procedure described in chapter 2.

In the following Figs. 4.6,4.7, and 4.9 the mixtures interface tension results are summarized.

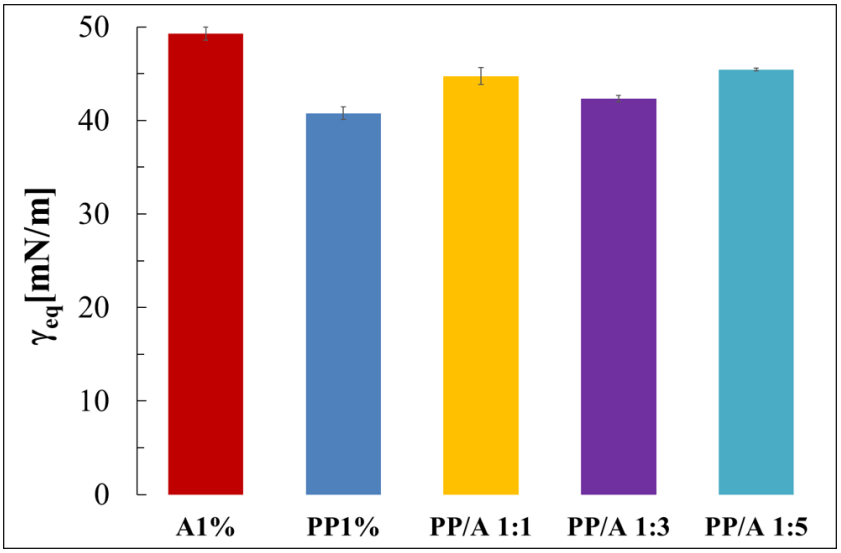

Figure 4.7: Comparison of equilibrium interfacial tensions of PP/A mixtures, compared to the pure proteins and starch mixtures.

In Fig.4.7 equilibrium interfacial tensions for PP/A mixtures are shown. As it can be seen, the values of the interfacial tension for the mixtures are in the middle between the pure proteins and the pure starch. This evidence could suggest the presence of a competitive effect between pea proteins and amylopectin. This topic will be discussed later. The mixture PP/A with a ratio of 1:3 has a mean interfacial value smaller than other mixtures. This could be explained assuming that there is an interfacial layer configuration for this ratio at which interactions between amylopectin and pea proteins are optimized.

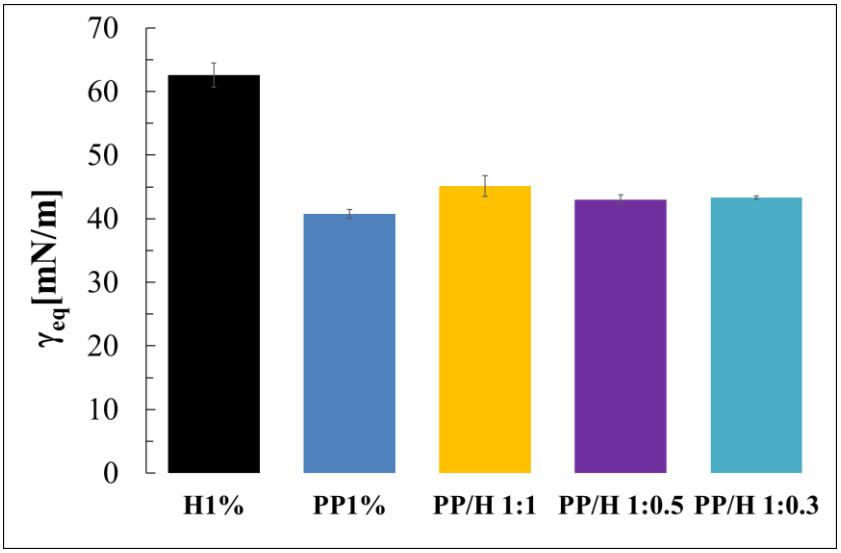

Figure 4.8: Comparison of equilibrium interfacial tensions of PP/H mixtures, compared to the pure proteins and starch mixtures.

In Fig.4.8, equilibrium interfacial tensions of PP/H mixtures are shown. As can be seen, interfacial tension values of mixtures are very similar to PP 1% value because a small amount of this starch was used, because from bulk results it was shown that Hylon was the most resistant starch, with a high structuring power compared to amioca starch. For this reason, because of future applications, just a little amount of Hylon resistant starch needs to be used.

Owing to the lower amount of amylopectin in this starch than previous starch, it can be said that the trend obtained is expected due to the amylose structure which can confer low interfacial activity to Hylon with respect to starches with a higher percentage of amylopectin inside (Ettalaie et al.,2016).

Even if the interfacial activity of pure Hylon is high, a positive effect can be observed of the interaction between hard-sphere like molecules, such as pea globulin, and linear molecules, such as amylose, especially at ratio 1:1.

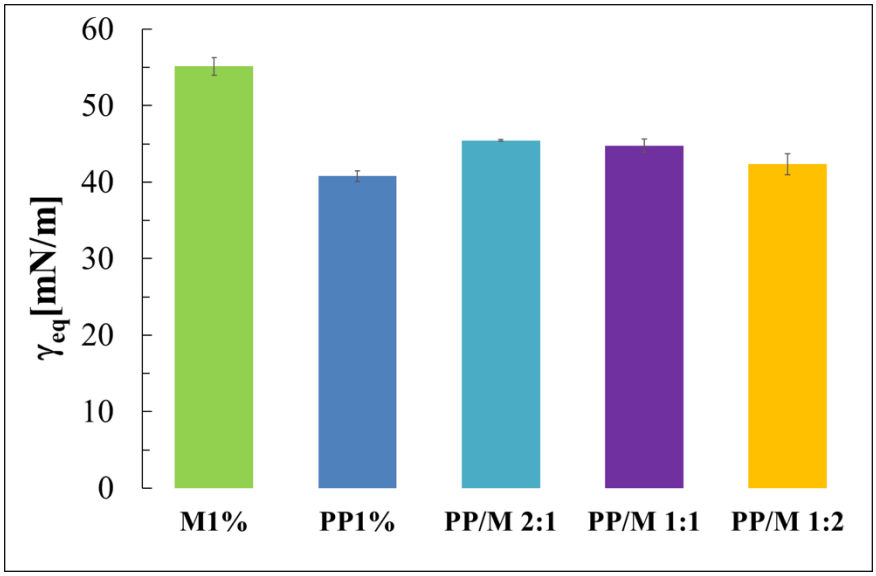

Figure 4.9: Comparison of equilibrium interfacial tensions of PP/M mixtures, compared to the pure proteins and starch mixtures.

In Fig.4.9 equilibrium interfacial tensions of PP/M mixtures are shown. As can be observed, M1% interfacial tension value is almost similar to H1%. This can be due to the similar composition between M and H resistant starches since both are rich in amylose (the former at least 56%, the second 70%). Mixtures equilibrium interfacial tension values are quite similar, all higher than PP1%. This could be due to a competitive effect between globular pea proteins and hard-sphere like amylopectin molecules present in Hi-maize starch, since both have a certain degree of hydrophobicity, and both aim to obtain interface and minimize interaction with water (Eliatte et al., 2016; Bos et al., 2001; Mezzenga et al., 2013).

4.2.2 Kinetic parameters

In this section, kinetic parameters are shown and discussed. As explained in Chapter 2, the kinetic mechanism involves three main steps: diffusion from bulk to interface, molecular adsorption at the interface; molecular rearrangement (Seta et al. 2011; Bos et al.,2001). In Fig.4.10 a schematic representation of the kinetic mechanism about soft proteins is shown.

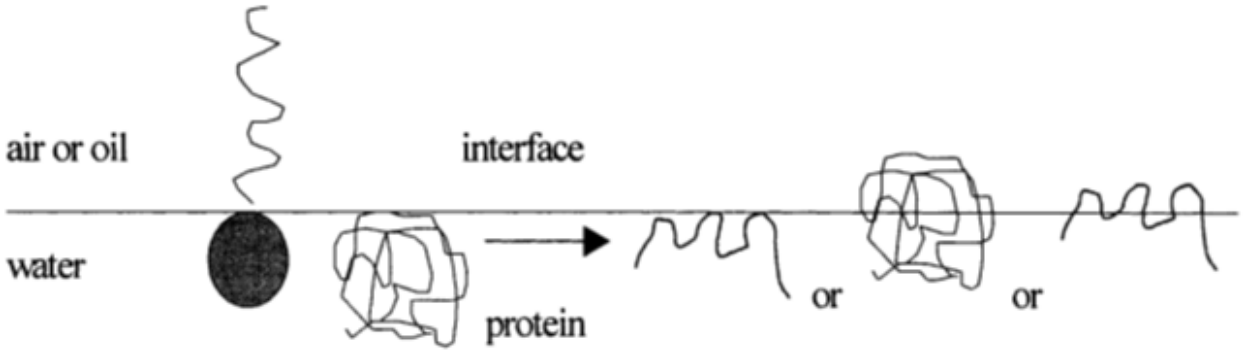

Figure 4.10: Schematic representation of three steps of the kinetic mechanism of proteins (Bos et al., 2001).

Molecular diffusion from the bulk to interface is determined by several factors like the molecular weight, the spatial conformation, the electrostatic interaction with solvent and the viscosity of the medium, other than temperature and solute bulk concentration (Bird et al, 2007; Seta et al. 2011; Best et al., 2002). It can be said that sphere-like molecules can diffuse better than random coil molecules (Bird et al., 2007; Callaghan et al., 1985). This information can be useful to explain the diffusion rate of the systems investigated.

Once solute molecules arrive at the interface, molecular adsorption occurs. Molecular interfacial adsorption is a very complex phenomenon, involving several factors, such as geometrical form, interactions with the solvent, steric factors and so on (Mezzenga et al., 2013). In pea proteins/resistant starches systems, there are hard-sphere-like molecules, such as pea globulins and amylopectin (Eliatte et al., 2016; van Vliet et al., 2002); linear hydrophilic molecules, such as amylose (Eliatte et al., 2016); albumins pea protein, with a soft-flexible structure (Mezzenga et al., 2013). Proteins adsorption can be often assumed irreversible, once equilibrium is reached. There is a difference between hard-sphere-like and flexible soft-structure molecules. Hard-sphere molecules, such as pea globulins, do not undergo any significant changes in their structural conformation during both adsorption and rearrangement, remaining in their spherical form and forming a compact interfacial layer thanks to hydrophobic effects and steric factors (Bos et al., 2001; Israelechvili, 2013). For molecules with flexible structure, such as albumins (Mezzenga et al., 2013), structural changes can occur thanks to which structure can be more stabilized, and thus the overall interfacial layer

(Mezzenga et al., 2013). This kind of stabilization, accomplished with the conformational change of soft molecules (called also molten globules) during adsorption and rearrangement, is due to the unfolding of the quaternary structure of albumins, by which they can expose hydrophilic groups toward the water, and hydrophobic ones toward the air, this way optimizing interactions (Mazzenga et al., 2013). Moreover, during rearrangement, further structure modifications can occur, and often flexible molecules, diffusing more slowly than hard-sphere like ones (Bird et al., 2007), can displace hard-sphere and rearrange at the interface (Bos et al., 2001; Mileti et al., 2019). Amylopectin, being made up of hydrophobic hard-sphere-like molecules (Eliatte et al., 2013), does not undergo any structural changes during both adsorption and rearrangement, realizing a compact insoluble layer, stabilized by hydrophobic and steric factors (Eliatte et al, 2013; Bos et al., 2001; Mezzenga et al. 2013). So, amylopectin hard-sphere molecules behave similarly to pea globulin. On the other hand, amylose linear molecules, having a certain degree of hydrophilicity, are able to stabilize the interfacial layer by extending the interaction range between the interface and bulk (Eliatte et al., 2013). Thus, after these considerations, it can be suggested that in these systems amylopectin and pea proteins adsorb first; during adsorption and rearrangement, albumins can change their conformational geometries and sometimes displace pea globulins; while amylose, adsorbing later thanks to its hydrophilicity, can interpose between the interfacial layer made up of globular species, interacting both with protein and amylopectin (with complex formations, hydrogen bonds, weak electrostatic interactions), this way extending the interfacial interactions range, and making the interfacial layer more "diffused" toward bulk (Mezzenga et al., 2013; Eliatte et al., 2016; Bos et al., 2001; Israelivchili et al., 2013). It is well known from the literature that the interfacial layer can be defined as the range of interactions in the region between two thermodynamic phases (Mezzenga et al., 2013; Israelivhili et al., 2013; Slattery et al., 2007). A compact insoluble monolayer, made up of hard-sphere-like molecules (such as amylopectin and pea globulins), has a relatively short interaction range; while, in the presence of hydrophilic molecules, such as amylose, the range of interaction can be increased, thus resulting in an extended and diffused interfacial layer.

In the light of the above, an attempt will be made to interpret the kinetic data. In Figs.4.11, 4.12, and 4.13 kinetic parameters for PP/A mixtures and the samples A1% and PP1%, taken as reference, are reported.

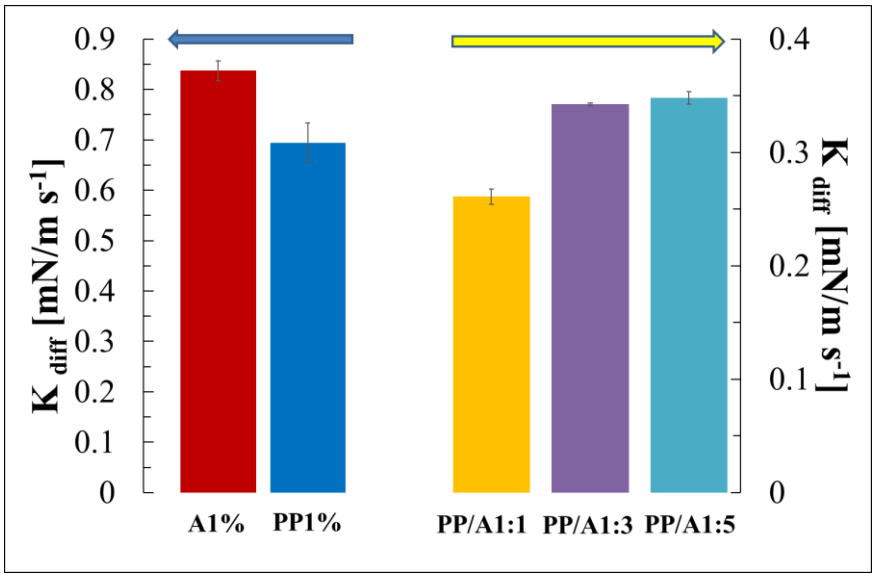

Figure 4.11: Diffusion rate for PP/A mixtures compared to A1%and PP1% pure samples.

In Fig.4.11 can be observed the K_{diff} coefficients for the samples analysed. The diffusion coefficient for the mixtures is reported in the right part of the graph due to the different scale compared to the pure substances, while pure materials are shown on the left axis.

As can be observed, the A1% and PP1% diffusion coefficients are much higher than those related to mixtures therefore they diffuse quickly at the interface compared to the mixtures. In general, in fact, the viscosity of suspensions of hard-sphere molecules, as can be considered amylopectin and pea globulins (Ettalaie et al., 2016; Barac et al., 2015) increases with the width of the hydrodynamic radius distribution (Bird et al., 1987; de Kruif et al., 1985). It can be observed to this end that in the mixtures a wide range of spherical molecules with different molecular radii is present since there are amylopectin and pea globulins, so the viscosity of the solution is higher, and the diffusion rate could be lower than in single materials systems for this reason. As a confirmation of this, it can be observed that in correspondence to the PP/A 1:1 mixture a minimum of the diffusion coefficient is present. In PP/A 1:1, there is a large amount of pea globulins and amylopectin. The pea globulins mean radius is smaller than amylopectin one (Eliatte et al., 2018; Barac et al., 2015) but since both species incomparable amount are present, the hydrodynamic radius distribution is wide. It can be speculated that the latter system has a molecular radius distribution higher than the other mixture analysed since it has a lower percentage of PP. In fact, the diffusion rate coefficient increases as A content in the system increases, since hydrodynamic radius distribution is less wide, being a higher percentual of one species, namely amylopectin. Thus, the trend observed can be explained in the light of the viscosity decrease passing from PP/A 1:1 to PP/A 1:5.

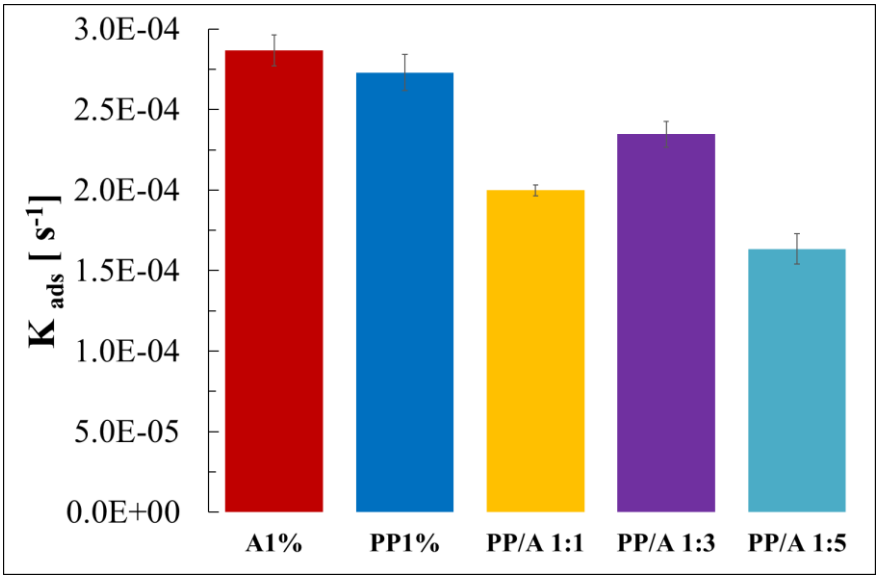

Figure 4.12: Adsorption rate for PP/A mixtures compared to pea protein and starch mixtures.

In Fig.4.12, adsorption rate coefficients for PP/A, A1% and PP1% are reported. For A1% and PP1%, the values of the adsorption coefficient are higher than the values relative to mixtures. The values of A1% and PP1% are almost similar, which could suggest that the adsorption mechanisms are the same, since both molecules have spherical geometries (Eliatte et al., 2016; Barac et al., 2015). Hard-sphere molecules tend to form a compact layer, at large concentrations (CMC), stabilised by steric factors (Bos et al., 2001). The adsorption coefficients of mixtures are lower than single components ones. This experimental evidence could suggest a competitive effect between amylopectin and pea proteins. Both species have a certain degree of hydrophobicity (Eliatte et al., 2016; Barac et al., 2015), so both aim to reach the interface to minimize the hydrophobic interactions. Hard-sphere molecules tend to form a compact interfacial layer, stabilized for steric factors and optimizing the packaging of spherical geometries at the interface. So, both species aim to occupy an interfacial site at the expense of the other. However, the PP/A mixture with a ratio of 1/3 has the higher adsorption rate value among the others and it could be suggested that at this ratio an optimum molecular packing is reached.

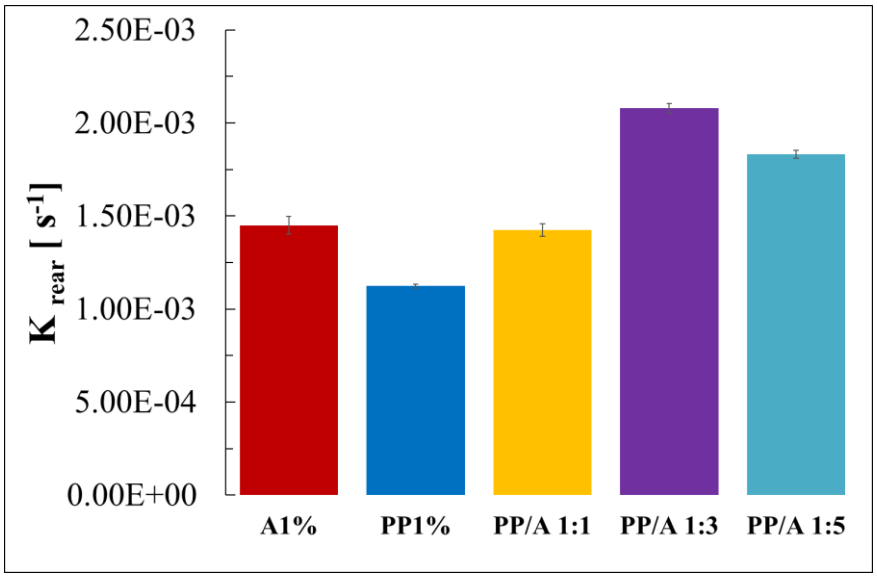

Figure 4.13: Rearrangement rate for PP/A mixtures compared to pea proteins and starch mixtures

In Fig. 4.13 rearrangement rate coefficients are reported. As can be observed, the A1% rate value is higher than PP1%. This can be due to the albumins present in the pea proteins that being a soft flexible protein can displace hard-sphere-like proteins from the interface, in a slow rearrangement mechanism (Bos et al., 2001; Mileti et al., 2019; Parkinson et al., 2005). For mixtures, it cannot be individuated a defined trend. For PP/A ratio 1:1, the rate value is similar to A1%, suggesting that the rearrangement mechanism is principally due to hard-sphere-like molecules, such as amylopectin and globulins, while a maximum value, relative to ratio PP/A 1:3, is reached according to the adsorption coefficient trend. In the following Figs. 4.14, 4.15 and 4.16, kinetic parameters about PP/H mixtures are reported, compared to H1% and PP1% pure samples.

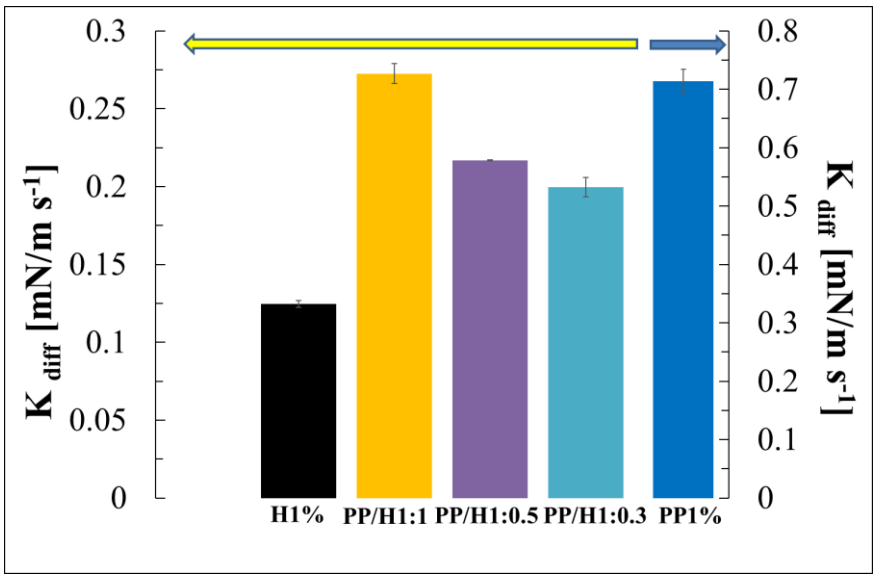

Figure 4.14: Diffusion rate for PP/H mixtures, compared to pea proteins and starch mixtures.

In Fig. 4.14, diffusion rate coefficients are shown: on the left axis, starchy systems are shown, namely H1% and PP/H mixtures. On the left axis, the pea proteins value is reported, since the PP1% value is too much higher than starchy mixtures. As can be seen, the PP1% value is much higher than H1% and PP/M mixtures. This trend reflects the predominant linear molecules present in the solution, such as amylose, for which the diffusion rate is smaller than the spherical ones (Bird et al., 1987). This could explain the reason for the smaller diffusion rate of H1% compared to PP1% and A1% (shown in Fig. 4.11).

The presence of amylose can be considered also very influential upon the PP/H mixtures diffusion mechanism. In fact, a sharp decrease in rate coefficients with regard to the PP1% solution is observed. The values slightly increase as H content decreases; thus, it can be concluded that also with a little percentage of H in the solutions, the diffusion rate decreases.

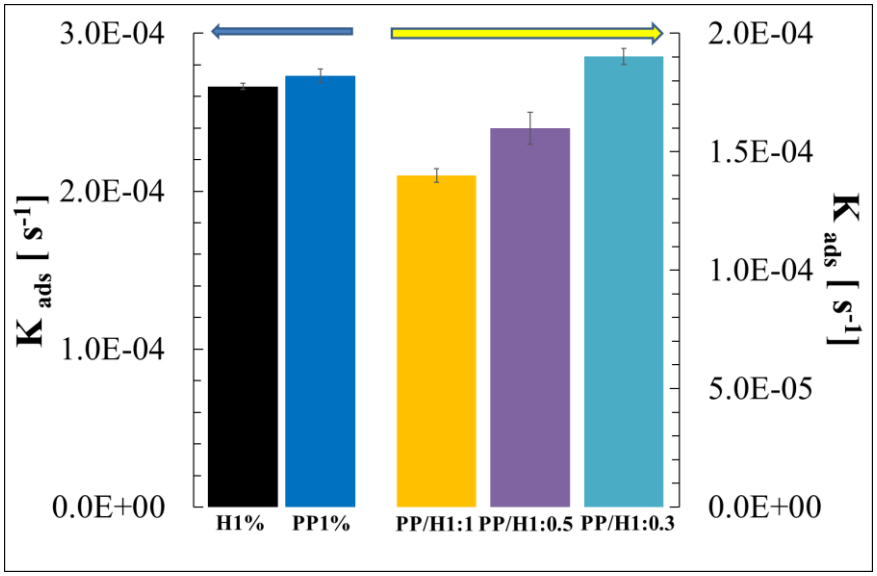

Figure 4.15: Adsorption rate for PP/H mixtures compared to pea proteins and starch mixtures.

In Fig. 4.15, the adsorption rate coefficients are shown. On the left axis, the single material K_{ads} values are reported, while the mixtures are shown on the right. The values for H1% and PP1% are almost the same. This can be explained considering that in H material there is also an amylopectin percentage, more hydrophobic than amylose, as explained above (Eliatte et al., 2016). For this reason, amylopectin can arrive first at the interface and adsorbs on it, while amylose, being linear and more hydrophilic, can remain in solution for more time. The claim can be supported by coefficient values for mixtures that are lower than the pure solution and increase with the decrease of the H percentage in the solution. This can be due to the competitive effect between amylopectin and globular pea

proteins, as described above. This competitive effect results minimized for PP/A 1:1/3, there being in the solution a lesser amount of amylopectin. The role of amylose in adsorption could be considered secondary, since it tends to remain in solution and, near the interface, to form a more diffused interfacial layer (Eliatte et al., 2016).

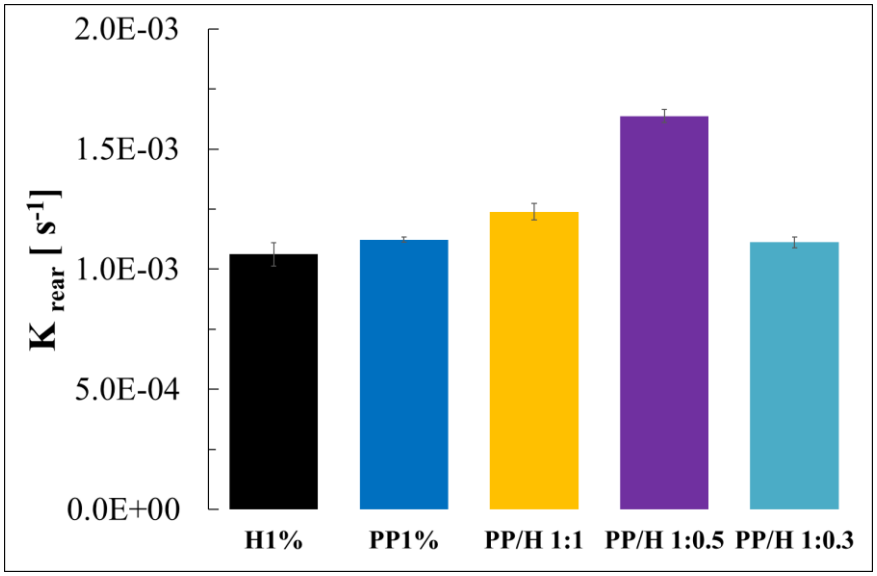

Figure 4.16: Rearrangement rate for PP/H mixtures, compared to pea proteins and starch mixtures.

In Fig.4.16, the rearrangement coefficient for PP/H mixtures, H1% and PP1% are reported. H1% and PP 1% values are quite similar. Soft flexible molecules play a crucial role in the rearrangement mechanism for both systems, although in different ways: the amylose stabilizing interface increasing the interfacial layer edge, formed by compacted packaged amylopectin spherical molecules (Eliatte et al., 2016); albumins by displacing globular proteins (Bos et al., 2001). The combinations of all these factors result in the rate values of mixtures. As can be seen, there is a ratio, PP/H 1:1/2, for which the rearrangement value is maximum. Consequently, this kind of interface is stabilized first, reaching equilibrium first. This will be confirmed by dilatational oscillating data and transient relaxation tests.

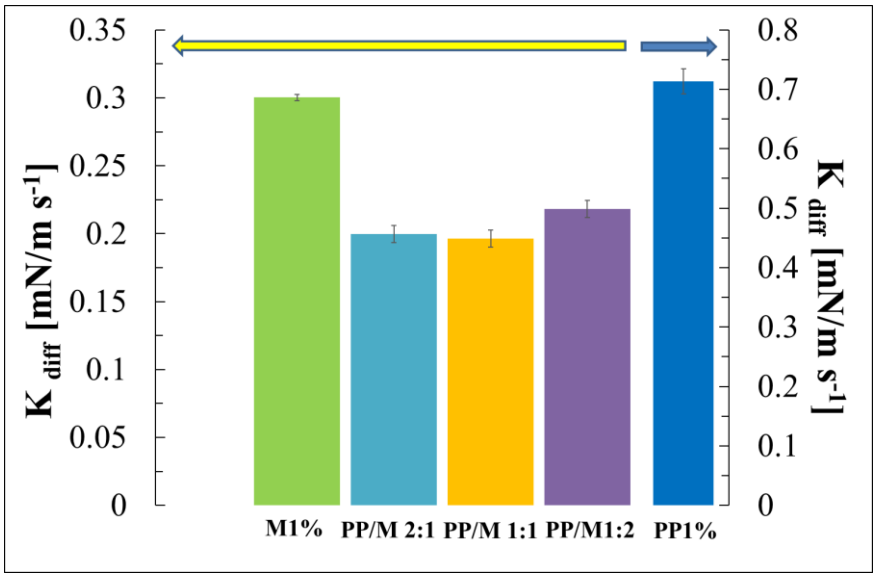

Figure 4.17: Diffusion rate for PP/M mixtures, compared to pea proteins and starch mixture.

Finally, Fig. 4.17 shows the diffusion rate values for PP/M mixtures, M1% and PP1%. Once more to appreciate values differences, starchy systems are shown on the left axis, while pea proteins on the right. PP1% value is higher than M1% and PP/M mixtures. In the light of the above considerations, M sample having a lower percentage (56%) of amylose than H sample (70%), it can be supposed that M1% rate diffusion is higher than H1% because it is richer in amylopectin. Diffusion rate values for the Mixtures are quite similar, so there is independence from the ratio utilized. Moreover, the PP/M rate diffusion values are very similar to the PP/H ones; so, an analogous diffusion mechanism in these kinds of system can be suggested. This was expected, because M and H resistant starches have a similar composition, as described in chapter 2.

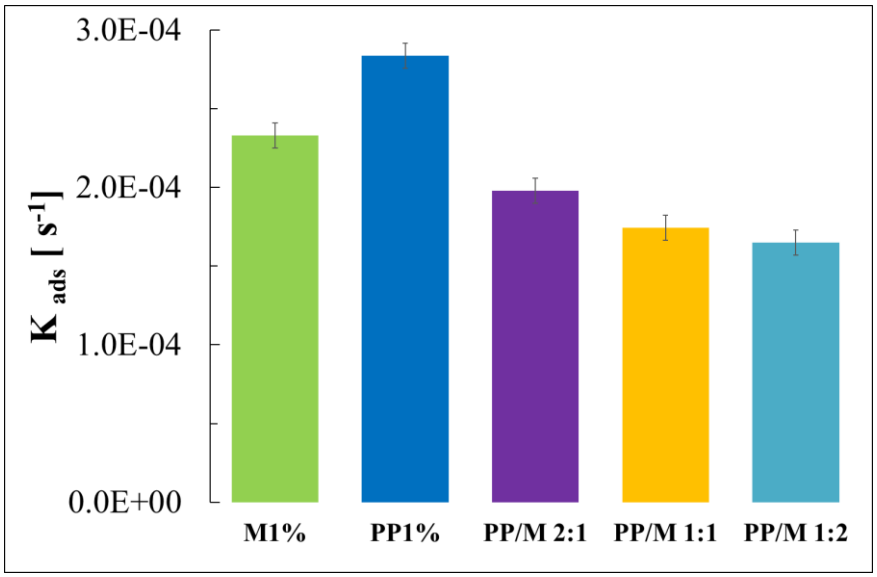

Figure 4.18: Adsorption rate for PP/M mixtures, compared to pea proteins and starch mixtures.

In Fig. 4.18 the adsorption rate for PP/M mixtures is shown, together with the M1% and PP1% values. From a comparison with PP/H mixtures values, it can be concluded that adsorption mechanisms are almost the same in both kinds of systems; the same can be assumed for the hypothesis introduced above for PP/H mixtures.

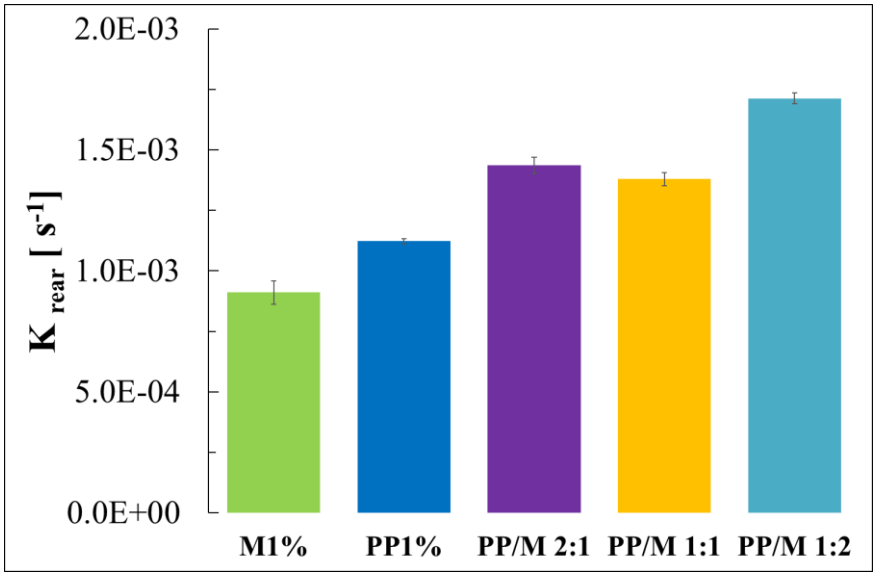

Figure 4.19: Rearrangement rate for PP/M mixtures compared to pea proteins and starch mixture

In Fig. 4.19, the rearrangement rate values for PP/M mixtures are shown. Also, for these systems, the amylose rule is determinant, since a larger amount of this (in sample PP/M 1:2) results in the highest rearrangement rate among both mixtures and single materials. So, the considerations assumed above about PP/H mixtures can be held here.

4.3: Dynamic oscillation tests: results and discussion

In this section, the dynamic oscillation tests results are presented and discussed. As described in section 2.3.4.2, in this test, in input interfacial area (A(t)) is varied according to a sinusoidal time function and information about the equilibrium interfacial structure can be obtained.

From the dynamic oscillation tests, the dilatational interfacial moduli can be evaluated: the storage modulus, E', and the loss one, E". In Fig. 4.20 a typical trend of E' and E" in the range of frequency analysed is reported.

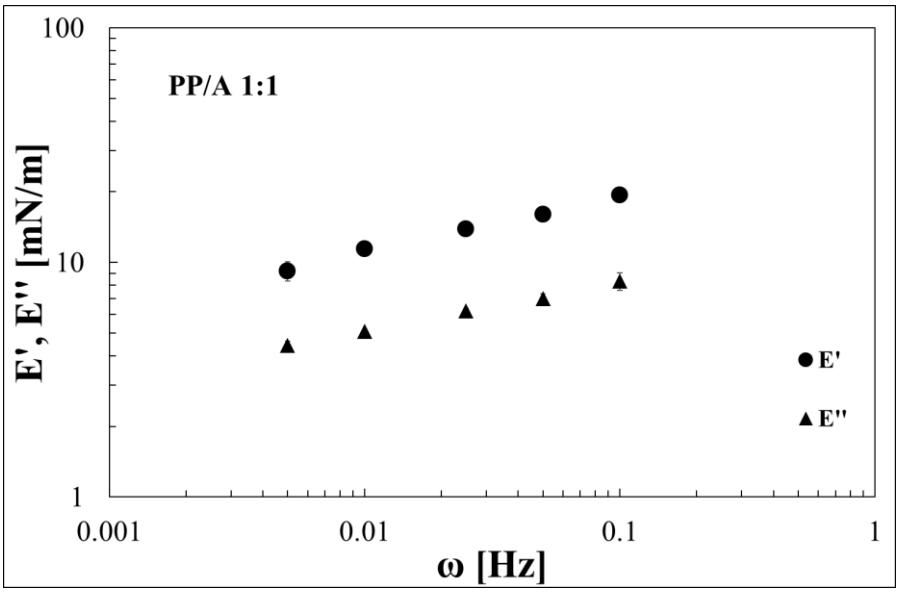

Figure 4.20: The typical trend of dilatational moduli E' and E" in the frequency range analysed.

In Fig.4.20 it can be observed that the dynamic moduli vary linearly with frequency in a log-log diagram (Bird et al., 1985) and are almost parallel in the windows analysed. Moreover, E' is always higher than E", therefore, the interfaces investigated show a solid-like behaviour and, plotting the complex modulus, E*, against the frequency, it is possible to fit the data with the gel model (eq.2.22) (Seta et al., 2012; Mileti et al., 2019).

For all the interfaces analysed, the phase angle δ is a weak function of the frequency, suggesting a gel-like behaviour and the complex modulus changes changing the system analysed. In Figs 4.21 and 4.22, the *A* and *n* parameters for PP/A mixtures and pure solutions (A1%, PP 1%) were reported.

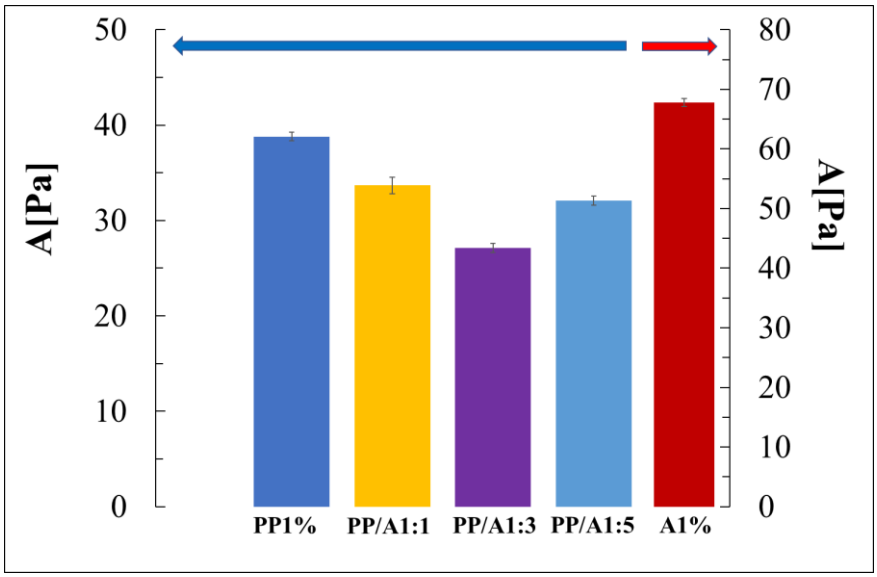

Figure 4.21: Comparison of *A* parameters for PP/A mixtures compared to pea proteins and resistant starch.

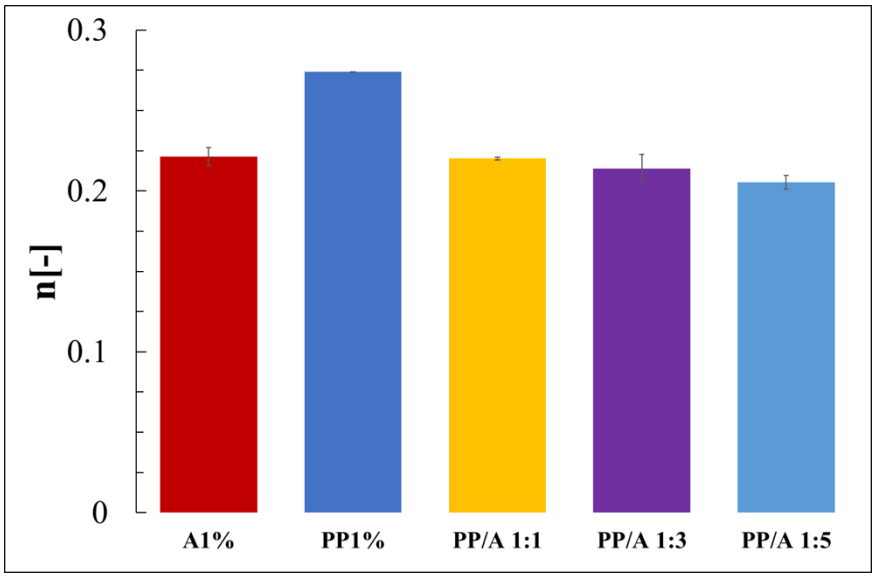

Figure 4.22: Comparison of *n* parameters for PP/A mixtures, compared to pea proteins and starch mixture

Sample A1%, shown on the right axis in Fig. 4.21, has the stronger structure among all the interfaces investigated. This could be related to the hydrophobic effect of spherical molecules of amylopectin, resulting in the formation of a strong insoluble interfacial layer (Eliatte et al., 2016). PP1% interface, rather, results less strong than A1%. Although the greater part of pea proteins are globulins, as said in section 4.1, it could be possible that the presence of albumin, able to replace globulin from the interface (Bos et al., 2001), can lead to a slight "weakening" compared to the just spherical and hydrophobic character of amylopectin in A1% (Eliatte et al., 2016). The mixture interface strength is lower both than the A1% and PP1% one. This experimental evidence suggests a weakening of the interfacial structure in terms of consistency, while the *n* parameter seems to improve by mixing A

and P in different proportions. This behaviour can be attributed to the high quantity of amylopectin, the conformation of which is hard spheres, present in mixtures.

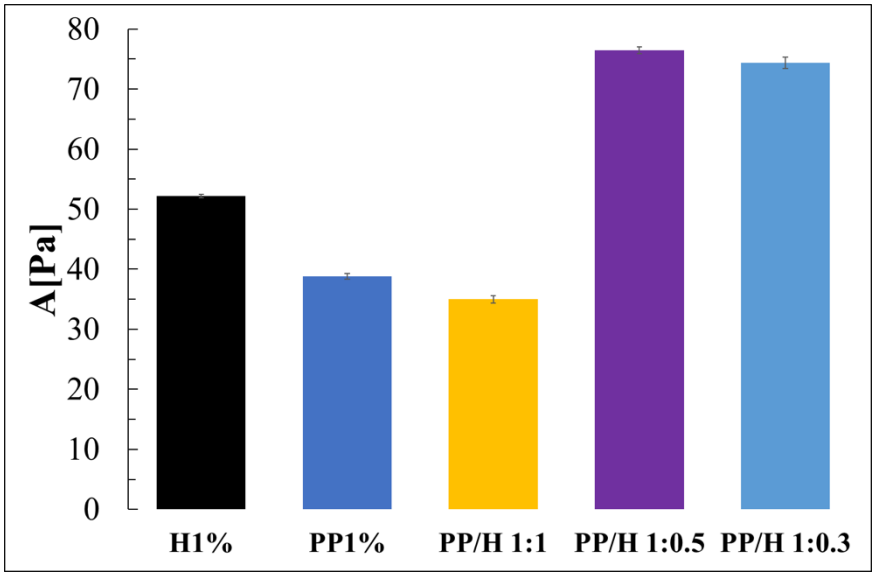

Figure 4.23: Comparison of *A* parameters for PP/H mixtures, compared to pea proteins and starch mixtures.

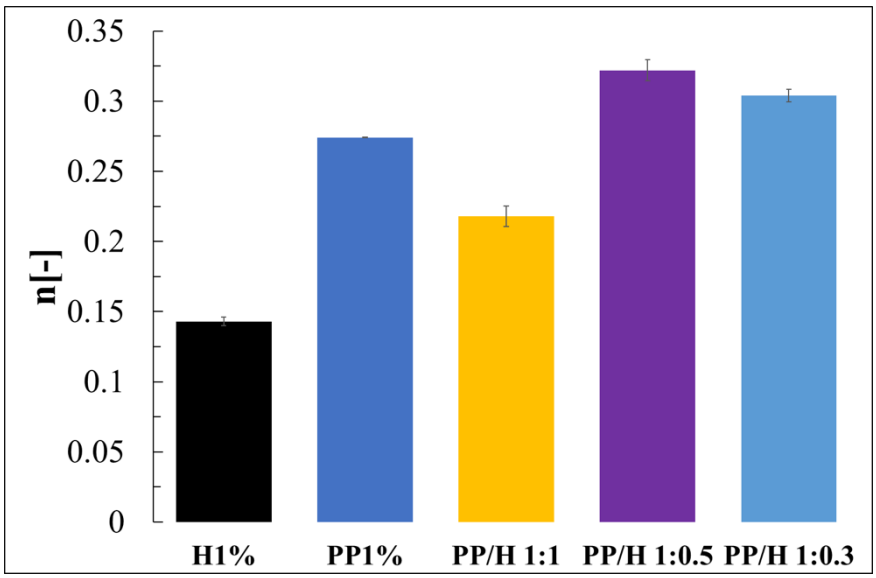

Figure 4.24: Comparison of *n* parameters for PP/H, compared to pea proteins and starch mixture.

In Figs. 4.23 and 4.24, the trend of H1% compared to PP1% and their mixtures can be observed. It is notable to observe that the mixtures at a low quantity of Hylon show a parameter different from those of the pure components, and this is probably due to a possible complex formation because of the different mechanical interfacial properties of the mixture in question compared to the two pure species.

An explanation could be due to the amylopectin/amylose quantity in the system. In fact, at a high percentage of starch, the amylose is preponderant in the system in relation to amylopectin, and an interfacial layer of amylopectin/pea proteins can be attained. This possible complex can increase the A parameter and lower the structuring degree (high n value) while increasing the Hylon quantity, because of the increase of the amylopectin inside, the *n* parameter is improved with a decrease in consistency (*A* parameter). The data of the higher amylopectin quantity in the latter mixtures are in accordance with the A and PP samples trend.

In Figs. 4.25 and 4.26, the *A* and *n* parameters of the PP/M mixtures, with M1% and PP1% values are reported.

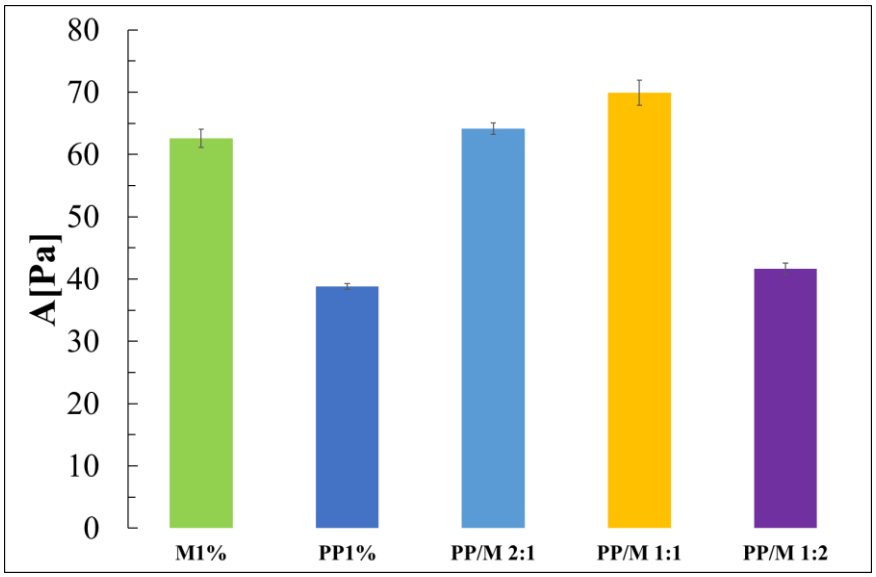

Figure 4.25: Comparison of *A* parameters for PP/M compared with pea proteins and starch mixture.

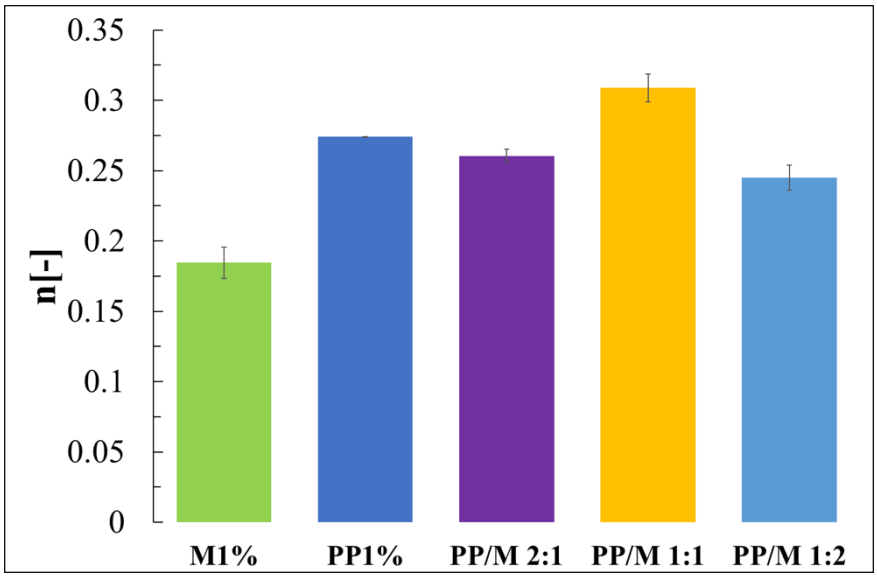

Figure 4.26: Comparison of *n* parameters for PP/M mixtures, compared to pea protein and starch mixture

As can be seen in Fig. 4.25, these kinds of mixture behave in an intermediary way between PP/A and PP/M.

For the PP/H mixtures, after a certain amount of amylopectin, it is possible to note a decrease of *n* and *A* as for the A/PP systems, whereas when the amount of amylose is more consistent compared to amylopectin in the mixture a different interface is obtained as for samples H/PP.

4.4 Transient Relaxation test: results and discussion

In this section, the transient relaxation test results are shown and discussed. Details about this type of test can be found in section 2.3.4.3. While in dynamic oscillatory tests it is possible to have information about the equilibrium interfacial structure, in the relaxation test the interfacial behaviour far from equilibrium is investigated, along with the relaxation and recovery mechanism.

A typical relaxation curve for the systems analysed is reported in Fig. 4.27.

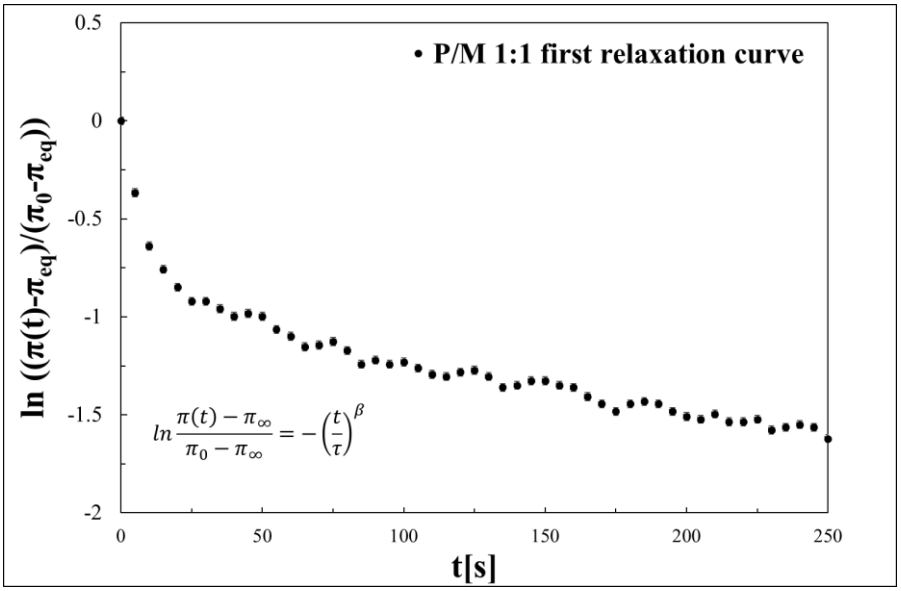

Figure 4.27: First relaxation curve of the P/M 1:1mixture.

The relaxation and recovery trends can be well fitted with a fractional exponential decay, shown in the graph and discussed in section 2.3.3.3, eq.2.28. In this equation, τ is the first relaxation time, while β is the relaxation time spectrum wideness coefficient (Schiessel et al., 1995). The β coefficient can vary only between 1 and 0; for β tending to 1, just a relaxation time characterize relaxation mechanism, while $\beta<1$, the relaxation time spectrum is wide, with several relaxation time values. Physically, this can correspond to different relaxation mechanisms, both of different molecules adsorbed at the interface and of the interfacial structure generated by the interaction among molecules.

The same holds for the recovery mechanism. From a physical point of view, understanding the reason underlying the relaxation and recovery mechanisms is very difficult (Bos et al., 2001), for many reasons. A step-area expansion modifies the interfacial structure very strongly, and in the following kinetic diffusion, adsorption and rearrangement occur, not necessarily in the same way as before (Bos et al., 2001).

The physical data interpretation is easier for the first expansion wave in relation to the others, since the starting point is the equilibrium condition, as described in section 2.3.3.3, whose characteristics are known from dilatation oscillatory tests. Moreover, it is known from the literature that strong interfaces, like those generated by hard-sphere-like molecules (such as amylopectin and pea globulins) or in the presence of species able to form a strong interfacial network (albumins), after a step-area expansion are fractured (Bos et al., 2001).

The relaxation mechanism is also determined by the extent of this fracture and of the depletion zones created during the sudden area deformation. On the contrary, during compression, the interfacial area is drastically reduced, thereby decreasing the specific area relative to each absorbed molecule. Moreover, compression lead to molecules overlapping, so they tend to depart from each other as soon as possible, both owing to electrostatic repulsion and steric reasons (Israelachvili, 2011). This consideration could be confirmed by the fact that for all the interfaces it was observed that recovery times are one order of magnitude lower than relaxations ones. Finally, analogously with the bulk relaxation mechanism, it can be stated that a higher relaxation time is linked to a more solid-like behaviour, that needs more time to relax the stress.

From the variation of interfacial tension following a stepwise expansion or compression, it is possible to evaluate interfacial elasticity and viscosity, as stated by Eqs. 2.29 and 2.30. The former is related to the resistance at expansion or compression: higher elasticity values are related to a more deformation-resistant interface; the second represents the dissipative terms of the kinematic applied (Wusteneck et al., 1999; Saulnier et al., 2011). Generally, in dilatational expansion, the elastic contribution is dominant with regard to the viscous one (Bird et al., 1985; Wusteneck et al., 1999).

In the following tables, the evaluated relaxation parameters are reported. Each table is divided into two sections, relative to expansion and compression respectively. For each section, parameters relative to the first and second wave are shown. In Tables 4.2 and 4.3 respectively, the elasticity and viscosity values for PP/A systems are shown with A 1% and PP 1% pure solutions.

	E [Pa]			
	Expansion		**Compression**	
	1st wave	2nd wave	1st wave	2nd wave
A 1%	26.86±1.80	17.70±0.51	11.63±1.65	9.36±0.26
PP 1%	24.19±0.72	21.31±2.14	22.55±2.14	29.51±0.056
PP/A 1:1	18.83±0.64	29.30±6.37	22.04±0.56	30.65±2.30
PP/A 1:3	14.98±1.57	20.12±3.78	13.70±1.70	30.45±2.29
PP/A 1:5	12.57±1.96	20.76±3.82	11.82±0.97	17.76±0.27

Table 4.2: Elasticity values of PP/A mixtures, compared to pea proteins and starch mixture.

	η [Pa s]			
	Expansion		**Compression**	
	1st wave	2nd wave	1st wave	2nd wave
A 1%	1.60±0.06	2.70±0.04	1.70±0.20	1.35±0.01
PP 1%	1.38±0.04	2.57±0.22	2.44±0.22	4.02±0.01
PP/A 1:1	1.06±0.03	3.25±0.70	3.04±0.10	4.44±0.18
PP/A 1:3	1.02±0.93	2.28±2.00	1.90±0.19	4.58±0.20
PP/A 1:5	0.70±0.12	1.46±0.32	1.57±0.10	2.30±0.40

Table 4.3: Viscosity values of PP/A mixtures, compared to pea proteins and starch mixture

In Table 4.2, the elasticity values for PP/A mixtures and reference A1% and PP1% values are reported. As can be observed, the A1% and PP1% elasticities are greater than those of the PP/A mixtures, while this trend is inverted for the second wave. A1% and PP1% have a strong equilibrium structure, while in the previous section it was shown that the PP/A interface is weaker than that of the single materials. This is confirmed by the elasticity values since those of the PP/A mixture are smaller than both A1% and PP1%. The elasticity decreases with the increase of A in the system.

In Table 4.3 the viscosity values are shown. It can be observed that each system viscosity value increases from the first to second expansion.

In the following Tables 4.4 and 4.5, the relaxation times τ and β coefficients for PP/A systems are reported.

	τ [s]			
	Expansion		**Compression**	
	1st wave	2nd wave	1st wave	2nd wave
A 1%	267.7±23.3	264.3±8.6	36.4±1.65	48.2±2.3
PP 1%	115.07±20.8	113±0.94	24.8±3.4	25.1±5.2
PP/A 1:1	178.3±17.8	128.6±16.5	26.1±5.2	25.8±2.6
PP/A 1:3	237±17	220±1.9	23.8±1.3	44.5±8.2
PP/A 1:5	139.52±30.	123.1±23.4	59.11±6.3	58.11±0.1

Table 4.4: Relaxation time values of PP/A mixtures, compared to pea proteins and starch mixture

	β [-]			
	Expansion		**Compression**	
	1st wave	2nd wave	1st wave	2nd wave
A 1%	0.66±0.01	0.43±0.11	0.23±0.03	0.52±0.05
PP 1%	0.62±0.06	0.61±0.02	0.46±0.02	0.29±0.03
PP/A 1:1	0.732±0.06	0.532±0.1	0.41±0.03	0.46±0.03
PP/A 1:3	0.60±0.01	0.65±0.02	0.37±0.07	0.36±0.01
PP/A 1:5	0.565±0.07	0.501±0.02	0.292±0.01	0.310±0.06

Table4.5: β coefficient of PP/A mixtures, compared to pea proteins and starch mixture

From Table 4.4, it results evident that the A1% relaxation time is higher than the others. This can be due to the strong interfacial amylopectin layer which is able to form this system. It is worth noting that PP/A 1:3 has a higher relaxation time among mixtures. This could confirm that at this ratio the interface is stabilized better, as results from the lower equilibrium interfacial tension and higher rate rearrangement coefficient, as shown in Fig. 4.4.

In Table 4.5 it can be seen that β coefficients are smaller than 1, denoting that there are several relaxation mechanisms. Although amioca is almost pure amylopectin, its β coefficient is smaller than one. It is well known from the literature (Bos et al., 2001; Mezzenga et al., 2013) that large hard-sphere-like hydrophobic molecules, such as amylopectin, can form a strong interfacial layer that, under sudden expansion, breaks in several points, thus generating several relaxation mechanisms. This can be the reason for a β coefficient smaller than1.

The degree of structuration is also confirmed by the small A1% *n* value in fig.4.18, denoting its solid-like behaviour.

In Tables 4.6 and 4.7, the elasticities and viscosities regarding the PP/H systems are shown.

	E [Pa]			
	Expansion		**Compression**	
	1st wave	2nd wave	1st wave	2nd wave
H 1%	26.86±1.80	17.70±0.51	11.63±1.65	9.36±0.26
PP 1%	24.19±0.72	21.31±2.14	22.55±2.14	29.51±0.056
PP/H 1:1	15.64±1.64	22.24±1.35	17.43±2.20	23.53±0.23
PP/H 1:0.5	23.90±1.50	21.70±3.75	20.78±1.70	29.63±2.50
PP/H 1:0.33	23.25±0.87	32.46±0.42	28.63±0.27	28.65±2.50

Table 4.6: Elasticity values of PP/H mixtures, compared to pea proteins and starch mixture

	η [Pa s]			
	Expansion		**Compression**	
	1st wave	2nd wave	1st wave	2nd wave
H 1%	1.60±0.06	2.70±0.04	1.70±0.20	1.35±0.01
PP 1%	1.38±0.04	2.57±0.22	2.44±0.22	4.02±0.01
PP/H 1:1	0.94±0.01	2.39±0.08	2.46±0.40	3.33±0.05
PP/H 1:0.5	1.30±0.06	2.91±0.54	3.60±0.28	4.32±0.46
PP/H 1:0.33	1.36±0.04	3.62±0.07	3.9±0.05	4.40±0.20

Table 4.7: Viscosity values of PP/H mixtures, compared to pea proteins and starch mixture

From the elasticities values reported in table 4.6, it can be observed that H1% has a higher value than other systems. This value can be related to the interface strength represented by parameter *A* in Fig. 4.23. It is worth noting that, among the mixtures, PP/H 2:1 has the higher mean value, confirming that a small amount of amylose in the system can lead to strong and elastic interfaces. As can be observed in Table 4.7, the dissipative term linked to the viscosities is for all the PP/H systems of the same order of magnitude.

	τ [s]			
	Expansion		**Compression**	
	1st wave	2nd wave	1st wave	2nd wave
H 1%	209±12.6	183±9.1	103.6±8.2	64.6±2.4
PP 1%	115.07±20.8	113±0.94	24.8±3.4	25.1±5.2
PP/H 1:1	113.9±13.2	151.2±3.5	19.3±1.3	53.5±0.7
PP/H 1:0.5	250.5±23.4	251.8±4.5	41.8±1.7	28.5±3.65
PP/H 1:0.33	242.09±20.6	230.7±22	32.8±2.7	52±5.2

Table 4.8: Relaxation time values of PP/H mixtures, compared to pea proteins and starch mixture

	β [-]			
	Expansion		**Compression**	
	1st wave	2nd wave	1st wave	2nd wave
H 1%	0.96±0.03	0.8±0.02	0.62±0.08	0.53±0.04
PP 1%	0.62±0.06	0.61±0.02	0.46±0.02	0.29±0.03
PP/H 1:1	0.65±0.02	0.72±0.05	0.34±0.3	0.37±0.3
PP/H 1:0.5	0.53±0.05	0.73±0.01	0.32±0.06	0.36±0.06
PP/H 1:0.33	0.60±0.08	0.61±0.07	0.38±0.09	0.5±0.06

Table 4.9: β coefficient values of PP/H mixtures, compared to pea proteins and starch mixture

From Table 4.8, it can be observed that the relaxation time increases as the H amount decreases, once more suggesting the stability and the strength of interfaces in a system containing a small amount of amylose. It is worth noting that the β coefficient for H1% is near to unit. This could be the amylose stabilizing effect upon the interfacial layer, making it more homogeneous and uniform. So, during a sudden expansion, the interfacial layer deforms homogeneously, giving just a relaxation mechanism. In Tables 4.10 and 4.11, the elasticities and viscosities of the PP/M systems are shown.

	E [Pa]			
	Expansion		**Compression**	
	1st wave	2nd wave	1st wave	2nd wave
M 1%	25.63±1.087	20.18±0.10	20.18±0.10	18.13±0.056
PP 1%	24.19±0.72	21.31±2.14	22.55±2.14	29.51±0.056
PP/M 1:1	16.85±1.18	28.05±0.71	20.85±0.55	23.80±1.16
PP/M 2:1	20.21±0.97	18.09±1.20	18.76±0.62	25.91±1.29
PP/M 1:2	15.62±0.43	13.31±1.86	9.03±1.03	9.74±0.39

Table 4.10: Elasticity values of PP/M mixtures, compared to pea proteins and starch mixture

	η [Pa s]			
	Expansion		**Compression**	
	1st wave	2nd wave	1st wave	2nd wave
M 1%	1.46±0.05	1.43±0.01	1.43±0.01	1.30±0.16
PP 1%	1.38±0.04	2.57±0.22	2.44±0.22	4.02±0.01
PP/M 1:1	0.93±0.06	2.70±0.04	2.82±0.08	3.38±0.18
PP/M 2:1	1.15±0.05	2.01±0.10	2.61±0.12	4.05±0.24
PP/M 1:2	0.91±0.02	1.44±0.19	1.28±0.005	1.32±0.08

Table 4.11: Viscosity values of PP/M mixtures, compared to pea proteins and starch mixture

Observing elasticity values in Table 4.10, it is evident that the elasticity value of M1% is similar to the H1% one. This was expected since the M and H composition are similar. The PP/M mixtures in which there is high content of M, namely PP/M 1:1 and PP/M 1/2, have poor elasticity, as confirmed also by the dilatational oscillation tests results. On the contrary, the PP/M 2:1 is better stabilized by the small presence of amylose, whereas a little amylopectin does not affect the interfacial properties because of the competitive effect with pea proteins. Finally, in Tables 4.12 and 4.13 the τ and β parameters are shown.

	τ [s]			
	Expansion		**Compression**	
	1st wave	2nd wave	1st wave	2nd wave
M 1%	193.1±3.3	150.9±8.72	24.8±3.4	24.7±2.7
PP 1%	115.07±20.8	113±0.94	24.8±3.4	25.1±5.2
PP/M 1:1	164.6±16.3	92.9±2.7	20.9±4.5	28.5±5.0
PP/M 2:1	224.8±18.36	215.4±4.1	43.7±2.3	35.2±1.12
PP/M 1:2	169.4±10.5	41.41±2.92	33.87±2.8	29±4.2

Table 4.12: Relaxation time values of PP/M mixtures, compared to pea protein and starch mixture

	β [-]			
	Expansion		**Compression**	
	1st wave	2nd wave	1st wave	2nd wave
M 1%	0.56±0.04	0.47±0.02	0.46±0.02	0.37±0.04
PP 1%	0.62±0.06	0.61±0.02	0.46±0.02	0.29±0.03
PP/M 1:1	0.6±0.07	0.53±0.03	0.37±0.03	0.5±0.1
PP/M 2:1	0.58±0.07	0.48±0.05	0.46±0.02	0.51±0.05
PP/M 1:2	0.57±0.06	0.3±0.01	0.33±0.04	0.33±0.02

Table 4.13: β coefficient values of PP/M mixtures, compared to pea proteins and starch mixture

From the data in Table 4.12, it can be seen that the M1% relaxation time is similar to H1%, as was expected since their composition is similar. The strongest interface among mixtures is worth noting, namely, PP/M 2:1, has also a higher relaxation time. This could confirm all the considerations stated above.

Bibliography

Arboleya J.C., Wilde P. J. (2005), Competitive adsorption of proteins with methylcellulose and hydroxypropyl methylcellulose, *Food Hydrocolloids* (19), 485-491

Baeza R., Pilosof A.M. R., Sanchez C. C., Rodrıguez Patino J.M. (2006), Adsorption and Rheological properties of Biopolymers at the Air-Water Interface, *AIChE Journal* (52), 2627-2638

Baeza R., Sanchez C. C., Pilosof A.M. R., Rodrıguez Patino J.M. (2004), Interfacial and foaming properties of prolylenglycol alginates. Effect of degree of esterification and molecular weight, *Colloids and Surfaces B: Biointerfaces* (36), 139–145

R. Byron Bird, Charles F. Curtiss, Robert C. Armstrong, Ole Hassager (1987)., Dynamics of Polymeric Liquids, Volume 2: Kinetic Theory, 2nd Edition, *Wiley*

Bos M.V. and van Vliet T. (2001), Interfacial rheological properties of adsorbed protein layers and surfactants: a review, *Advances in Colloid and Interface Science* (91), 437-471

Camino N. A., Perez O. E., Sanchez C. C., Rodriguez Patino J. M., Pilosof A. M.R. (2009), Hydroxypropylmethylcellulose surface activity at equilibrium and adsorption dynamics at the air−water and oil−water interfaces, *Food Hydrocolloids* (23), 2359−2368

Daniel C. Carter and Joseph X. Ho (1994), Structure Of Serum Albumin, *Advances In Protein Chemestr*y153 1994 By Academic Press, Lnc., Vol. 45

C. G. de Kruif, E. M. F. van Iersel, A. Vrij, and W. B. Russel (1985), Hard sphere colloidal dispersions: Viscosity as a function of shear rate and volume fraction, *J. Chem. Phys*. 83, 4717.

Dickinson E. (1999), Adsorbed protein layers at fluid interfaces: interactions, structure and surface rheology, *Colloids and Surfaces B: Biointerfaces* (15), 161-176

Dickinson E. (2010), Mixed biopolymers at interfaces: Competitive adsorption and multilayer structures, *Food Hydrocolloids* (25), 1966-1983

Rammile Ettelaie, Melvin Holmes, Jianshe Chen, Amin Farshchi (2016), Steric stabilising properties of hydrophobically modified starch: Amylose vs. amylopectin, *Food* Hydrocolloids,Volume 58, July, Pages 364-377.

T.J. Faber, A. Jaishankar, G.H. McKinley (January 2017), Describing the firmness, springiness and rubberiness of food gels using fractional calculus. Part I: Theoretical framework, *Food Hydrocolloids*, Volume 62, Pages 311-324

Freer E.M., Yim Kang Sub, Fuller G. G., Radke C.J. (2004), Shear and Dilatational Relaxation Mechanisms of Globular and Flexible Proteins at the Hexadecane/Water Interface, *Langmuir* (20), 10159-10167

Jaishankar, A. & G. H. McKinley (2013) Power-law rheology in the bulk and at the interface: quasi-properties and fractional constitutive equations. *Proceedings of the Royal Society a-Mathematical Physical and Engineering Sciences*, 469.

Ivanov, I. B., K. D. Danov, K. P. Ananthapadmanabhan & A. Lips (2005) Interfacial rheology of adsorbed layers with surface reaction: On the origin of the dilatational surface viscosity. *Advances in Colloid and Interface Science*, 114, 61-92.

Mezzenga R., Fischer P. (2013), The self-assembly, aggregation and phase transitions of food protein systems in one, two and three dimensions, *Reports on Progress in Physics* (76) 046601 (43pp)

Mileti, Olga; Cerra, Maria Carmela; Gabriele, Domenico; de Cindio, Bruno; Baldino, Noemi (2019), Interface rheology of structured food, PhD Thesis, *UNICAL*

Mondy L., Brooks C., Grillet A., Moffat H., Koehler T., Yaklin M., Reichert M., Walker L., Cote R., Castañeda J. (2010), *Surface Rheology and Interface Stability*, SANDIA REPORT SAND 2010-7501

Emma L. Parkinson, Rammile Ettelaie, and Eric Dickinson (2005),, Using Self-Consistent-Field Theory to Understand Enhanced Steric Stabilization by Casein-Like Copolymers at Low Surface Coverage in Mixed Protein Layers, *Biomacromolecules* 6, 3018-3029

Perez A. A., Carrara C. R., Sánchez C. C., Santiago L.G., Patino J. M. R. (2009), Interfacial dynamic properties of whey protein concentrate/polysaccharidecmixtures at neutral pH, *Food Hydrocolloids* (23), 1253-1262

Ravera, F., G. Loglio & V. I. Kovalchuk (2010) Interfacial dilational rheology by oscillating bubble/drop methods. *Current Opinion in Colloid & Interface Science*, 15, 217-228

Saulnier, P., F. Boury, A. Malzert, B. Heurtault, T. Ivanova, A. Cagna, I. Panaiotov & J. E. Proust (2001), Rheological model for the study of dilational propertie s of monolayers. Comportment of dipalmitoylphosphatidylcholine (DPPC) at the dichloromethane (DCM)/water interface under ramp type or sinusoidal perturbations. *Langmuir*, 17, 8104-8111.

Slattery, John C., Sagis, Leonard, Oh, Eun-Suok (2007), Interfacial Transport Phenomena, *Springer*,

Scott J. McClellan, Elias I. Franses (2003), Effect of concentration and denaturation on adsorption and surface tension of bovine serum albumin, *Colloids and Surfaces B: Biointerfaces* 28 63/75

Seta L., Baldino N., Gabriele D., Lupi F.R., de Cindio B. (2012), The effect of surfactant type on the rheology of ovalbumin layers at the air/water and oil/water interfaces, *Food Hydrocolloids* (29) 247-257

van Vliet T., Martin A.H., Bos M.A. (2002), Gelation and interfacial behavior of vegetable proteins, *Current Opinion in Colloid & Interface Science* (7), 462-468.

Wilde P.J. (2000), Interfaces: their role in foam and emulsion behavior, *Current Opinion in Colloid & Interface Science* (5), 176-181

Wustneck, R., N. Wustneck, D. O. Grigoriev, U. Pison & R. Miller (1999) Stress relaxation behaviour of dipalmitoyl phosphatidylcholine monolayers spread on the surface of a pendant drop. *Colloids and Surfaces B-Biointerfaces*, 15, 275-288.

Chapter 5:
Potential applications

In this final chapter, potential applications are described and discussed. In the first phase of experimental work, materials bulk characteristics were studied, focusing attention on their behaviour during thermal treatment, as explained in Chapter 3. In the second part, namely interfacial analysis, mixtures between protein and resistant starches were investigated, aiming to understand the interfacial properties of the air /water interfaces generated in these kinds of system. Finally, information derived both from bulk characterization and interfacial analysis were matched together, to realize whether final product characteristics can be predetermined and, in the future, designed.

5.1 Introduction

The final part of this work is focused on creating bakery products, trying to obtain the desired characteristics in the light of the results obtained both from a bulk and interfacial analysis and matching between them. As seen in Chapter 3, from time cure information about the gelatinization a mechanism was derived, with particular attention to the onset and peak temperatures, along with gelatinization velocity and the evaluation of the complex modulus at peak temperature (Baldino et al., 2018). In Chapter 4, the air/water interface was investigated, to understand both equilibrium and non-equilibrium rheological properties. Although oven conditions during the cooking process are different from those achieved with the strain-controlled rheometer used in this work, the thermal treatment investigation in linear conditions and with a controlled ramp temperature was useful to understand the evolution of the system during gelatinization. It is well known that during the cooking process, the dough expands, both owing to the air entrapped within, and for water evaporation caused by temperature increases. The bubble expansion in dough is determined by several factors (Carnevale et al., 2014):

- Gelatinization mechanism: during bubble expansion, the gelatinization process is still taking place. If the gelatinization process is too short, the structure crystallizes quickly and could prevent bubble expansion. On the contrary, if the gelatinization mechanism is not quick, the bulk structure has the time to evolve and the bubbles have the time to expand during cooking.

In other words, a quick gelatinization process means that G^*_{peak} is reached sooner, preventing this way bubble expansion. This kind of information could be confirmed also comparing the bulk structure strength of the resistant starches analysed, evaluated with a frequency sweep. a stronger and more compact structure will oppose more resistance, while in a weaker one, bubbles are facilitated in expansion. Information derived by frequency sweep should consider also starch retrogradation phaenomena, but, as explained in chapter 3, samples were analysed soon after cooling, so retrogradation effects do not alter structure characteristics in a significant way. On the light of these consideration, the right compromise has to be found.

- Interfacial properties: as can be studied in Bird et al. (1985) for the bubble expansion problem, the interfacial tension is very important in stress balance at the interface. So, it can be said that bubble expansion is determined not only by bulk properties and behaviour, but also by interfacial characteristics, both in equilibrium and far from it. Interfaces with strong structure will expand with more difficultly, and vice versa.

In the light of the above, two extreme mixtures were realized and investigated: the first one rich in Hylon and the second in Amioca. In each mixture, the same pea proteins content was used. This choice was made in light of the results presented in Chapters 3 and 4. Hi-Maize resistant starch has a similar composition that is intermediate between Hylon and Amioca, therefore, in this preliminary evaluation, its use was avoided. From a qualitative point of view, it was expected that the rich amioca mixture would give a more expanded final product since its systems exhibited the weakest structure and the less structuration degree in bulk and a good structuring degree at the interface. So, the system could expand easier because of the strong interface and low bulk consistency. On the other hand, the Hylon-based system has in bulk a stronger structure than Amioca-based systems, but a lower structuring degree of the interfacial layer. Therefore, a less expanded final product was expected. Even if a possible cause of a low expansion could be the high differences between the T_0 temperatures. In fact, Hylon has a higher T_0 than Amioca and this could stop the expansion of the second system during the thermal treatment. Moreover, these two mixtures were not investigated only to test the capability to design a certain kind of products, but also because these two mixtures could satisfy some food industrial applications: amioca-rich mixture could be suitable for the design of aerated systems, such as some kinds of bread or cream puffs; hylon-rich one could be useful for the design of more compact bakery products, such as biscuits or protein bars.

5.2 Results and discussion

In this section, the time cure results will be shown first. In conclusion, the final product images are reported and discussed. In the Fig. 5.1, complex modulus G* and phase angle δ trends for mixture A, are shown.

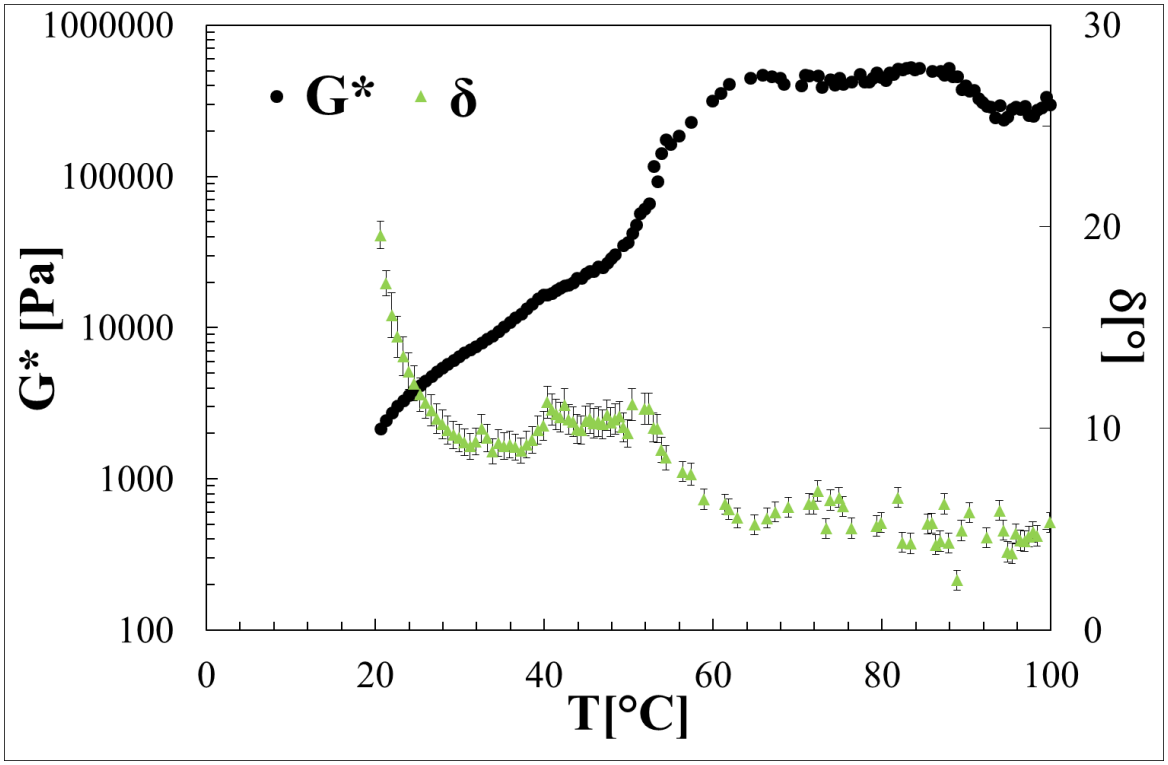

Figure 5.1: Complex modulus G* and phase angle δ for Mixture A

As can be seen from Fig.5.1, this sample has a certain consistency. The modulus value is very high, and the phase angle is very low, showing a strong solid-like behaviour. As can be observed, the onset and peak temperature cannot be well identified because modulus G* always increases during the temperature ramp without a well-defined slope change. In Fig.5.3, complex modulus G* and phase angle δ trends for mixture B, rich in amylopectin, are shown.

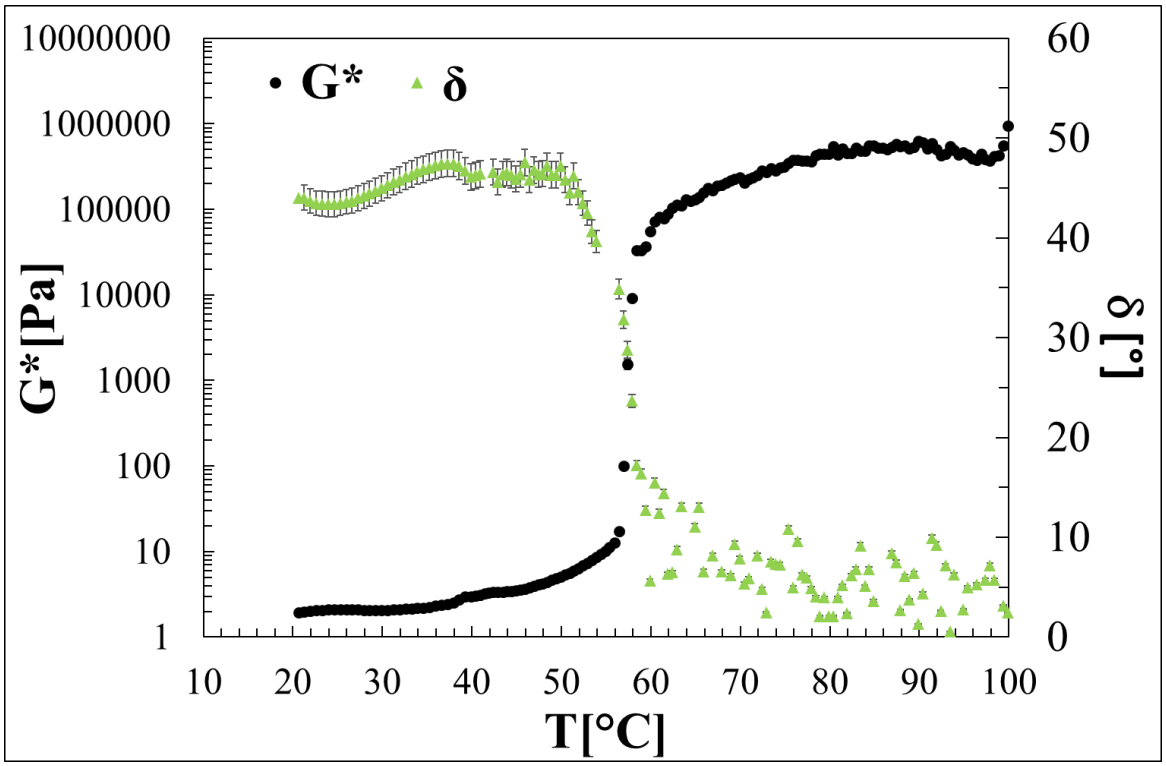

Figure 5.2: Complex modulus G* and phase angle δ for Mixture B

In Fig.5.3, it can be seen that at low temperatures both G*and δ vary because of the kinetic effects (Baldino et al.2018). For this type of recipe, it is possible to evaluate the onset temperature at 58.0 ± 1.8°C. At high temperature, the complex modulus still increases, but with a much lower slope than that registered after onset temperature until 62.0 ± 0.5 °C. This evidence could result from a combination of factors, such as kinetic effects (Baldino et al., 2018), the evolution of structure (Fweng Xie et al., 2020; Chen Li et al., 2020) and recrystallization (Jinchuan et al., 2020).

For both the mixtures analysed, the structural changes and gelatinization process are determined by several factors, principally: pea protein denaturation and gelatinization, described in 3.2, resistant starch gelatinization, described in 3.1 and the interaction between these.

In the figure below, a comparison between the internal structures of cooked mixtures is shown.

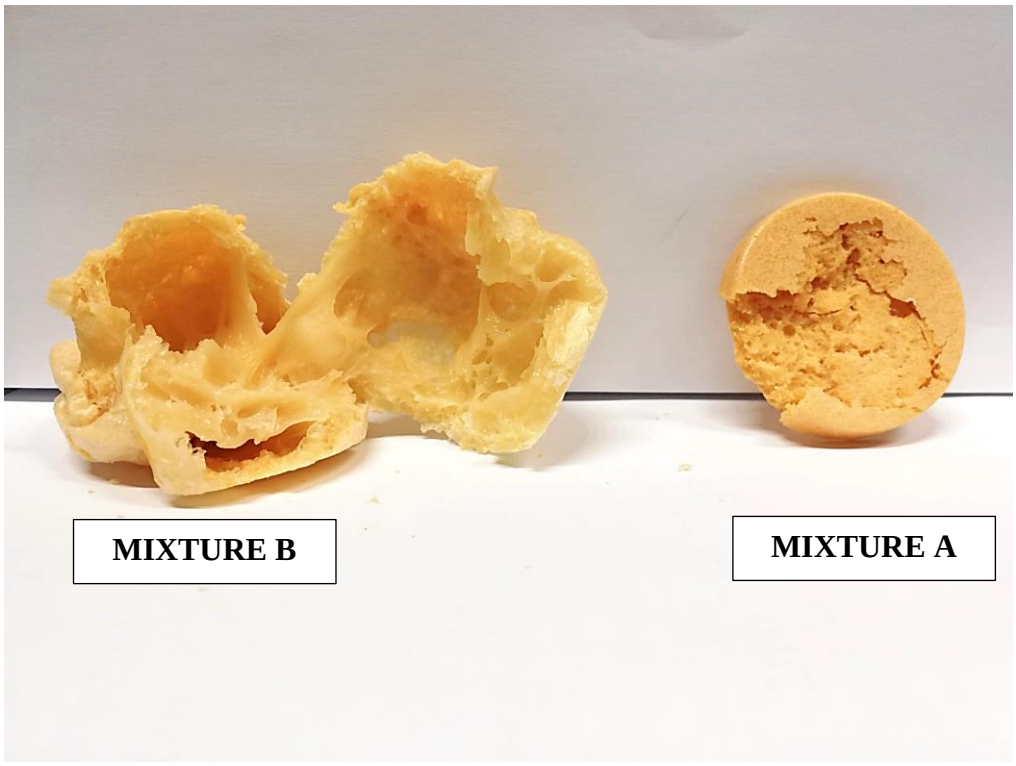

Figure 5.3: Comparison between internal structure of mixture A, rich in hylon, on the right, and mixture A, rich in amioca, of the left.

From the comparison in Fig.5.3, it can be seen that cooked mixture A, rich in Hylon, has a very compact structure, with a certain "hardness" (Faber et al., 2017), brittle, with small bubbles as expected, while cooked mixture B has large holes in the structure, indicating that the structure gave to the bubbles the possibility of expanding within the sample, other than a major "softness" (Faber et al., 2017) of the cooked mixture B.

This type of behaviour was expected by the analysis of both in the bulk and interfacial properties. In fact, from bulk characterization, it was obtained that the H system, rich in amylose and B-type amylopectin (Jinchuan et al., 2020) can give a much stronger structure with a high degree of structuration, compared to the A-system, made up of A-type amylopectin, as discussed both in Chapter 3 and 4. This was confirmed from time cure and frequency results. In the interfacial analysis, pea PP/H interfaces showed a very strong structure compared to PP/A ones, but a lower structuration degree.

For this reason, it was expected that the H rich system would have a stronger structure, in which the bubble would have little expansion capacity since the strength of the structure network would have stopped them; while the A rich system, having a weaker bulk structure, can give more expansion capacity to the bubbles dispersed inside. From the interfacial analysis, it was obtained that PP/H

mixtures are less structured than PP/A ones. So, the interfacial resistance to expansion was different and, in particular, in favour of PP/A mixtures rther than PP/H ones.
The combination of all these factors leads to final product characteristics. According to the final products “hardness” or softness” desired, a different blend can be used, once both bulk and interfacial single materials features are known. So, it has been shown that the information derived with bulk and interfacial characterization can be matched together to pre-determine and design the final product characteristics.

Bibliography

Baldino Noemi, Francesca Laitano, Francesca R. Lupi, Stefano Curcio, Domenico Gabriele (2018), Effect of HPMC and CMC on rheological behavior at different temperatures of gluten-free bread formulations based on rice and buckwheat flours, *European Food Research and Technology* 244:1829–1842

Carnevale Ilaria, Noemi Baldino, Bruno de Cindio (2014), Modeling of mixing and drying processes in pasta production, PhD thesis, *DIMES, UNICAL*.

Cheng Li, Bo Gong (2020), Insights into chain-length distributions of amylopectin and amylose molecules on the gelatinization property of rice starches, *International Journal of Biological Macromolecules* 155 721–729

T.J. Faber, A. Jaishankar, G.H. McKinley (January 2017, Describing the firmness, springiness and rubberiness of food gels using fractional calculus. Part I: Theoretical framework, *Food Hydrocolloids*, Volume 62, Pages 311-324.

Gohar Khachatryan, Lidia Krzeminska-Fiedorowicz, Ewelina Nowak, Maciej Fiedorowicz (2014), Molecular structure and physicochemical properties of Hylon V and Hylon VII starches illuminated with linearly polarised visible light, LWT, Food Science and Technology 58 256e262

Fengwei Xie, Long Yu, Bing Su, Peng Liu, Jun Wang, Hongshen Liu, Ling Chen (2009), Rheological properties of starches with different amylose/amylopectin ratios, *Journal of Cereal Science* 49 371–377

Hui-Huang Chen *, Hong-Yi Kang, Su-Der Chen (2008), The effects of ingredients and water content on the rheological properties of batters and physical properties of crusts in fried foods, *Journal of Food Engineering* 88 45–54.

Jinchuan Xu, Andreas Blennow, Xiaoxi Li, Ling Chen, Xingxun Liu (2020), Gelatinization dynamics of starch in dependence of its lamellar structure, crystalline polymorphs and amylose content, *Carbohydrate Polymers* 229 115481

Juan Mario Sanz-Penella, Małgorzata Wronkowska, Maria Soral-S´mietana, Concha Collar, Monika Haros (2010), Impact of the addition of resistant starch from modified pea starch on dough and bread performance, *Eur Food Res Technol* 231:499–508

Claire D. Munialo, Erik van der Linden, Komla Ako, Hamen H.J. de Jongh (2015), Quantitative analysis of the network structure that underlines the transitioning in mechanical responses of pea protein gels, Food Hydrocolloids 49 104-117

Conclusions

This work aimed to find rheological relationships for complex food systems and tried to use them in rheological product design. Since foods are multiphasic structured systems, in which both the continuous phases and interfaces have to be modelled with complex constitutive equations, bulk characterization and interfacial analysis must be performed.

Nowadays, the demand for foods with high nutritional added value is increasing. Furthermore, new needs related to health, ethical and religious issues are arising. One of these is linked to vegetable proteins as an alternative to meat ones. Vegetable proteins are healthy, with a lot of nutritional and functional properties, which make them suitable to be used in the food industry, both for adding value and for their stabilizing effect on multiphasic food, such as foams or emulsions. On the other hand, increasing celiac and gastrointestinal system diseases, other than obesity, makes the use of an alternative to wheat flours necessary. Resistant starches constitute a valid alternative to wheat flour for the structuration of bakery products and the design of gluten-free foods. Therefore, in this work vegetable proteins/resistant starches complex systems were investigated. As vegetable proteins, peas were used, while as resistant starches three different species were investigated: Hylon VII®, Hi-Maize® and Amioca®. Both pea proteins and resistant starches were supplied by INGREDION (Westchester, Illinois).

In the first part of the experimental work, bulk characterization on single materials was performed, in which dependency upon concentrations, temperature, stress and frequency was investigated. On single materials, different concentrations suspensions time cure tests were performed, to understand the gelatinization mechanisms of each material. Onset and peak temperatures at different concentrations were evaluated. For all resistant starches, onset and peak temperatures with concentrations plot showed a sigmoidal trend. It was observed that amylose-rich systems, such as Hylon and Hi-maize samples, gelatinized at a higher temperature than the amylopectin rich.

It was also demonstrated that amylose has a higher structuration capacity than amylopectin in bulk and on pregelatinized starches, frequency sweep tests were performed at different concentrations to understand the level of structuration and the mechanical behaviour. Finally, rheological data were obtained and interpreted with a proper constitutive equation. The same procedure was also performed on pea protein at different concentrations. From the time cure tests, a sigmoidal trend for the onset temperature was found. From frequency sweep data, it was also found that structure strength slightly increases with a concentration in the range analysed. All pregelatinized samples showed solid-like behaviour.

Once understood single materials bulk behaviour, an interfacial analysis was performed. Both single materials solutions and their mixtures were investigated. Mixtures ratios were chosen on bulk results. Since Hylon was found to be the most resistant, a high ratio systems pea proteins/Hylon was investigated; on the other hand, it was found to be less resistant, so small ratio mixtures of pea protein/amioca were analysed. Interfacial properties were investigated in static, dynamic and transient conditions. From static measurements, equilibrium interfacial tension and kinetic parameters were evaluated. The Gibbs adsorption isotherm for single materials was evaluated. For each material, equilibrium interfacial tension with concentration showed a usual trend, in which amylose-rich systems were found to have a lesser interfacial activity than the amylopectin-rich ones. This was explained suggesting that amylopectin is more hydrophobic, while amylose is more hydrophilic.

Pea proteins adsorption isotherm showed an almost sigmoidal trend, typical for several vegetable proteins. From static measurements on mixtures, equilibrium surface tension and kinetic parameters were evaluated. It was discussed how experimental data were the results of several factors, such as electrostatic interaction, steric hindrance, molecular geometry and so on.

It was found that pea protein/amioca mixtures could present a competitive effect between amylopectin and pea proteins, while a stabilizing effect of amylose in mixtures both with hylon and hi-maize was hypothesised. These considerations were confirmed by dynamic results. In fact, pea protein/amioca were found to have the weakest structure, while it was found that a small amount of amylose increases interfacial strength and structuration. Also, relaxation tests showed that pea proteins/amioca have a lower elasticity, while pea proteins/Hylon have the higher one.

Finally, intending to design a possible bakery aerated product, two mixtures of pea protein/resistant starch were chosen: the first amylose rich, using Hylon resistant starch; whereas the second was rich in amylopectin by using amioca. The characteristics of cooked samples have confirmed the hypothesis made, since the amylose-rich system was more compact in structure, hard and brittle, with small bubbles because of the bulk mechanical properties and the low structuring of the interface compared to amylopectin-rich systems. In conclusion, it is possible to say that matching information coming from both the bulk and interfacial analysis allows the choice of the right blend to design a final product with desired characteristics. It is worth noting that in this work an attempt to conjugate bulk and interfacial analysis to understand how to design then final products deriving from complex systems was done. Thus, in further works, the same way could be followed, especially because in the post-modern era dietary problems will be predominant, for environmental sustainability, human health and ethical issues. The industry will have to supply new products in which classical wheat flour could be partly or substituted by alternative materials, as resistant starches. Moreover, protein supply derived from animal sources should be substituted by vegetable ones. This kind of products

should have the same features as classical ones, and consequently, bulk and interfacial rheology, matched together could be helpful to achieve this goal. More specifically, from a bulk rheology perspective, it could be interesting to find optimal resistant starch blends, suitable to be processed and get desired final products. Moreover, the interaction between resistant starch and vegetable protein during thermal treatment and the resulting structure could be studied in more depth. It could be useful also to investigate these systems with transient tests, such as creep or relaxation tests, to study their time dependency. From an interfacial point of view, all the systems analysed in this work should be investigated in shear kinematic to understand the long time stability phenomena.

In this work, only pea proteins were used, then it could be interesting to investigate the interaction between resistant starches and other vegetable proteins, such as soy, lentil, fava, hemp or rice. Finally, it could be interesting to understand how key parameters, such as onset and peak temperature, or structure strength and network extension varies in function of the system constituents and on the thermal conditions.

Appendix:
Theoretical Background: a brief overview

A.1: Introduction

The theoretical background deals with two main distinct questions: rheological constitutive models to be used and the definition of the interface. These two items are strictly related. In the first part, the rheological constitutive models will be introduced shortly, together with the philosophy inspiring them. In the second part, the different definitions of the often-used interface will be discussed focusing interest on the critical point and suggesting a possible solution.

A.2: A short comparison between viscoelastic and fractional paradigms

From the experimental results obtained both on the bulk and on the interface, the considered material shows a behaviour between solid and liquid. This behaviour can be approached by associating it with the existence of an internal supramolecular structure corresponding to a temporary network rheological model.

A.2.1: Viscoelastic models

Temporary networks can be studied by viscoelastic models based upon the superposition principle: the elastic and viscous component of the mechanical material behaviour are added to obtain the system response to any deformation history. These models describe the behaviour of materials rather well that, from a microrheological point of view, are a network as it occurs for polymers. In this case, long chain molecules entangle together to form a network, in which the chains are very strong (often covalent C bonds); therefore, they cannot be destroyed, while during deformation the topological nodes of the network untie inducing a change of the overall system conformation. This is well described by Rouse and the temporary network model.

According to these models, the complex modulus measured under linear oscillating deformation can be expressed as:

$$E_d^*(\omega) = \sqrt{E'(\omega)^2 + E''(\omega)^2} \tag{A.1}$$

Where *E'* and *E''* are the storage and the loss modulus respectively. The phase angle is related to the two as:

$$tan\delta = \frac{E''}{E'} \tag{A.2}$$

This result is coherent with a general constitutive Maxwell viscoelastic model that according to a single relaxation mechanism can be written:

$$\frac{d}{dt}\boldsymbol{\Sigma} + \frac{E_0}{\eta_D}\boldsymbol{P} = 2E_0A_0\frac{d\boldsymbol{P}}{dt} \tag{A.3}$$

Where $\boldsymbol{\Sigma}$ and $\boldsymbol{P}$ are deformation and stress tensors respectively. The two material parameters are E_0 and η_D and their ratio is the relaxation time τ_D:

$$\tau_D = \frac{\eta_D}{E_0} \tag{A.4}$$

When an asymptotical oscillation kinematic is applied, the values of the storage E' and loss E'' moduli become:

$$E' = E_0\frac{\omega^2{\tau_D}^2}{1+\omega^2{\tau_D}^2} \tag{A.5}$$

$$E'' = E_0\frac{\omega\tau_D}{1+\omega^2{\tau_D}^2} \tag{A.6}$$

The ratio leads to:

$$tan(\delta) = \frac{1}{\omega\tau_D} \tag{A.7}$$

Therefore, the value of E_0 can be obtained by the measured values of $E^*_{d,exp}$ and $\tau_{D,exp}$:

$$E_0 = E^*_{d,exp}\frac{\sqrt{1+\omega^2{\tau_D}^2}}{\omega^2{\tau_D}^2} \tag{A.8}$$

If eqs.5 and 6 are plotted, the following plot is obtained:

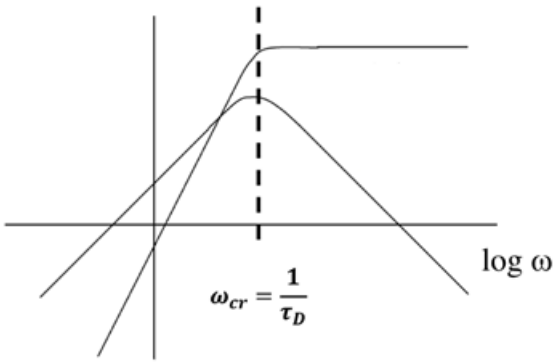

Figure A.1: E' and E'' plot for a material with viscoelastic behavior

It appears that there is a critical value of the frequency, corresponding to:

$$\omega_{cr} = \frac{1}{\tau_D} \tag{A.9}$$

At this frequency it holds:

$$E' = E'' = E_0/2 \tag{A.10}$$

where:

$$E_d^* = E_0/\sqrt{2} \tag{A.11}$$

Finally, for $\omega < \omega_{cr}$ it holds:

$$E'' \propto \omega \tag{A.12}$$

$$E' \propto \omega^2 \tag{A.13}$$

While when $\omega > \omega_{cr}$, it results:

$$E' \sim E_0/2 \tag{A.14}$$

$$E'' \propto \omega^{-1} \tag{A.15}$$

Often, experimental data do not respect them. This means that given an available frequency range it happens that at low frequencies the two slopes *2* and *1* in a log-log plot of *E'* and *E''* vs ω are not found, and even that at high frequencies slope 0 and -1 are absent. On the contrary, it often happens that the complex modulus shows a linear trend with a constant slope lower than 1. According to that there is a double choice. The first is to assume that the trend towards the quoted viscoelastic slopes is attained only at frequencies much lower than those experimentally investigated: this is coherent with the presence of a very wide relaxation spectrum due to a large distribution of the molecular weight or in turn of a large sub-chain (defined as those between two entanglements) distribution. This approach explains also the absence of the crossover between E' and E'' moduli observed in numerous cases. A second possibility is to change the approach by stating that the power behaviour is just the typical behaviour of a class of materials following an alternative rheological paradigm as illustrated below.

A.2.2 Fractional models

Many materials belonging to the so-called "soft matter" class exhibit a rheological behaviour that often cannot be modelled through the classic network theory, built for polymeric materials. Soft materials are characterized by weak interactions (London forces and H bond) therefore the deformation is not due to entanglement untying, as happens for polymers, but to the chain destruction. On the other hand, through the linear viscoelastic theory, an attempt is made to combine properties and material characteristics that are opposite to each other: the elastic modulus, typical of a Hooke solid, and the viscosity, fully defined for the Newtonian fluid. Hence the need to find possible alternative modelling without the Newton and Hooke constraints. A possibility consists in the fractional models for which the slope of the complex modulus becomes a material constitutive parameter. This is a rather old topic, dating back to a letter from Leibniz to de l'Hôpital. In the rheological field, one of the first attempts in this direction was carried out by Nutting, in the 1920s. However, it was G.W. Scott Blair who considerably expanded Nutting's work, proposing the use of differential equations of fractional order and introducing a new rheological unit, the spring-pot, a sort of combination of spring and dashpot viscoelastic mechanical elements. Instead, to sum these two

latter models by weighting them (superposition principle) to generate a visoelastic model, the principle of "intermediation" is applied and the "quasi-properties", are defined to characterize the material rheologically. According to the intermediation principle, it can be asserted that the overall material behaviour is intermediate between solid and liquid, but it does not result from the superposition of the two effects. Over the years, it has been seen that the behaviour of numerous materials can be modelled through a "power law". In the dynamics of complex materials, constituted at the microscopic level by a fractal-like structure, relaxation processes are often encountered that cannot be modelled using the usual Debye function, but they show a "stretched" stress decay (Kohlraush-Williams-Watts), that can be analysed with a function such as:

$$\Phi(t) \propto e^{-\left(\frac{t}{\tau}\right)^{\alpha}} \tag{A.16}$$

with $0 < \alpha < 1$.

Fractional calculus can be used in viscoelastic theory by replacing the whole order derivatives $\frac{d^n}{dt^n}$, with fractional derivatives $\frac{d^\beta}{dt^\beta}$, with $0 < \beta < 1$. However, this formal procedure does not ensure that constitutive equations built in this way have a full physical sense. To overcome this problem, it is necessary to build constitutive equations that are intrinsically fractional. For this purpose, fractional elements need to be defined. Following Scott-Blair approach, the basic fractional element spring-pot model is introduced as that which possesses rheological properties intermediate between those of a Hooke's solid and a viscous Newton's fluid.

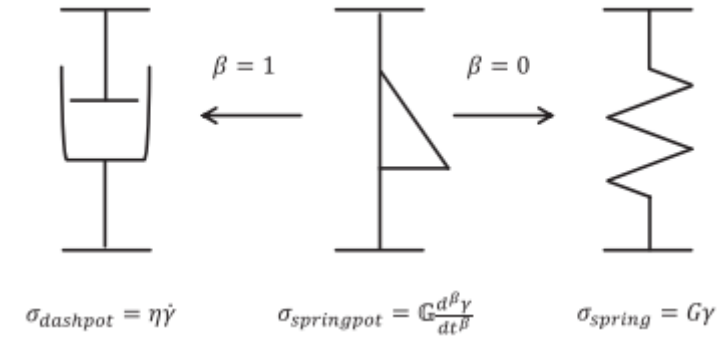

Figure A.2: schematic representation of the spring-pot constitutive equation and its relationship with classic ones (Faber et al.,2017)

As can be seen from fig.2 according to the following constitutive equations, Hooke solids have a unique material parameter i.e. the elastic modulus G, Newton's fluid have the viscosity η as material parameter, while the Scott-Blair element, is characterized by the order of derivation, β, the relaxation time τ, and the "quasi-property" $\mathbb{G}$, dimensionally equal to Pa s $^{(-\beta)}$ (see fig 2). It is evident how the Scott-Blair element reduces to a Newton element for β = 1 and to a Hooke element for β = 0.

Fractional constitutive models are, therefore, more general than classic ones, which represent the extreme behaviours in terms of derivative power.

To write the constitutive equation in the fractional approach, we can start from the Lodge constitutive equation, in which the memory function is introduced through a causal convolution:

$$\sigma(t) = \int_{-\infty}^{t} dt' G(t-t') \frac{d\varepsilon(t')}{dt'} \tag{A.17}$$

In this approach it is assumed that the different mechanical state exhibited during time can be summed according to a time superposition principle of the effects, expressed by the Boltzmann integral, is valid for processes that are homogeneous over time.

Now if we consider a system subjected to a step shear deformation, the time stress decay is classically expressed by a power law (eq.16). Therefore, the relaxation modulus, *G (t-t')* assumes the form:

$$G(t) = \frac{\mathbb{G}}{\Gamma(1-\beta)} \left(\frac{t}{\tau}\right)^{-\beta} \tag{A.18}$$

where $\mathbb{G}$ is the quasi-property as already defined. By substituting in the time superposition integral (eq.17), is obtained:

$$\sigma(t) = \frac{\mathrm{G}\,\tau^{\beta}}{\Gamma(1-\beta)} \int_{-\infty}^{t} (t-t')^{\beta} dt' \frac{d\varepsilon(t')}{dt'} \tag{A.19}$$

The second member of this equation is a fractional integral. In fact, according to Riemann's definition we have:

$${}_cD_t^{-\gamma} f(t) = \frac{1}{\Gamma(\gamma)} \int_c^t dt' \frac{f(t')}{(t-t')^{1-\gamma}} \tag{A.20}$$

Where it holds $\gamma > 0$.

The fractional integral includes two special forms: for c = 0, it falls within the Riemann-Liouville formalism, while the case of $c \rightarrow -\infty$ corresponds to the Weyl formalism.

The fractional differentiation of order $\gamma > 0$, is obtained by fixing an integer n ($n > \gamma$) and writing a fractional integral of order γ-n, followed by an ordinary differentiation of order n:

$${}_cD_t^{\gamma} f(t) = \frac{d^n}{dt^n} \left({}_cD_t^{\gamma-n} f(t) \right) \tag{A.21}$$

Using Weyl's formalism, it can be written $\frac{d^{\beta}}{dt^{\beta}} = {}_{-\infty}D_t^{\beta}$.

Through the given definitions, eq.19 may by written as:

$$\sigma(t) = \mathrm{G}\,\tau^{\beta} \frac{d^{\beta}\varepsilon(t)}{dt^{\beta}} \tag{A.22}$$

This equation represents the constitutive model for a single springpot.

From the physical point of view, Weyl's formalism corresponds to consider an arbitrary deformation history beginning in the remote past ($c \rightarrow -\infty$), while the Riemann-Liouville formalism, later developed by Caputo, restricts the deformation history to only positive times, capable of solving a problem with initial values, in which the Cauchy conditions must be specified. Several authors

(Schiessel et al. 1995, Faber et al. 2016) have found the same functions for module G (t) and compliance J (t), while using the two different formalisms of Weyl or Riemann- Liouville (or Caputo). In the case of oscillatory experiment for a single springpot it is found:

$$G'(\omega) = \mathrm{G}\omega^{\beta} \cos\left(\frac{\pi\beta}{2}\right) \quad \text{(A.23)}$$

$$G''(\omega) = \mathrm{G}\omega^{\beta} \sin\left(\frac{\pi\beta}{2}\right) \quad \text{(A.24)}$$

While for relaxation and creep, the following expressions are found:

$$G(t) = \frac{\mathrm{G}}{\Gamma(1-\beta)}\left(\frac{t}{\tau}\right)^{-\beta} \quad \text{(A.25)}$$

$$J(t) = \frac{1}{\mathrm{G}}\frac{1}{\Gamma(1+\beta)}\left(\frac{t}{\tau}\right)^{\beta} \quad \text{(26)}$$

It can be easily verified that for β = 0 and β = 1, the results obtained with the fractional model coincide respectively with the elastic solid and the viscous fluid.

Finally, it should be noted that from a structural point of view the fractional models well represent conditions where the elasticity is not only due to different configurations (entropy) but also to the chain rupture (enthalpy). Therefore, it appears that classic viscoelastic models can be valid for strong network system (entropic elasticity), while fractional models can be used for soft materials (Helmotz free energy elasticity), in which a cluster model seems to represent better the physical behaviour with respect to networks.

A3: Interface and interfacial constitutive models: some definitions

The aim of this section is to introduce a theoretical model of interface and to investigate the rheological time-dependent equations of state. In order to reach this goal, it is necessary to give a definition of interface. The interface is classically defined as the area between two immiscible fluids. The assigned geometry directly affects the modelling of the physical system.

There are essentially two types of approach:

- Two-dimensional interface;
- Three-dimensional interface;

In the first approach, the interface is considered as a mathematical surface separating two bulks often with fluid behaviour. From a strictly mathematical point of view, the surface is obtained by making the thickness of the volume to tend to zero, which is interposed between the two continuous phases.

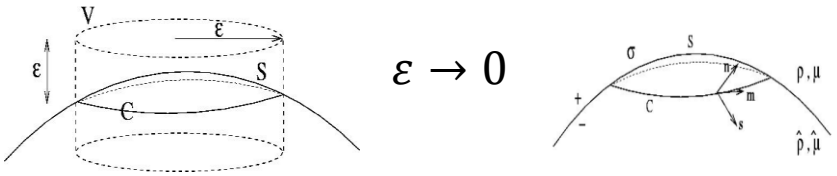

Figure A.3: Schematic representation of interface definition. In two-dimensional approach, the thickness is sent to zero by a limit operation. In three-dimensional approach, the thickness is considered very little, but still finite.

In the second approach, the interface is considered as a volume of small thickness but not zero, which can be studied with the classic methods of continuum mechanics. The critical aspects affecting the two-dimensional approach will be discussed later, leading to the need to develop a three-dimensional approach, which is more complicated from a modelling point of view, but that is characterised by a full physical meaning. In the two-dimensional approach, the interface is considered as an ideal mathematical surface interposed between two immiscible phases placed in mutual contact. The so-defined interface constitutes a singularity surface on which some of the variables of the system have a discontinuity of the first kind, namely concentration and stress. On this surface it is defined the so-called surface tension. This surface property is classically referred to as a scalar field, although it intrinsically embodies the concept of force and would therefore be represented by a tensor. From a mathematical point of view, if an interface volume is considered with an edge ε, a two-dimensional interface is equivalent to evaluate the limit volume for $\varepsilon \to 0$. This operation is valid only in the continuum approach. The two-dimensional approach has some aspects that are extremely critical, although it continues to be the most-used one, and, albeit poor, a wide literature is devoted to this subject. First of all, there is a difficulty to make physical sense of a purely mathematical and immaterial surface. Whenever it is be assumed that it is possible to assign a mass to an interface, the question how to define a surface density will remain open, because the mass is strictly a volume property and not a surface one. Another difficulty is related to the exact spatial placement of the interface: in fact, it is questionable to say whether the interface belongs to one phase or to the other. The importance of defining the exact boundary separating two phases is crucial especially for complex systems, because the surface-active agents aggregate into three-dimensional structures more than 2D ones.

The surface tension, although being defined as a force, in many cases it continues to be considered as a pure scalar, uniform on the surface (thus neglecting any eventual inhomogeneities and anisotropies). On the contrary, it should be defined by a tensor, in perfect analogy with the bulk stresses in the three-dimensional continuum. The two-dimensional tensor introduces a concept of tension overcoming the

scalar definition, however, it is affected by the problems concerning the nature of the interfacial surface. It is observed that the dimensions of the materials parameters defined by constitutive equations are at least ambiguous by referring to surfaces and not to the contour lines. In conclusion, this makes the use a 2D tensor critical. Finally, there is a discontinuity in concentrations at the interface: it is difficult to believe that it is physically acceptable that in a single step a component can possess a number of moles different from those that it owns in the adjacent phase, however, in the presence of an immaterial separation surface. Starting from this inherent difficulty, Gibbs proposed a radically different solution, in which the interface is considered as a three-dimensional continuum, with boundaries not exactly defined, positioned in the portion of space that separates the two phases, in which the physical properties are different from those of the two bulk fluids. The concentration of the surface-active agents in the interface volume, shows a strong gradient compared to that of the two bulk phases, owing to their properties to be adsorbed at the interface. Therefore, the concentration does not show any discontinuity that would be physically unacceptable. In any case, the problem of defining the interface volume remains, but there is the possibility of applying a mathematical treatment using the principles of continuum mechanics, no longer applied to a *bulk*, but to the volume containing the interface. In accordance with that, it is possible to define a three-dimensional surface tensions tensor of the second order, the coefficients of which represent the stress state of the interfacial volume. The need to avoid discontinuity of concentrations at the interfacial surface, coupled with the advanced studies of thermodynamic equilibrium and adsorption of substances with interfacial activity, led Josiah Willard Gibbs to conclude that the interface was made up of a volume, interposed between two immiscible phases, with characteristics different from those of the two bulk fluids. The thickness of this volume on a microscopic scale is determined by the intermolecular and intramolecular interactions. From the macroscopic point of view the continuum mechanics principles can be used, just in the same way as they are used for any bulk phase. Thus, in the interfacial volume a second order tensor can be defined, analogously to the Cauchy stress tensor, which is called surface tension tensor and has to be related to the applied deformation/motion tensor with a specific constitutive equation. In this way, the physical meaning of material parameters is recovered while, when using a two-dimensional interface approach, many doubts arise about their physical meaning. The thickness of Gibbs volume can be related to the molecular interactions of the system, but this seems to be rather complex due to the dimensions of the volume. In fact, to accomplish that it is necessary to find a function relating the surface tension tensor to the macroscopic variables, namely, concentration and temperature. When considering a no-time-dependent isothermal system, the tensor is a function of the single strength, and there are two ways to define the concentration functionality:

the first makes use of Gibbs theory (thermodynamic approach), the second is based on the film theory, considering the transport phenomena within the system.

Coming back to a two-dimensional interface, it is possible to introduce a scalar variable, namely surface tension, which accounts for the discontinuity of stresses on the interface. In static conditions, this statement leads to the Young-Laplace equation:

$$p_1 - p_2 = \gamma \left(\frac{1}{R_1} + \frac{1}{R_2}\right) \tag{A.26}$$

where the stresses of the two bulks are obviously represented by static pressures.

When the system is no longer in static equilibrium, i.e. the two bulks separated by the interface are in motion, also the interface undergoes to a deformation/motion. In this case it is necessary to describe the phenomenon through the complete forces balance (Bush, Lecture 2), thus the tensional state of interface must be referred to the two phases bulk stress tensor, according to the classic fundamentals of continuum mechanics. Since the reference volume element is characterized by size ε, the acceleration and the field forces will be proportional to ε^3, while the terms of surface forces will be dependent on the factor ε^2. With the operation of limit, the volume integrals vanish, and the terms of surface forces remain, which must be balanced. In static conditions, the force difference at the interface is proportional to the curvature of the interface, through a coefficient that assumes the physical sense of dynamic surface tension. The general form of the force balance with scalar surface tension reads:

$$\boldsymbol{n} \cdot \boldsymbol{T} - \boldsymbol{n} \cdot \widehat{\boldsymbol{T}} = \gamma \boldsymbol{n} (\nabla_S \cdot \boldsymbol{n}) - \nabla_S \gamma \tag{A27}$$

It is evident that equation (2) is a generalization of the Laplace equation.

To obtain the tensions, it is necessary to introduce the constitutive equations for the two bulks and to indicate how surface tension is determined by the flow/deformation field which the interface undergoes.

The physical interpretation of the terms in eq.2 is:

- $\boldsymbol{n} \cdot \boldsymbol{T}$: Tension exerted by the upper fluid on the interface;
- $\boldsymbol{n} \cdot \widehat{\boldsymbol{T}}$: Tension exerted by the lower fluid on the interface;
- $\gamma \boldsymbol{n} (\nabla_S \gamma \cdot \boldsymbol{n})$: Normal forces of curvature connected with the local curvature of interface $\nabla \cdot \boldsymbol{n}$;
- $\nabla_S \gamma$: Shear stresses related to surface tension gradients.

On the interface, both normal and tangential stresses must be balanced. The components are obtained by multiplying the force balance at the interface respectively for the normal unit vector $\boldsymbol{n}$ and for the tangential unit vector $\boldsymbol{t}$.

The balance of normal stresses takes the form:

$$\boldsymbol{n}\cdot\boldsymbol{T}\cdot\boldsymbol{n}-\ \boldsymbol{n}\cdot\widehat{\boldsymbol{T}}\cdot\boldsymbol{n}=\gamma(\nabla_S\cdot\boldsymbol{n}) \tag{A.28}$$

The jump of normal stresses at the interface is balanced by the curvature force per unit area. It should be noticed that, for a surface with any curvature, $\nabla_S\cdot\boldsymbol{n}\neq 0$ holds, therefore, there is a discontinuity of the normal stresses across the interface, this obviously does not occur for flat surfaces.

The tangential component is presented as:

$$\boldsymbol{n}\cdot\boldsymbol{T}\cdot\boldsymbol{t}-\ \boldsymbol{n}\cdot\widehat{\boldsymbol{T}}\cdot\boldsymbol{t}=-(\nabla_S\gamma\cdot\boldsymbol{t}) \tag{A.29}$$

The first member, similarly to the normal component, is the jump of tangential stresses at the interface, while the second member contains the tangential stress deriving from the presence of a no-zero value of $\nabla_S\gamma$, an evidence that can occur in the presence of temperature or chemical composition gradients at the interface. It has to be noticed how the first member is constituted only of velocity gradients, and pressure is absent, this implies that the presence of a no-zero gradient of surface tension, leads always to a flow condition.

The force balance at the interface when using a surface stress tensor takes the following form:

$$\boldsymbol{n}\cdot\boldsymbol{T}-\boldsymbol{n}\cdot\widehat{\boldsymbol{T}}=\boldsymbol{n}\,[\boldsymbol{\gamma}\colon\boldsymbol{\nabla}\mathbf{n}]-\boldsymbol{\nabla}\cdot\boldsymbol{\gamma} \tag{A.30}$$

The first term in the second member represents the curvature tension, the second term is present only in flow condition. The form of balance of forces is derived by the assumptions made on the interface and on the form and functionality of the surface tensor.

When using a 2D surface tensor, the interface is still a discontinuity surface for stresses, but in this case, the discontinuity factor is represented in tensorial form. In this case, it is possible to define the surface tensions tensor as (Miller et al.):

$$\boldsymbol{\gamma}=-\gamma_0\boldsymbol{I}+\boldsymbol{\gamma}_{\boldsymbol{dev}}=-\gamma_0\begin{pmatrix}1&0\\0&1\end{pmatrix}+\bar{\gamma}\begin{pmatrix}1&0\\0&1\end{pmatrix} \tag{A.31}$$

This expression must be substituted into the force balance (eq.5). In this way, the surface tensions assume a more physical meaning although they are defined referring to a line element, and not to a surface. In a three-dimensional approach, the tensional state of the surface is defined by a second order surface tensions tensor, which takes the following form to be substituted into eq.5:

$$\boldsymbol{\Gamma}=\begin{pmatrix}\gamma_{11}&\gamma_{12}&\gamma_{13}\\\gamma_{21}&\gamma_{22}&\gamma_{23}\\\gamma_{31}&\gamma_{32}&\gamma_{33}\end{pmatrix} \tag{A.32}$$

The tensor components are called surface tension coefficients and have the dimension of force per unit area. The diagonal terms act along the direction normal to the surface. The surface tension tensor can be split into two contributions: an isotropic contribution and a deviatoric contribution:

$$\boldsymbol{\Gamma}=-\gamma_0\boldsymbol{I}+\boldsymbol{\Gamma}_{\boldsymbol{dev}} \tag{A.33}$$

From which is obtained:

$$\boldsymbol{\Gamma_{dev} = \Gamma + \gamma_0 I} \tag{A.34}$$

In matrix notation, it reads:

$$\boldsymbol{\Gamma_{dev}} = \begin{pmatrix} \overline{\gamma_{11}} & \overline{\gamma_{12}} & \overline{\gamma_{13}} \\ \overline{\gamma_{21}} & \overline{\gamma_{22}} & \overline{\gamma_{23}} \\ \overline{\gamma_{31}} & \overline{\gamma_{32}} & \overline{\gamma_{33}} \end{pmatrix} = \begin{pmatrix} \gamma_{11} & \gamma_{12} & \gamma_{13} \\ \gamma_{21} & \gamma_{22} & \gamma_{23} \\ \gamma_{31} & \gamma_{32} & \gamma_{33} \end{pmatrix} + \boldsymbol{\gamma_0} \begin{pmatrix} 1 & 0 & 0 \\ 0 & 1 & 0 \\ 0 & 0 & 1 \end{pmatrix} \tag{A.35}$$

The deviatoric part of the stress tensor is the only one determined by the deformation and the deformation history.

The introduction of a tensor of the surface tensions of the second order allowed the ambiguities linked to the nature of the surface tension to be resolved, no longer defined as a scalar, but rather as a tensor, with components that are forces per unit area and not per unit length. A crucial question remains open: despite the concept of volumetric interface having been introduced, the balance of forces is correctly written for any surface within the interfacial volume, following the continuum mechanics approach. If the balance of forces on the entire volume is written, with reference to fig.1 (right side), a balance of forces on the surfaces separating Gibbs (interface) volume from the α phase and on those separating from the β phase can be written. Assuming a cartesian reference system of unit vectors $(\boldsymbol{n, m, s})$, the balance of forces on the surface in contact with the α phase, i.e. $\mathbf{S_1}$ with contour $\mathbf{C_1}$, can be written as:

$$\boldsymbol{\int_{S1}[t(n)]dS + \int_{C1} t_s\, dl = 0} \tag{A.36}$$

It should be noted that the stress discontinuity disappears because the interface is no longer considered as a surface of discontinuity but, instead, an interface volume. Thus, the tension acting on the interface can be expressed by applying the Cauchy theorem and the theorem of Stokes on line integral. This leads to:

$$\boldsymbol{-n_{S1} \cdot T_\alpha = (n\,[\Gamma : \nabla n])_{S1} - \nabla \cdot \Gamma_{S1}} \tag{A.37}$$

By operating similarly on the surface in contact with phase $\boldsymbol{\beta}$, indicated with $\boldsymbol{S2}$ the volume contour, is obtained:

$$\boldsymbol{n_{S2} \cdot T_\beta = (n\,[\Gamma : \nabla n])_{S2} - \nabla \cdot \Gamma_{S2}} \tag{A.38}$$

By subtracting the first equation to the second, is obtained:

$$\boldsymbol{n_{S2} \cdot T_\beta - n_{S1} \cdot T_\alpha = [(n\,[\Gamma : \nabla n]_{S2}) - (n\,[\Gamma : \nabla n])_{S1}] + (\nabla \cdot \Gamma_{S1} - \nabla \cdot \Gamma_{S2})} \tag{A.39}$$

So far, we have considered only the forces acting on the contour of the interface volume. It should be considered that inside the Gibbs volume can be present both concentration and temperature gradients, which induce an internal flow. The corresponding momentum flux will vary as a function of position,

temperature and concentration inside the interfacial layer, as well as of the time for time-dependent materials:

$$\boldsymbol{J}(\boldsymbol{t},\boldsymbol{c},\boldsymbol{T}) = \mathfrak{J}(\boldsymbol{\nabla c},\boldsymbol{\nabla T},\boldsymbol{t}) \tag{A.40}$$

The function must be specified through appropriate constitutive equations and experimental tests. The influence of this flux term is hidden in the variation of rheological interfacial properties. With this new term eq.12 becomes:

$$\boldsymbol{n_{S2}}\cdot\boldsymbol{T_{\beta}} - \boldsymbol{n_{S1}}\cdot\boldsymbol{T_{\alpha}} = [(\boldsymbol{n}\,[\boldsymbol{\Gamma}\colon\boldsymbol{\nabla}\mathbf{n}]_{\boldsymbol{S2}}) - (\boldsymbol{n}\,[\boldsymbol{\Gamma}\colon\boldsymbol{\nabla}\mathbf{n}])_{\boldsymbol{S1}}] + (\boldsymbol{\nabla}\cdot\boldsymbol{\Gamma_{S1}} - \boldsymbol{\nabla}\cdot\boldsymbol{\Gamma_{S2}}) + \boldsymbol{J}(\boldsymbol{t},\boldsymbol{c},\boldsymbol{T}) \tag{A.41}$$

To build the interfacial constitutive equations that correlate the stress to deformation, the flow field that that characterizes the interface must be defined. In conclusion, it can be said that although the two-dimensional interface model is widely used in the scientific literature, it shows several critical points, which could be resolved with a three-dimensional approach, as briefly explained above. The latter, however, has the problem of defining the thickness of the volume and of measuring it. Therefore, a possible solution is to consider a thin layer, approximating it to a geometrical surface. This makes it possible to use the same rheological constitutive models proposed for bulk rheology but referred to the Gibbs volume.

Bibliography

Bird, Hassager, Armstrong (1987), Dynamic of polymeric liquids, *Wiley-Interscience*.

Bos M.V. and van Vliet T. (2001), Interfacial rheological properties of adsorbed protein layers and surfactants: a review, *Advances in Colloid and Interface Science* (91), 437-471

T.J. Faber, A. Jaishankar, G.H. McKinley (January 2017), Describing the firmness, springiness and rubberiness of food gels using fractional calculus. Part I: Theoretical framework, *Food Hydrocolloids*, Volume 62, Pages 311-324

Jaishankar, A. & G. H. McKinley (2013) Power-law rheology in the bulk and at the interface: quasi-properties and fractional constitutive equations. *Proceedings of the Royal Society a-Mathematical Physical and Engineering Sciences*, 469.

Krotov V. V. (2009), “Basics of interfacial rheology”, in Interfacial Rheology, Miller R. & Liggeri *L. (Ed.s), Brill: Leiden (The Netherlands)*, 1-36

Rusanov (2005), Surface thermodynamics revisited, *Surface Science Reports* 58 111–239

H Schiessel et al 1995, Generalized viscoelastic models: their fractional equations with solutions *J. Phys. A: Math. Gen*. 28 6567

Acknowledgments

At the end of this PhD course I would like to sincerely thank people that guided and accompanied me during these three years: Prof. Baldino Noemi and Prof. Bruno de Cindio, who with their experience and knowledge guided me in the work, and first of all for the “parental affection” shown to me during dark moments. Thanks also to Professor Lupi Francesca and Gabriele Domenico for hints given during my studies. Special thanks to my collegues: Ilaria Carnevale, Elisabetta Bruno, Francesco Petrosino and Gaudio Maria Teresa for their friendships. Finally, a special mention for my dear Ylenia Marchesano, Samuele Salvino and Mileti Olga, who filled there three years with their presence and affection.